THE ROLE OF A NEURON-SPECIFIC V-ATPASE IN SYNAPSE SPECIFICATION, FUNCTION, AND MAINTENANCE

APPROVED BY SUPERVISORY COMMITTEE

P. Robin Hiesinger, Ph.D. (Advisor) _____

Adrian Rothenfluh, Ph.D. (Chair) _____

Ege Kavalali, Ph.D. _____

Helmut Kramer, Ph.D. _____

DEDICATION

For RAM

THE ROLE OF A NEURON-SPECIFIC V-ATPASE IN SYNAPSE SPECIFICATION, FUNCTION, AND MAINTENANCE

by

Wallace Ryan Williamson

DISSERTATION

Presented to the Faculty of the Graduate School of Biomedical Sciences

The University of Texas Southwestern Medical Center at Dallas

In Partial Fulfillment of the Requirements

For the Degree of

DOCTOR OF PHILOSOPHY

The University of Texas Southwestern Medical Center at Dallas

Dallas, Texas

November, 2011

THE ROLE OF A NEURON-SPECIFIC V-ATPASE IN SYNAPSE SPECIFICATION, FUNCTION, AND MAINTENANCE

WALLACE RYAN WILLIAMSON, Ph.D.

The University of Texas Southwestern Medical Center at Dallas, 2011

PETER ROBIN HIESINGER, Ph.D.

The Vacuolar-type (V-) adenosine triphosphatase (ATPase) is a proton-pumping nanomachine consisting of two multi-subunit, reversibly associating protein sectors, the cytosolic V1 sector and the membrane-bound Vo sector. The V1/Vo holoenzyme hydrolyses ATP to translocate protons across biological membranes thereby modulating lumenal and extracellular pH. Additionally, accumulating evidence suggests that the Vo sector has a role in membrane fusion when dissociated from the V1 sector, its proton-pumping partner. Published evidence for this includes a null allele for the neuron-specific a subunit in the *Drosophila* Vo sector, *v100*, which leads to defects in synaptic function that are unrelated to pH regulation. My project emerged from the need to

explain why *v100* has two additional phenotypes that are absent in other synaptic function mutants: functional and structural degeneration in photoreceptor cells and patterning defects in the visual system neuropil. I proposed that v100 has a previously undocumented role on a neuron-specific endo/lysosomal pathway in addition to its documented role in neurotransmitter secretion.

To test my hypothesis in the context of only one of the two purported v100 functions, I generated transgenic animals with v100 mutations designed to specifically disrupt either acidification or membrane fusion. Using these genetic tools, I discovered that v100 has an essential role in sorting cargo into an endo-lysosomal pathway that concomitantly requires v100 for the acidification-dependent maturation of degradation-competent organelles. This 'sort-and-degrade' mechanism for v100 defines a neuron-specific degradation pathway that is required for synaptic specification, function, and maintenance. In developmental stages, v100 is required to 'sort-and-degrade' guidance receptors as part of the synapse specification program. In the adult, the 'sort-and-degrade' mechanism provides additional degradative capacity to neurons, a cell type that must often maintain homeostasis for unusually long periods of time. Finally, I provide evidence that the role for V100 in membrane fusion requires a direct, physical interaction with Syntaxin-1, an interaction that can be specifically disrupted *in vitro* and *in vivo*.

In brief, my results provide mechanistic insight into the acidification-independent role of v100 and reveal the existence of a neuron-specific endo-lysosomal pathway on which v100 functions to 'sort-and-degrade' cargo in order to meet the special needs of a neuron in development, function, and maintenance.

PREFACE AND ACKNOWLEDGEMENTS

With the blessing of my thesis committee, I have included in this dissertation three complete manuscripts for which I am either first author or co-first author. The manuscripts have been reformatted to serve as chapters two, three, and four. In the materials and methods chapter of this dissertation, I distinguish my direct contributions to these projects from the contributions from others. I am grateful for the helpful critiques of preliminary manuscripts we received from Michael Buszczak, Bassem Hassan, Ilya Bezprozvanny, Nikos Giagtzoglou, Adam Haberman, Daniel Epstein, Nevine Shalaby, Grace Zhai, Tanja Rosenmund, Christian Rosenmund, Hugo Bellen and the members of the Hiesinger lab. I would like to thank Helmut Krämer, Thomas Neufeld, Hugo Bellen, Bill Trimble, Matt Scott, Damian Crowther, Grace Zhai, Craig Montell, John Abrams, Karl Fischbach, David Bilder, Trudi Schupbach, the Bloomington Stock Center and the University of Iowa Developmental Studies Hybridoma Bank for reagents. I am especially grateful to Sanchali Ray and Helmut Krämer for providing the eye sections shown in chapter two. I would like to acknowledge the funding sources that supported me and my collaborators: grants from the NIH (RO1EY018884), the Welch Foundation (I-1657), the Whitehall Foundation and the American Federation for Aging Research. My graduate mentor P. Robin Hiesinger is an endowed Eugene McDermott Scholar in Biomedical Research, and our collaborator on the role of the V-ATPase in *Drosophila* development, Jonathan R.Terman, is a Rita C. and William P. Clements, Jr. Scholar in Medical Research at UT Southwestern Medical Center.

I am also grateful in ways that cannot be duly expressed in a peer-reviewed publication. I must extend my deepest gratitude to my mentor, Robin Hiesinger, for the quality of his guidance and mentorship. His hand impacted my graduate experience most directly, fostering an opportunity for growth I will never forget. I thank my lab mates and colleagues who directly and indirectly enriched my research and writing experiences, especially Dong Wang, Daniel Epstein, Adam Haberman, Chih-Chiang Chan, and Elzi Volk. I thank my thesis committee for their time, their effort, and for their genuine concern for my success. I especially thank my chair, Adrian Rothenfluh, for the consistently invaluable advice on which I came to rely. My mother and father have provided consistent and dependable support for as long as I can remember. I would not be writing this if it were not for their persistent encouragement, love, and faith. Lastly, I would like to thank my wife, Angela, and my step-son, Malachi, for their patience, love, and devotion. They alone have made this effort and achievement worth the while.

TABLE OF CONTENTS

PUBLICATIONS

Wang, D.*, **Williamson, W.R.***, Srinivasan, S., Epstein, D., Haberman, A., Quiocho, F., Hiesinger, P.R. (in preparation). A SNARE-dependent vesicle sorting function of V0-ATPase subunit a1. *equal contribution

Haberman, A., **Williamson, W.R.**, Wang, D., Epstein, D., Meinertzhagen, I., and Hiesinger, P.R. (in revision). A role of the synaptic vesicle SNARE neuronal Synaptobrevin in endolysosomal degradation and neurodegeneration. The Journal of Cell Biology.

Williamson, W.R., Yang, T., Terman, J., and Hiesinger, P.R. (2010). Guidance Receptor degradation is required for neuronal connectivity in the *Drosophila* nervous system. PLoS Biology 8(12): e1000553.

Williamson, W.R.*, Wang, D.*, Haberman, A.S., and Hiesinger, P.R. (2010). A dual function of V0-ATPase a1 provides an endolysosomal degradation mechanism in Drosophila melanogaster photoreceptors. The Journal of Cell Biology 189, 885-899. *equal contribution

Williamson, W.R., and Hiesinger, P.R. (2010). Preparation of Developing and Adult Drosophila Brains and Retinae for Live Imaging. Journal of Visualized Experiments, e1936.

Williamson, W.R., and Hiesinger, P.R. (2010). On the role of v-ATPase V0a1–dependent degradation in Alzheimer Disease. Communicative & Integrative Biology 3, 604-607.

Williamson, W.R., and Hiesinger, P.R. (2008). Synaptic Patterning by Morphogen Signaling. Science Signaling 1 (18), pe20.

LIST OF FIGURES

CHAPTER THREE FIGURES

CHAPTER FOUR FIGURES

LIST OF DEFINITIONS

α-SNAP	Soluble N-ethylmaleimide-sensitive fusion protein-Attachment Protein
AV	Autophagic vacuole
Avl	Avalanche
Brp	Bruchpilot
Car	Carnation
CSP	Cysteine String Protein
Dor	Deep Orange
EE	Early Endosome
ERG	Electroretinogram
Fas2	Fasciclin II
Fmi	Flamingo
L3	3rd-Instar Larva
MARCM	Mosaic Analysis with a Repressible Cell Marker
MVB	Multivesicular Body
N-Cad	N-Cadherin
NSF	N-ethylmaleimide Sensitive Fusion protein
PMSF	Phenylmethylsulfonyl Fluoride
RE	Recycling Endosome

Rst	Roughest
SM	Sec1/Munc18-like
SNAP-25	Synaptosomal-Associated Protein 25
SNARE	Soluble NSF Attachment Protein REceptor
Spin	Spinster
Sun	Sunglasses
SV	Synaptic Vesicle
Syb	Synaptobrevin
Syx	Syntaxin
TEM	Transmission Electron Microscopy
TGN	Trans-Golgi Network
V-ATPase	Vacuolar Adenosine Triphosphatase

CHAPTER ONE

General Introduction

Nervous systems contain an organized network of neurons and their supporting cells, collectively charged with the task of receiving, processing, and storing sensory information. The functional unitary carrier of information is a specialized cell known as a neuron. Many of the cell biological processes that are common to all eukaryotic cells are required for cell division, maintaining homeostasis, and gene expression. In complex organisms composed of multiple cell types, each cell type is functionally specialized to some degree. Their special tasks are accomplished by expressing unique proteins that collaborate to accomplish biological processes that maintain the functional and physical characteristics which define a particular cell type. In some cases, loss of a specialized process will not affect common processes such as homeostasis. For example, I have observed that a mutation in the gene required for neurotransmitter production in *Drosophila* photoreceptors leads to defects in neurotransmission in cells that are otherwise healthy. For my graduate thesis, I have discovered a modified biological process that is dispensable for cell viability yet essential for neuron-specific needs in development, function, and maintenance. Evidence for this pathway comes from my work on a dual-functioning V-ATPase subunit, v100, which couples acidification and membrane fusion for a subset of endo/lysosomal compartments in neurons.

1.1 STRUCTURE AND FUNCTION OF THE V-ATPASE

The Vacuolar- (V-) ATPase is a multi-subunit holoenzyme with the primary function of translocating protons across biological membranes to modulate pH (reviewed by Jefferies et al., 2008; Marshansky and Futai, 2008). This enzyme is found ubiquitously in all eukaryotic cells and is required for their viability under normal conditions. Within a cell, the V-ATPase is responsible for acidifying the lumen of vesicles and organelles along the secretory and endo/lysosomal pathways (Figure 1.1). Many secretory vesicles carry antiporters that utilize the potential energy of a proton gradient. By harnessing energy from the incidental proton gradient, these antiporters load their secretory vesicle with the appropriate molecules destined for exocytosis. For example, antiporters on synaptic vesicles utilize a proton gradient to load the vesicle with a specific neurotransmitter (Forgac, 2007). Other types of secretory vesicles require acidification to activate enzymes which convert precursor molecules into functional hormones prior to exosomal secretion. This process is known to be essential for insulin secretion (Moriyama et al., 1992). Along the endocytic pathway, the acidification of early endosomes is a mechanism for dissociating ligands such as low-density lipoprotein (LDL) from their receptors, which are then free to be recycled back to the plasma membrane (Maxfield and McGraw, 2004). Lysosomes require acidification for the release of proteases from their mannose-6-phosphate receptors and subsequent activation (Ghosh et al., 2003). In some mammalian tissues, the V-ATPase is targeted to the apical membrane of certain cells to locally acidify the extracellular environment. For example, osteoclasts acidify the extracellular matrix to activate enzymes that participate in bone resorption (Toyomura et al., 2003). Dysfunction leads to the well-documented human genetic disorder osteopetrosis. Extracellular acidification is also required in mammals for renal function, inner-ear hair cell function, and sperm maturation in the male reproductive

tract (Karet et al., 1999; Pietrement et al., 2006; Wagner et al., 2004). Because of its fundamental role in eukaryotic cell biology as well as its relevance to mammalian physiology and disease, the V-ATPase has long-been of keen interest to basic science and medicine.

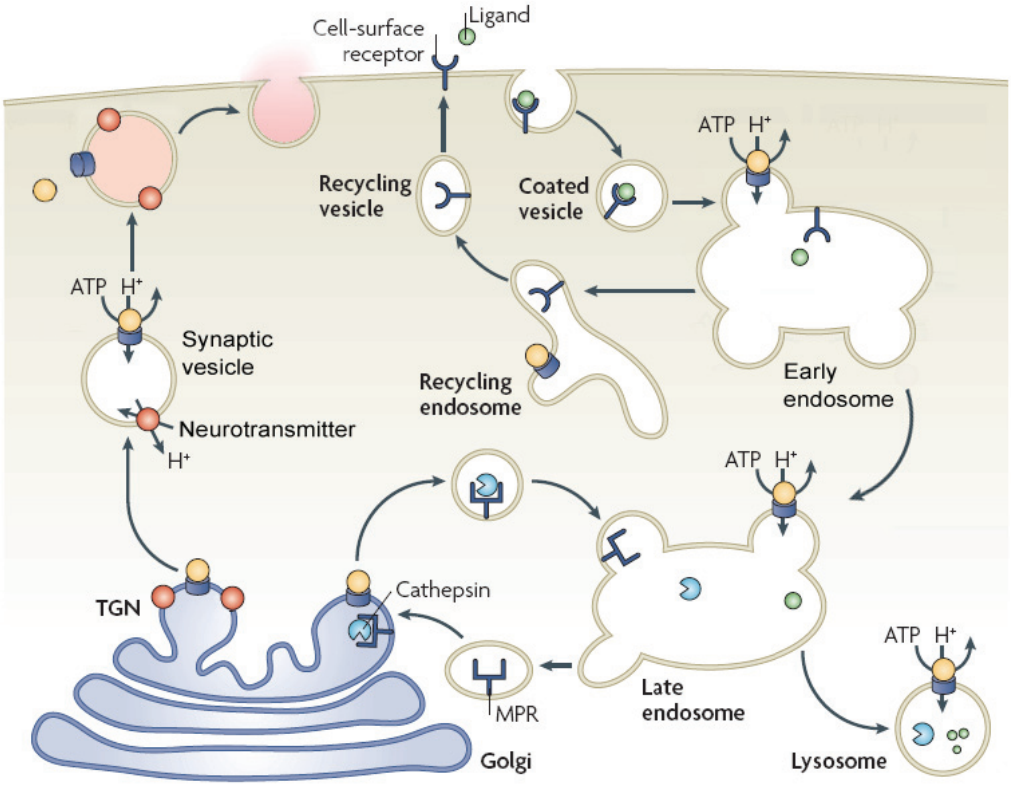

Figure 1.1: Roles or the V-ATPase in secretion, endocytosis, and degradation.

Assembly of the V-ATPase is competed in the Golgi. In neurons, synaptic vesicles are loaded with neurotransmitter by antiporters which utilize proton gradients generated by the V-ATPase. Mild acidification of early endosomes is required for receptor/ligand dissociation. In lysosomes, an acidic environment activates proteolytic enzymes like Cathepsin. Additionally, the Vo sector may have a role in exocytosis (see below). (adapted from Forgac, 2007)

The V-ATPase holoenzyme is composed of two multi-subunit sectors, V1 and Vo, which can reversibly associate and dissociate in a process regulated by other

enzymes (Seol et al., 2001; Xu and Forgac, 2001). In order to function as a proton pump, however, the V1 and Vo sectors must be associated (Figure 1.2). V1 is found in the cytosol when dissociated from Vo, and is responsible for harnessing the energy from ATP hydrolysis which drives proton translocation through the Vo sector, which is integrated with the membrane (Kane, 2006). The V1/Vo holoenzyme is structurally very similar to its better-characterized relative, the F-ATP synthase (Marshansky and Futai, 2008). Both have a stator that contains nucleotide-binding sites and a spinning rotor through which protons pass. However, they are functionally opposed. While the F-ATP synthase harnesses energy from a proton gradient to synthesize ATP, the V-ATPase hydrolyses ATP to establish a proton gradient. Additionally, the V-ATPase must localize to many parts of the cell and establish a specific lumenal or extracellular pH, while the F-ATP synthase is found only on the mitochondrial inner membrane and has the sole task of synthesizing ATP as efficiently as possible. To meet these additional demands, the cell utilizes a repertoire of subunit isoforms that can be differentially assembled to produce a specific V-ATPase that will reach the appropriate destination and pump protons with the appropriate efficiency, as part of the pH-regulation program (Toei et al., 2010). Most of this specificity is achieved by the specific subunit isoforms incorporated into the Vo sector. Vo sectors are composed of a stereotyped subunit stoichiometry: a (1), c (4), c' (1), c'' (1), d, and e (Figure 1.2). The a subunit provides the targeting sequence and has a specific affinity for the V1 sector depending on the isoform. Additionally, the c subunit isoforms couple protons with variable efficiencies. Multiple subunit isoforms are also available to the V1 sector, which has the following stoichiometry: A (3), B (3), C, D, E, F, G (2), and H (2) (Figure 1.2). Subunits B, C, E, and G are available in multiple isoforms in mammals and are known to interact with other proteins that regulate V1/Vo assembly and disassembly (Toei et al., 2010).

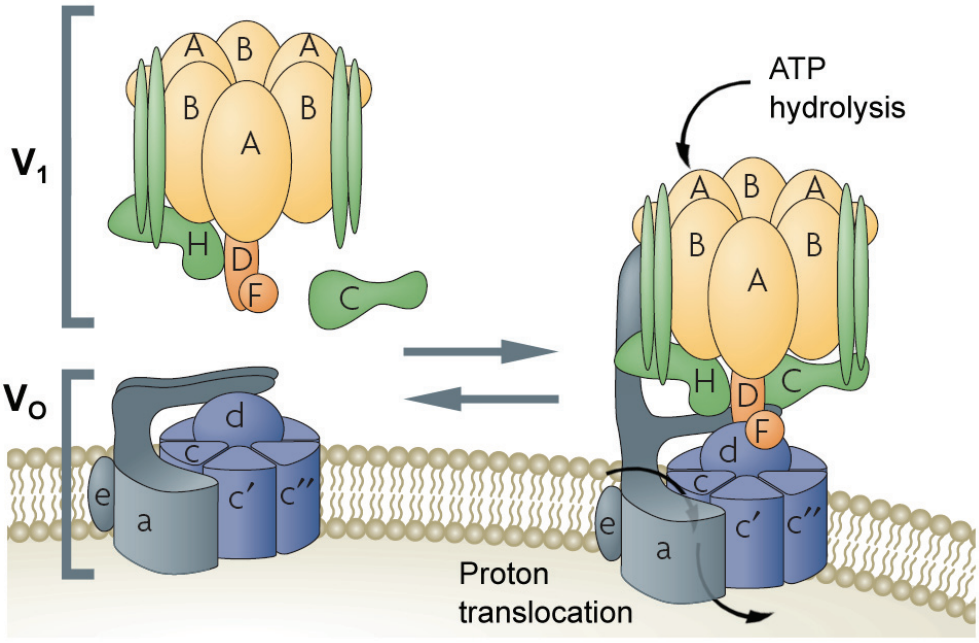

Figure 1.2: Schematic of the Vacuolar- (V-) ATPase.

The V-ATPase is a proton-pump that translocates protons across biological membranes using the energy from ATP hydrolysis. When the cytosolic V1 sector is dissociated from the membrane-bound Vo sector, the enzyme is inactive. When associated, ATP hydrolysis can occur in the A and B subunits of the V1 sector, inducing conformational changes which turn the Rotor (the D, d, and c-subunits) This rotation drives cytosolic protons through the a subunit and into the lumen or extracellular space. (adapted from Forgac, 2007)

Null mutations in V-ATPase subunits are often recessive cell lethal due to the vital requirement for lumenal pH regulation in many fundamental cell biological processes including the preparation of certain golgi-derived vesicles and lysosomal degradation (Forgac, 2007). However, phenotypes caused by mutations in some Vo sector subunit isoforms have been attributed to defects in specific membrane fusion events rather than defects in pH regulation (Hiesinger et al., 2005; Lee et al., 2006; Peri and Nusslein-Volhard, 2008). Accumulating evidence suggests that one or more of the subunits in Vo may have a direct role in membrane fusion (El Far and Seagar, 2011).

1.2 THE CORE MACHINERY IN MEMBRANE FUSION

Membrane fusion is a fundamental biological process that facilitates the controlled transport of cargo along the endocytic and secretory pathways (Reviewed in Jahn and Scheller, 2006b; Sudhof and Rothman, 2009). One of the best-studied examples is the fusion of synaptic vesicles to the pre-synaptic membrane to release neurotransmitter into the synaptic cleft following an action potential. Like most occurrences of membrane fusion, the synaptic vesicle fusion event is tightly regulated to ensure that neurotransmitter is released at the appropriate time and place. After trafficking a vesicle to the correct subcellular location (e.g. the synapse for synaptic vesicles), the vesicle is 'tethered' at close proximity to its target membrane (Bröcker et al., 2010). Although SV 'tethering' is poorly understood, other types of vesicles have known tethering factors with cytosolic domains that typically interact with Rab-GTPases and/or SNARE proteins that are present on the target membrane (Bröcker et al., 2010). Soluble N-ethylmaleimide-sensitive factor attachment protein receptor (SNARE) proteins are central to membrane fusion because they provide the energy that drives the energetically unfavorable process of lipid-mixing (Sollner et al., 1993; Sudhof and Rothman, 2009). The functional unit is a SNARE complex, a four-helical bundle of four 'SNARE motifs,' which are characteristic domains that define SNARE proteins (Figure 1.3). For a SNARE complex to be fusion-competent it must include at least one SNARE protein that is anchored to the vesicle and another that is anchored to the target membrane, thus forming a 'trans-SNARE complex' (Nichols et al., 1997). At the neuronal synapse, the SV donates a single vesicle- or v-SNARE, Synaptobrevin, which must specifically interact with the target or t-SNAREs Syntaxin and SNAP-25 on the presynaptic membrane. Synaptobrevin (Syb) and Syntaxin (Syx) each donate a single SNARE motif while SNAP-25 donates two to form a highly stable 'ternary SNARE complex' (Sudhof,

2004). SNARE complex formation is so energetically favorable that SNARE proteins are not found in isolation, preferring to interact promiscuously with one another. When unregulated, they can form a variety of four-helical SNARE complexes that are less-stable than the Syb/Syx/SNAP-25 SNARE complex described above (Margittai et al., 2001; Misura et al., 2001). Therefore, the controlled assembly of the SNARE complex is essential for SV fusion.

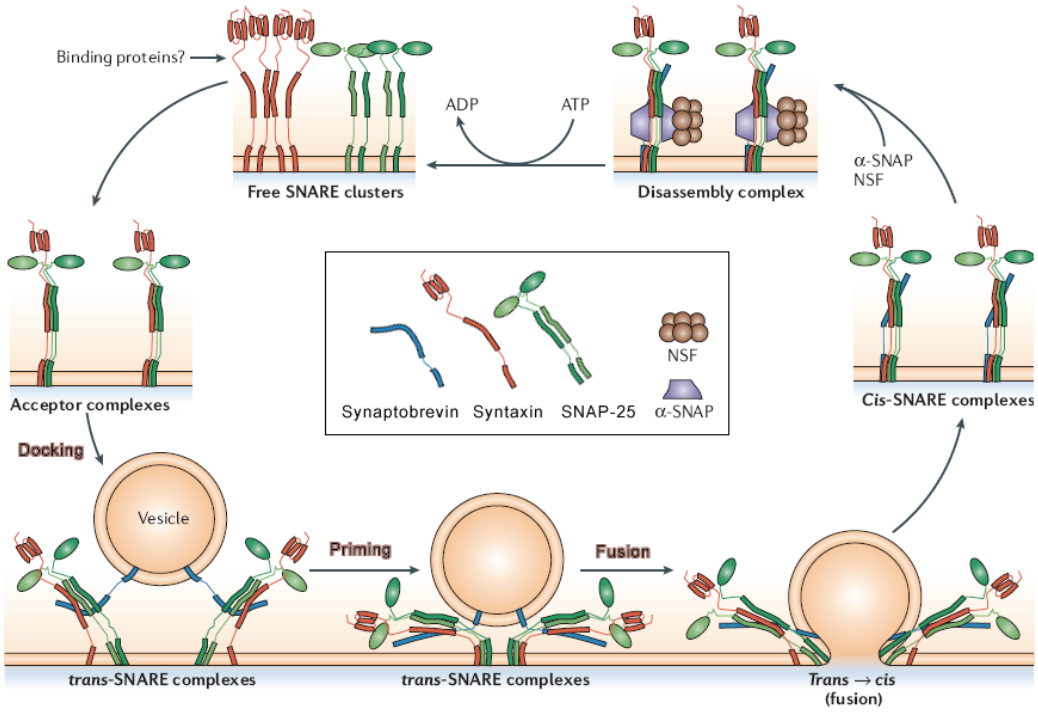

Figure 1.3: The synaptic vesicle cycle.

Following a fusion event, synaptic vesicle SNARE proteins remain in a 'cis' conformation until disassembled by NSF and α-SNAP. Unknown 'binding proteins' may stabilize the free SNARE proteins as t-SNARE complexes are prepared to receive an incoming v-SNARE protein. A regulated, stepwise process primes the newly-formed 'trans'-SNARE complex prior to fusion. (adapted from Jahn and Scheller, 2006b)

Immediately after the vesicle fuses, the SNARE complex remains stable in 'cis' on the target membrane (Figure 1.3). For another round of fusion to occur, the t-SNAREs Syx and SNAP-25 must be free to receive the v-SNARE Syb from an incoming, tethered vesicle to form a trans-SNARE complex in a process known as 'docking' (Sudhof, 2004). Dissociation of SNAREs in a cis-SNARE complex is performed by the ATPase NSF, its chaperone α-SNAP, and the energy from three ATPs. The process of trans-SNARE assembly following the dissociation of cis-SNARE complexes by NSF and α-SNAP is not completely understood and may involve unknown SM (Sec1/Munc18-like) proteins, a class known to be required for trans-SNARE complex formation (Carr and Rizo, 2010).

Synaptic vesicle fusion is ultimately triggered by an influx of calcium through voltage-gated calcium channels that open in response to an action potential. In preparation for this event, a process known as 'priming' brings the trans-SNARE complex close to its most-stable conformation, just shy of the activation energy required for membrane fusion (Sudhof and Rothman, 2009). Complexin is a SNARE complex-binding protein that maintains the primed state of the trans-SNARE complex (Krishnakumar et al., 2011). In the current model, calcium influx causes the calcium sensor Synaptotagmin to displace Complexin, allowing the SNARE complex to assume its most stable conformation and release enough energy to generate the final fuseogenic push (Maximov et al., 2009). Synaptotagmin-dependent neurotransmitter release in response to an action potential is known as 'evoked synchronous-release' and occurs on the narrowest timescale documented to date (Pang and Südhof, 2010). Electrical recordings indicate the synchronous transfer of charge that could only result from synchronized channel openings in response to the synchronous release of

neurotransmitter from the presynaptic cell. However, this describes only one class of response commonly observed in post-synaptic cells. Indeed, there are two additional physiologically relevant classes of calcium-mediated SV exocytosis (Pang and Südhof, 2010). Occasionally, an asynchronous transfer of charge is observed in the post-synaptic cell shortly after the synchronous event, indicating asynchonous channel openings in response to asynchronous neurotransmitter release. This calcium-dependent phenomenon is more dramatic when synaptotagmin function is inhibited or lost, indicating the presence of a second calcium sensor that may even compete with synaptotagmin. Finally, the response to spontaneous neurotransmitter release can be recorded in a post-synaptic cell. This class of release known as 'spontaneous miniature release' is also calcium-dependent and yet loss of synaptotagmin, the only known calcium sensor for synaptic vesicle release, is not required for spontaneous release. The identity of the calcium sensor(s) involved in asynchronous release and spontaneous release remains unknown (Pang and Südhof, 2010).

1.3 V100, THE a1 SUBUNIT OF THE V-ATPase IN *DROSOPHILA*

In an effort to identify unknown components of synaptic vesicle fusion machinery, a forward screen in *Drosophila* was conducted in the Hugo Bellen lab at the Baylor College of Medicine in Houston, TX led by my current advisor Robin Hiesinger when he was a postdoctoral fellow. Proteins involved in SNARE-mediated membrane fusion are often available in many isoforms that have specific subcellular destinations and are tailored to participate in specific fusion events. Because of this, the synaptic vesicle fusion machinery is often dispensable for the viability of cells yet required for the viability of an adult animal. In order to facilitate screening for synaptic function mutants

that would normally result in embryonic lethality, the eyFlp method was used to generate heterozygous, viable adults are homozygous for potential mutant alleles only in photoreceptor cells. To isolate genes specifically required for synaptic function, alleles chosen for analysis were demonstrably dispensable for photoreceptor development and function yet required to evoke a post-synaptic response when stimulated with visible-light. One such gene isolated in the screen was previously uncharacterized and was later given the name v100 (Hiesinger et al., 2005).

Multiple alleles of *v100* were isolated in the screen, one of which was demonstrated to be a null allele. The *Drosophila* gene v100 is orthologous to the V-ATPase a1 subunit. Loss of *v100* specifically in photoreceptor cells results in synaptic dysfunction, a phenotype that can be rescued by expressing wild type cDNA specifically in photoreceptors using the gal4/UAS system. When all cell types are homozygous for the *v100* null allele, the animal dies as a fully-developed embryo that exhibits uncoordinated muscle contractions. Indeed, electrophysiological recordings at the embryonic neuromuscular junction indicated loss of the evoked response in the muscle in addition to a dramatic reduction in the frequency of responses to spontaneous release events. Neuron-specific expression of wild type cDNA reverses these defects and restores viability through adulthood, demonstrating that v100 is required only in neurons. Antibody labeling in wild type animals demonstrates localization of V100 to the synapse, and labeling is lost at synapses in animals homozygous for the *v100* null allele. The a1 subunit was previously known in other systems to localize to synaptic vesicles where proton gradients generated by the V-ATPase power the antiporter that loads synaptic vesicles with neurotransmitter. Unexpectedly, however, the authors demonstrated that synaptic vesicles in the v100 null were properly loaded with neurotransmitter and that the

number of docked vesicles is normal, suggesting that the defects in synaptic vesicle release at the NMJ are directly related to defects in membrane fusion.

The fly gene v100 is one of four a subunit orthologs (a1-a4) conserved from *C. elegans* to humans. Indeed, the a1 subunit in *Drosophila*, is more homologous to the human a1 protein than it is to the other *Drosophila* a subunits a2-a4 (Hiesinger et al., 2005). The single-celled eukaryote *S. cerevisiae*, on the other hand, has only two a subunit isoforms, Stv1 and Vph1, while all other V-ATPase subunits lack multiple isoforms (Toei et al., 2010). Vo sectors containing Stv1 localize the V-ATPase to the trans golgi network, while Vph1 localizes the V-ATPase to the yeast vacuole. In 2003, Bayer et al. published evidence that while Vph1-containing V-ATPases are responsible for the acidification of the vacuole, Vph1 in a dissociated Vo sector directly participates in vacuolar membrane fusion (Bayer et al., 2003).

1.4 THE PUTATIVE ROLE IN MEMBRANE FUSION FOR SECTOR Vo

In 2001, Peters et al. demonstrated that the c subunit proteolipid pore in the *S. cerevisiae* V-ATPase Vo sector is required for vacuole fusion downstream of SNARE assembly (Peters et al., 2001). This finding legitimized the possibility that Vo sector subunits have an essential role in at least a subset of membrane fusion events. In the decade following this discovery, all Vo sector subunits would be implicated in at least one instance of membrane fusion, distinct from their roles in acidification, with examples coming from multiple model systems. In addition to the *Drosophila* a1 subunit being involved in synaptic vesicle exocytosis, the mammalian a3 subunit has been implicated in insulin secretion from murine pancreatic beta-cells (Sun-Wada et al., 2006). The a1 subunit in zebrafish is required for phagosomal/lysosomal fusion in glia (Peri and

Nusslein-Volhard, 2008). Exosomal secretion of Hedgehog-related protein is mediated by the a subunit in *C. elegans* (Kolotuev et al., 2009). Loss of the d2 subunit in mice impairs osteoclast fusion (Lee et al., 2006). Also in mice, a specific cytosolic fragment of the c-subunit directly interacts with synaptobrevin *in vitro* (Di Giovanni et al., 2010). When the same c subunit fragment is present in the cytosol, synaptic vesicle exocytosis was diminished. Collectively, these findings suggest that the role of the Vo sector in membrane fusion is more than just an ancient mechanism, with relevance to mammalian physiology.

1.5 RATIONALE AND SUMMARY

Unpublished observations in certain neuronal cell types devoid of v100 led to the inception of my thesis project. Photoreceptor cells null for v100 exhibit slow, adult-onset degeneration that correlates with a reduced electrical response to visible light as well as structural deterioration of the rhabdomeres. Additionally, loss of v100 in a subset of CNS neurons leads to defects in neuronal connectivity, a genetically-encoded developmental process that occurs independent of synaptic activity. My objective was to explain how loss of a protein thought to exclusively reside on synaptic vesicles could result in defects not seen in other synaptic function mutants. The answer would require characterization of a novel role for v100 in neural cell biology, in the context of its two putative functions: acidification and/or membrane fusion.

The primary hypothesis that guided my work was that mutations can be generated in a dual-functioning gene to specifically disrupt one function while leaving the other intact (Figure 1.4). Previous work done in yeast proves guidance and credence to this idea. A highly conserved Arginine in the yeast a subunit Vph1 is absolutely required for proton translocation (Kawasaki-Nishi et al., 2001). Mutations that result in a residue

change specifically disrupt acidification without affecting assembly or localization of the V-ATPase. By inducing a similar mutation in Drosophila, I was able to genetically isolate the fusion role of v100 by specifically disrupting the acidification role. In this genetic background, phenotypes were observed that were strikingly distinct from those observed both in the wild type animal and in the v100 null. Using this tool, I was able to characterize a novel role for v100 in neuronal cell biology and to attribute specific phenotypes to the v100 role in acidification or in membrane fusion.

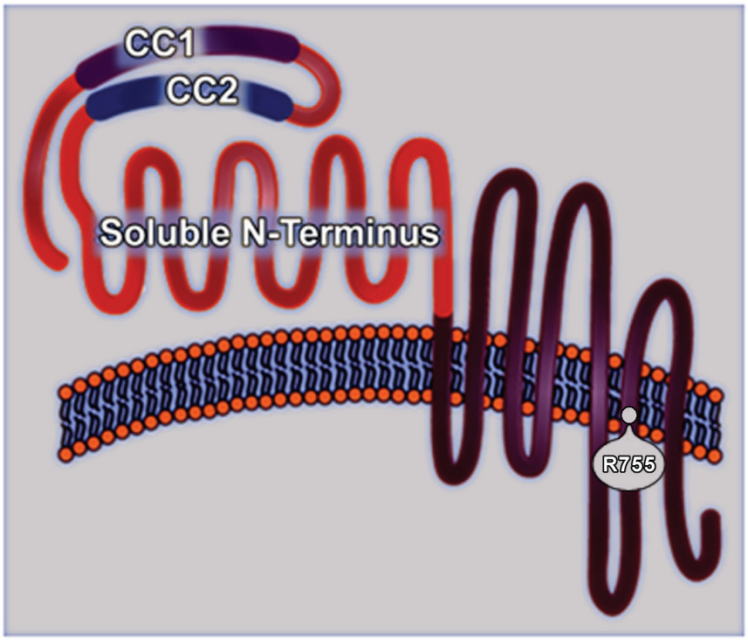

Figure 1.4: Schematic of the Drosophila *V-ATPase a1 subunit,* v100

The *Drosophila* a1 subunit v100 is comprised of a soluble N-terminal sequence which contains the two coiled-coil domains within which mutations were induced in an attempt to specifically disrupt SNARE protein interactions and the putative role for v100 in membrane fusion. Arginine-755 is located in the membrane-bound C-terminus of v100 and is homologous to the yeast Arg-735, shown to be absolutely required for proton translocation. We mutated the *Drosophila* Arg-755 to specifically disrupt acidification.

Despite the numerous reports implicating Vo subunits in membrane fusion events, the scientific community remains skeptical that the role in membrane fusion is direct. This is most likely because the molecular mechanism has yet to be established. A few hints can be found in published literature, however, that may place the Vo sector in context with known players in membrane fusion. Hiesinger et al. demonstrated a direct interaction with the t-SNAREs Syntaxin and SNAP-25 under exclusion of synaptobrevin in vitro. Additionally, a direct interaction with synaptobrevin has been demonstrated with a fragment of the mammalian c subunit. Finally, imunoprecipitation experiments from rat brain extracts indicate a protein complex exists *in vivo* that includes the a, c, and d subunits along with SNAP-25 and Synaptobrevin (Galli et al., 1996). These observations beg the question whether Vo subunit interactions with SNARE proteins are physiologically relevant. To test this, I generated mutations in v100 that disrupt SNARE binding *in vitro* and have characterized the consequence *in vivo* of expressing this SNARE-binding-deficient mutant. The results indicate that the SNARE interaction is physiologically relevant, supporting the hypothesis that the dual functions of v100 can be dissected genetically. Furthermore, these genetic tools have made it possible to test whether unknown neuronal cell biological roles exist for v100 in the context of its two putative functions: acidification or membrane fusion (Figure 1.5).

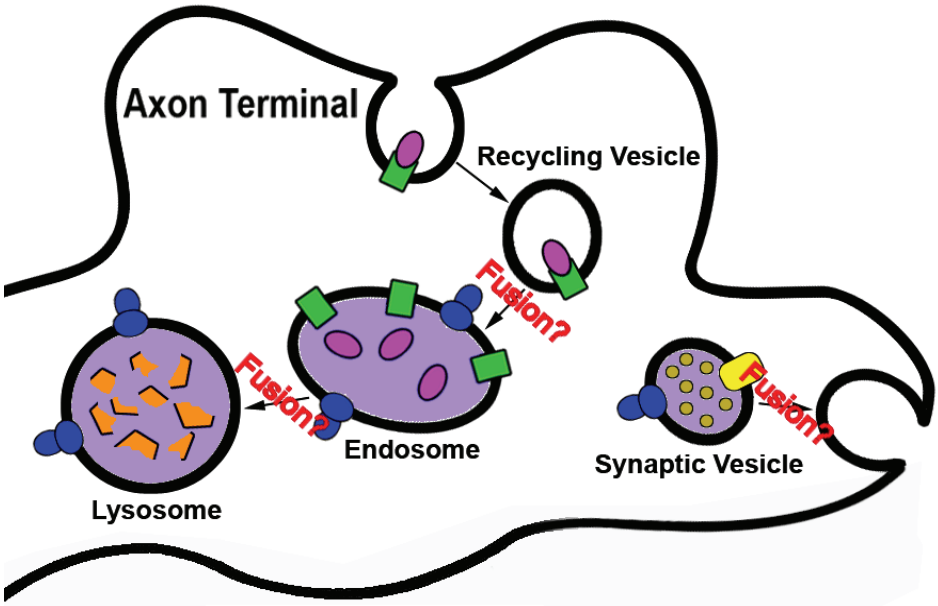

Figure 1.5: Axon terminal schematic to highlight experimental design rationale.

The candidate roles in neuronal cell biology that would explain phenotypes observed for *v100* could mechanistically require one or both of the two reported v100 functions. Genetic manipulations were designed to specifically disrupt either acidification or membrane fusion, and the cell biological consequences were analyzed to discern between the two.

CHAPTER TWO

A dual function of V0-ATPase a1 provides an endolysosomal degradation mechanism in *Drosophila* photoreceptors

Previously published in: **Williamson, W.R.***, Wang, D.*, Haberman, A.S., and Hiesinger, P.R. (2010). A dual function of V0-ATPase a1 provides an endolysosomal degradation mechanism in Drosophila melanogaster photoreceptors. The Journal of Cell Biology 189, 885-899. *equal contribution

2.1 ABSTRACT

The vesicular ATPase is a proton-pump that acidifies intracellular compartments. In addition, mutations in components of the membrane-bound v-ATPase V0 sector cause acidification-independent defects in yeast, worm, fly, zebrafish and mouse. Here we present a dual function for the neuron-specific V0 subunit a1 ortholog *v100* in *Drosophila*. A *v100* mutant that selectively disrupts proton translocation rescues a previously characterized synaptic vesicle fusion defect as well as vesicle fusion with early endosomes. Correspondingly, V100 selectively interacts with Syntaxins on the respective target membranes and neither synaptic vesicles nor early endosomes require *v100* for their acidification. In contrast, V100 is required for acidification once endosomes mature into degradative compartments. As a consequence of the complete loss of this neuronal degradation mechanism, photoreceptors undergo slow neurodegeneration, while selective rescue of the acidification-independent function accelerates cell death by increasing accumulations in degradation-incompetent compartments. We propose that V100 exerts a temporally integrated dual function that increases neuronal degradative capacity.

2.2 INTRODUCTION

Neurons have highly specialized demands on intracellular trafficking during development and function (Sann et al., 2009). While disruption of endosomal sorting typically leads to early developmental defects, aberrant late endosomal, lysosomal or autophagic functions have been implicated in neurodegeneration (Mizushima et al., 2008; Nixon et al., 2008; Tooze and Schiavo, 2008). Many disease-causing mutations directly affect degradation pathways, and a common hallmark of neurodegenerative disorders are accumulations of undegraded proteins. Disruption of the autophagy pathway in post-developmental neurons in mice leads to neurodegeneration within weeks (Hara et al., 2006; Komatsu et al., 2006). Despite the apparent susceptibility of neurons in particular, the intracellular degradation machinery is thought to be shared with other cell types and there is little evidence for a dedicated neuronal degradation mechanism.

Most intracellular compartments require acidification to function, and all require targeted membrane fusion to obtain and deliver intracellular cargo. The vesicular ATPase is a multi-subunit complex that consists of the membrane-bound V0 sector and a cytosolic V1 sector. V0 and V1 assembly is reversible. The V0/V1 holoenzyme acidifies intracellular compartments and is required for membrane protein sorting and degradation (Marshansky and Futai, 2008; Nishi and Forgac, 2002). Loss of v-ATPase-dependent acidification leads to signaling defects in early development in *Drosophila* (Yan et al., 2009) and *C. elegans* (Kolotuev et al., 2009). In addition, several studies in yeast, worm, fly, zebrafish and mouse suggest acidification-independent roles for the V0 complex in secretion or membrane fusion. These roles include yeast vacuolar fusion (Peters et al., 2001), synaptic vesicle exocytosis in *Drosophila* (Hiesinger et al., 2005), Hedgehog secretion in *C. elegans* (Liegeois et al., 2006), insulin secretion (Sun-Wada et al., 2006)

and osteoclast fusion (Lee et al., 2006) in mouse, and phagosome-lysosome fusion in zebrafish (Peri and Nusslein-Volhard, 2008). The v-ATPase thus represents a molecular machine that may regulate intracellular trafficking by integrating the two basic cellular functions acidification and membrane fusion (Nishi and Forgac, 2002; Wada et al., 2008). The reversible assembly of the V0 and V1 sectors provides an elegant regulatory mechanism for V0/V1 holoenzyme activity. V0/V1 disassembly may also regulate the availability of the V0 sector in the membrane for acidification-independent functions (Marshansky and Futai, 2008; Nishi and Forgac, 2002). It is unclear how both functions could be coordinated and integrated to regulate intracellular trafficking.

The *Drosophila* gene *vha100-1* (henceforth *v100*) encodes subunit a1 of the V0 sector. Mutations in *v100* were originally identified in a genetic screen for synaptic malfunction (Hiesinger et al., 2005). The genomes of *Drosophila, C. elegans*, mouse and human contain four subunit a1-a4 homologs (Marshansky and Futai, 2008). Mutations in subunit a2 have been shown to cause autosomal recessive cutis laxa type II (wrinkly skin syndrome), and mutations in subunit a3 cause osteopetrosis (Kornak et al., 2008; Kornak et al., 2000). *Drosophila* and *C. elegans* subunit a1 orthologs exhibit neuron-specific expression and a mammalian subunit a1 was originally cloned from a vesicle preparation from bovine brain (Perin et al., 1991). Neuronal expression of *v100* in null mutant embryos is sufficient to rescue embryonic lethality to adulthood in *Drosophila* (Hiesinger et al., 2005). In addition to this cell-specificity, subunit a1-a4 homologs confer intracellular compartment specificity. For example, in yeast there are two subunit 'a' homologs, whereas all other 13 core subunits are encoded by a single gene. Of these two, Vph1p localizes to the vacuole and Stv1p localizes the v-ATPase to the Golgi and endosomal compartments (Kane, 2007; Manolson et al., 1994). A *Torpedo* a1 subunit was shown to be specifically sorted to nerve terminals (Morel et al., 2003). How this

compartment-specific targeting of the v-ATPase is mediated by subunit ‘a’ homologs is unknown. An active role of subunit a1-a4 homologs in targeting of vesicle populations or their cargo has to our knowledge not been shown.

Here we report a dual function of subunit a1 in *Drosophila* that provides an integrated neuronal degradation mechanism. First, V100 directs vesicle fusion independently of acidification. Second, V100 is required for the acidification of a subset of neuronal lysosomes and autophagosomes, but not synaptic vesicles and early endosomes. Taken together these findings show how two completely different molecular functions can be temporally and functionally integrated to provide a cell biological mechanism of *’sort-and-degrade’*. We propose that V100’s dual function provides a neuronal degradation mechanism that functions only after neuronal differentiation in addition to essential endolysosomal function and bestows neurons an increased degradative capacity.

2.3 RESULTS

2.3.1 A putative v100 acidification mutant that rescues neurotransmission

We previously reported synaptic transmission defects in neurons mutant for *v100*, the gene that encodes the v-ATPase V0 subunit a1 in *Drosophila*. Importantly, electrophysiological recordings revealed normal neurotransmitter content of synaptic vesicles in this mutant. Since neurotransmitter loading requires synaptic vesicle acidification, we concluded that V100 is not part of the proton pump that acidifies synaptic vesicles (Hiesinger et al., 2005). These findings not only suggest a second function for *v100*, but also raise the question whether it has a v-ATPase-dependent acidification function elsewhere.

To genetically dissect the two putative functions of V100, we set out to generate a mutation that specifically disrupts the proton translocation function of V100. Such a mutation has been described previously for the yeast ortholog *vph1*: Mutation of Arginine 735 to Alanine (R735A) in *vph1* leads to the specific disruption of proton translocation without affecting assembly of the v-ATPase or its localization (Kawasaki-Nishi et al., 2001). This Arginine lies in a 17 amino acid region that is 100% conserved in V100 homologs from yeast to humans and corresponds to R755 in V100 (Fig. 1A). Neurotransmission in *v100* null mutant photoreceptors can be rescued using the Gal4/UAS system (Brand and Perrimon, 1993) by exclusively expressing *v100* presynaptically (Hiesinger et al., 2005). We generated and selected two independent UAS-$v100^{R755A}$ lines that exhibit indistinguishable expression levels of the synaptically localized protein compared to control UAS-$v100^{WT}$ (data not shown). Remarkably, synaptic transmission, as indicated by the 'on'-transient of the electroretinogram (ERG),

is significantly restored by *v100*^{R755A} expression in *v100* mutant photoreceptors (Fig. 1B, C). Surprisingly, however, the rescue of the ERG 'on'-transient is accompanied by a significant decrease in ERG depolarization (Fig. 1D). This reduction in response amplitude does not occur in *v100* null mutants. Furthermore, the decrease in depolarization is more pronounced when *v100*^{R755A} is expressed in mutant photoreceptors compared to its overexpression in wild type neurons (Fig. 1B, D). A reduction in response amplitude often indicates an unhealthy neuron. Indeed, even mildly elevated levels of *v100*^{R755A} in mutant neurons leads to a reduced eye size and loss of photoreceptors (Fig. 1E-I). In contrast, this phenotype is not observed when *v100*^{R755A} is expressed at the same level in the presence of wild type *v100* (compare Fig. 1G and I). Higher levels of expression (>24C) lead to almost complete abolishment of the eye when *v100*^{R755A} is expressed in *v100* null mutant photoreceptors and a milder rough eye phenotype when *v100*^{R755A} or wild type *v100* are expressed in wild type photoreceptors (data not shown). Hence, *v100*^{R755A} has a strongly detrimental effect on photoreceptor viability only when wild type *v100* is absent. These observations raise two questions: First, how can expression of *v100*^{R755A} rescue neurotransmitter release yet cause cell death when expressed at higher levels in mutant neurons? Second, why is *v100*^{R755A} strongly detrimental to cell viability *only* in the absence of wild type *v100*? *v100*^{R755A} exhibits a genetically unusual behavior: It is not a dominant negative, because it causes a phenotype that is very different from the null mutant and because it does not cause the same phenotype when expressed in a wild type background. If V100^{R755A} is selectively disrupted in proton translocation, a straightforward hypothesis would be that *v100*^{R755A} rescues a second, acidification-independent function that is sufficient to restore neurotransmitter release, but causes detrimental effects to the cell only in the absence of a wild type protein.

2.3.2 V100 is required for the acidification of a subset of neuronal degradative compartments

First, we needed to know whether $V100^{R755A}$ is indeed acidification-defective. No acidification role of V100 has so far been characterized (Hiesinger et al., 2005). We therefore performed live measurements of intracompartmental pH using the fluorescent probe Lysotracker in the null mutant, $v100^{R755A}$ and control photoreceptors. Lysotracker is a membrane-permeable compound that can be added to the bath of a live *Drosophila* larval or pupal eye-brain culture and selectively labels strongly acidified compartments. To quantitatively assess even slight differences in Lysotracker labeling we generated 50% fluorescently labeled mutant clones in developing photoreceptor neurons (MARCM technique (Lee and Luo, 1999)). As a further control, we confirmed that wild type MARCM clones cause no effect (data not shown). As shown in Figure 2A, Lysotracker labeling of mutant and control cells is indistinguishable in L3 larval eye discs, i.e. at the time point when neuronal differentiation and *v100* expression commence. Remarkably, however, in mutant cells at 20% of pupal development (P+20%) the Lysotracker signal reduces slightly, but significantly (data not shown). At P+40% the Lysotracker signal is reduced to approximately 50% (Fig. 2B, D). A level of ~50% Lysotracker labeling is maintained in 1-day adult photoreceptors (data not shown). This phenotype is rescued by expression of wild type *v100* (Fig. 2D). The change of Lysotracker fluorescence is reflected in a corresponding loss of Lysotracker-positive compartments in mutant compared to control clones from 100% in L3 to 67% at P+20% and 47% at P+40%. These observations indicate that developing photoreceptors exhibit a progressive reduction of strongly acidified compartments after neuronal differentiation.

Next, we tested whether expression of $v100^{R755A}$ under the same conditions that rescue neurotransmitter release also rescues this acidification defect. As shown in Fig.

2C-D, expression of *v100*^{R755A} in *v100* mutant photoreceptors does not rescue the Lysotracker defect observed in *v100* mutant neurons. This result supports a direct acidification function of V100 for at least some Lysotracker-positive compartments in neurons.

Since Lysotracker labeling indicates normal levels of acidification prior to neuronal differentiation, we wondered whether these compartments are acidified by other v-ATPase subunits. We tested this idea pharmacologically with the v-ATPase-specific blocker Bafilomycin 1A. Indeed, 10 minutes preincubation with Bafilomycin A1 fully prevents any Lysotracker labeling in both mutant and control cells, indicating that these Lysotracker-positive compartments are acidified in a v-ATPase-dependent manner (Fig. 2F-H). The finding that strongly acidified compartments persist in *v100* mutant neurons shows that *v100* cannot be required equally for the acidification of all compartments.

We assessed the molecular nature of Lysotracker-positive compartments in the live preparation by expressing YFP-tagged versions of the early endosomal maker Rab5, the late endosomal marker Rab7, and the recycling endosomal marker Rab11 (Zhang et al., 2007) as well as the autophagosomal marker Atg8-GFP (Chang and Neufeld, 2009). As shown in Fig. 2E and Suppl. Fig. 1A-B, Lysotracker rarely marks Rab5 or Rab11-positive compartments. In contrast, 32% of Lysotracker-positive compartments are Rab7-positive, ring-shaped late endosomes. In addition, 20% of Lysotracker-positive compartments are Atg8-GFP positive (Fig. 2E; Suppl. Fig. 1C-D). This ratio of Rab7 and Atg8-positive strongly acidified compartments is unaltered in the mutant (Fig. 2E; Suppl. Fig. 1E-F). Hence, neither compartment type is lost in the mutant. Instead, these findings indicate a loss of a neuronal subset of these compartment types. Taken together our data suggest that V100 is required for the acidification of a neuronal subset of late

endosomal and autophagosomal compartments and that this acidification function is not rescued by $v100^{R755A}$.

2.3.3 V100 is enriched on early endosomes

To comprehensively characterize V100-positive compartments in wild type, we used a panel of 16 markers for colocalization analyses in developing and adult photoreceptors. We performed these experiments using high-resolution 3D confocal microscopy that allows the visualization of distinct subcellular compartments at the resolution limit of light (Hiesinger et al., 2001). To quantify compartment colocalization, we identified clearly discernible intracellular V100-positive compartments and counted how many of these were positive for a given other intracellular compartment marker as shown in Suppl. Fig. 2A-D for the synaptic vesicle marker CSP and the late endosomal marker Rab7. As shown in Figure 3A-B, wild type V100 colocalizes to a varying degree with several markers of membrane compartments, including endosomes, lysosomes and synaptic vesicles (marked *endo, lyso* and *syn.ves.* in Fig. 3B). Most strikingly, only immunolabeling of the early endosomal marker Syntaxin7/Avalanche (Syx7/Avl) exhibits a localization pattern that is almost identical to V100 (Fig. 3C-D). Syx7/Avl acts together with Rab5 in vesicular fusion with early endosomes (Lu and Bilder, 2005). Indeed, the second most colocalizing marker ofV100-positive compartments is the early endosomal marker Rab5 (Fig. 3B; Suppl. Fig. 3E, F). This colocalization pattern is substantiated in a complementary experiment using photoreceptor-specific expression of GFP-Rab5 (Wucherpfennig et al., 2003). GFP-Rab5 exhibits strong labeling along the developing rhabdomeric structure in the cell bodies (green arrowhead in Fig. 3E) as well as in photoreceptor axon terminals (blue arrow in Fig. 3E). V100 immunolabeling colocalizes with GFP-Rab5 at the axon terminals (blue arrow), but only little in the cell

bodies (Fig. 3E). These data suggest that V100 is enriched together with synaptic endosomes. In contrast, co-labeling with the lysosomal marker Sun/CD63 (Xu et al., 2004) reveals little V100 colocalization and a converse distribution pattern (increased levels in the cell bodies (red arrowhead in Fig. 3E) and very low levels in developing synaptic regions; Fig. 3E). Similarly, expression of fluorescently tagged V100 in *v100* null mutant neurons (that rescues its function) reveals partial colocalization with the endosomal markers Hrs and Rab11 (Lloyd et al., 2002; Pelissier et al., 2003), but less colocalization with the lysosomal marker Spin/Bnch (Dermaut et al., 2005; Sweeney and Davis, 2002) Suppl. Fig. 3G-I). Taken together our wild type compartment characterization yields the surprising finding that V100 most strongly colocalizes with early endosome markers in addition to synaptic vesicles and exhibits comparably less colocalization with lysosomal markers.

2.3.4 Loss of v100 causes endosomal and autophagosomal accumulations

To understand the trafficking defects in *v100* mutant photoreceptors we examined changes of the 16 intracellular compartment markers presented in the previous section. We again engineered MARCM flies in which 50% of all photoreceptors are rendered mutant and positively labeled with a fluorescent marker, whereas the other 50% serve as control in the same brain. As shown in Fig. 4A-B, photoreceptor terminals of 1-day old adults exhibit upregulation specifically of endosomal and lysosomal compartment markers. The most prominently upregulated markers include the early endosomal Syntaxin Syx7/Avl, the early and late endosomal *rab* GTPases Rab5 and Rab7 and the lysosomal marker Sun/CD63. In contrast, markers for the synaptic target-membrane Syntaxin 1A, the Golgi/lysosomal Syntaxin 16 and several other membrane proteins remain largely unaltered. Hence, we find upregulation of specific markers along the

endolysosomal pathway that suggest accumulations of both early and late endosomal compartments. Correspondingly, Western Blot analysis of total protein extract from 2-day old *v100* mutant eye-lamina complexes shows a clear increase of the endosomal proteins Syx7/Avl and Hrs (Suppl. Fig. 3A-C). These data support the idea of a protein degradation defect.

We have previously performed transmission electron microscopy (TEM) of 1-day adult *v100* mutant photoreceptors. In our previous study we found a significant increase of vesicular content, but no alterations of active zones or mitochondria (Hiesinger et al., 2005). To identify ultrastructural correlates of the endolysosomal accumulations, we analyzed the TEM data for morphologically abnormal membranous compartments. As shown in Fig. 4C-E, quantitative analysis reveals a significant increase of highly heterogeneous enlarged structures, many of which appear morphologically as multivesicular bodies (MVBs; arrowhead in Fig. 4D) or double-membrane autophagosomal vacuoles (AVs; arrow in Fig.4D; quantification in Fig. 4E). We did not observe any multilamellar structures that represent failed degradation in aberrant lysosomal structures, as are apparent for example in micrographs of photoreceptor terminals of the lysosomal storage mutant *spinster/bnch* (Dermault et al., 2005). Instead, accumulations of both MVBs and AVs are indicative of compartments prior to lysosomal degradation.

Lastly, we performed a series of experiments using fluorescent reporters of the different trafficking and degradation compartments. As a marker for MVBs we used YFP-Rab7, for AVs LC3/dATG8-GFP and for early endosomes YFP-Rab5 and 2xFYVE-GFP. Expression of any of these four markers results in large accumulations in *v100* mutant 1-day adult photoreceptors (Fig. 4F-M). Immunolabeling for Syx7 reveals substantial colocalization with endosomal Rab5, Rab7 and 2xFYVE accumulations (Fig.

4F-I and data not shown). In contrast, Atg8-positive autophagosomal compartments are mostly non-overlapping with the Syx7-positive endosomal accumulations (Fig. 4J-K). Similarly, both the early endosomal markers GFP-2xFYVE (Wucherpfennig et al., 2003) and the lysosomal marker Sun/CD63 (Xu et al., 2004) accumulate, but do so in mutually exclusive compartments (Fig. 4L-M). These data suggest that early endosomal markers, including Syx7, do not accumulate in a single type of Atg8-positive AV or Sun/CD63-positive lysosome. Instead, accumulations occur at the level of endosomes in addition to lysosomal and autophagosomal degradative compartments.

2.3.5 V100 exerts an acidification-independent function on early endosomes

The accumulation of late endosomes and autophagosomes is consistent with the acidification defects of late endosomal and autophagosomal compartments shown in Figure 2. But why is V100 predominantly localized on early endosomes? Early endosomal compartments can mature into late endosomal compartments (Rink et al., 2005). V100 may thus exert an acidification-independent function on early endosomes that later mature into degradative compartments and require increased acidification. To assay how loss of *v100* affects the pH of endosomal compartments, we expressed the membrane-tagged fluorescent probe synapto-pHluorin in photoreceptors. Synapto-pHluorin (henceforth pHluorin) is a genetically encoded pH-sensitive GFP variant that can be used to measure the pH of synaptic vesicles and other intracellular compartments (Ng et al., 2002). Synaptic vesicles and other endocytic vesicles can fuse with endosomal compartments and pHluorin was previously shown to localize to endosomes (Machen et al., 2003).

At wild type photoreceptor synapses pHluorin labeling is very similar to the synaptic vesicle marker Cystein String Protein (CSP) (Fig. 5A). In addition, pHluorin

marks regions enriched for the early endosomal marker Rab5 (Suppl. Fig. 3D), but colocalizes very little with the late endosomal marker Rab7 and the recycling endosomal marker Rab11 (data not shown). Remarkably, in *v100* mutant terminals, the colocalization of pHluorin with the synaptic vesicle markers CSP is mostly lost (Fig. 5B). Instead, accumulations of pHluorin partially colocalize with the early endosomal markers Syx7/Avl (Fig. 5C) and Rab5, the late endosomal marker Rab7 and the recycling endosomal marker Rab11 (Suppl. Fig. 3E-G). Photoreceptor-specific expression of wild type *v100* fully recues this phenotype (Suppl. Fig. 3H-K). These data indicate that pHluorin accumulates in *v100* mutant terminals in compartments along the endosomal pathway, including Syx7/Avl-positive endosomes.

To measure the acidification of these compartments, we again used the v-ATPase-specific inhibitor Bafilomycin 1A. pHluorin has reduced fluorescence when exposed to acidic pH and loss of acidification results in a fluorescence increase. In our photoreceptor preparation, the pharmacological block of all v-ATPase function leads to a 1.37-fold pHluorin fluorescence increase in the wild type and a statistically not significantly different 1.42-fold increase in the mutant (Fig. 5H-N). This finding indicates that pHluorin-positive compartments are acidified in *v100* mutant neurons. We further confirmed that pHluorin accumulates in acidified compartments in cell bodies and at synapses using a calibrated alkalization/acidification protocol based on NH_4Cl washes as described in the Materials and Methods and shown in Suppl. Fig. 4A-D. Taken together with the wild type localization data, these data suggest that V100 is an endosomal protein that is not required for endosomal acidification.

Next, we tested how $v100^{R755A}$ expression affects the pHluorin localization and measurements in *v100* mutant neurons. Surprisingly, fluorescence levels reveal a dramatic further increase of pHluorin accumulations in *v100* mutant photoreceptors

expressing *v100*^{R755A} compared to the mutant alone (Fig. 5D-F; Suppl. Fig. 4E). This finding follows the previously observed pattern of phenotypes worsened by *v100*^{R755A} expression on the ERG amplitude and cell death (Fig. 1). Since *v100*^{R755A} expression causes massive photoreceptor cell loss only when expressed in null mutant photoreceptors (Fig. 1G-I), we wondered whether the same is true for pHluorin accumulations. Fig. 5G shows a mosaic of synaptic terminals of 1-day old photoreceptors where wild type terminals are marked with RFP (magenta), whereas the *v100* null mutant terminals are unmarked. In addition, we co-expressed both *v100*^{R755A} as well as pHluorin at identical levels in all photoreceptors. Remarkably, only *v100*^{R755A} expression in *v100* mutant photoreceptors, but not in a wild type control clone, causes dramatic pHluorin accumulations at the synaptic terminals (Fig. 5G). This finding shows that the pHluorin accumulation phenotype indeed follows the same pattern as the reduction in ERG depolarization and eye size: in all cases *v100*^{R755A} causes more severe phenotypes in the absence of wild type *v100*.

Finally, we performed acidification measurements using the same Bafilomycin protocol as before. As shown in Fig. 5H-N, pharmacological block of all v-ATPase function in photoreceptors with *v100*^{R755A} expression in a mutant background causes a 1.79-fold increase in fluorescence. This finding indicates that the increased accumulations occur in compartments that are at least as acidified as in wild type and null mutant (Fig. 5N). Indeed, the 1.79-fold increase is significantly higher than in the null mutant, which is likely due to the dramatic increase in the amount of pHluorin. The accumulation of pHluorin in acidified compartments was again confirmed using calibrated NH_4Cl washes (Suppl. Fig. 4E). Our findings support the notion that selective rescue of an acidification-independent function causes protein accumulations only when no wild type protein provides acidification.

2.3.6 V100 interacts with the early endosomal Syntaxin7/Avalanche, but not the Golgi/lysosomal Syntaxin16

Our findings raise the question about the molecular mechanism of the acidification-independent function. An important hint comes from the observation that V100 is an endosomal protein that is not required for endosomal acidification. We were intrigued by the Syx7 colocalization with V100 in wild type as well as the Syx7 accumulation in the *v100* mutant, since previous studies suggested acidification-independent functions of V100 and its homologs in SNARE-mediated membrane fusion (Bayer et al., 2003; Hiesinger et al., 2005; Liegeois et al., 2006; Peri and Nusslein-Volhard, 2008). Syntaxins are key SNARE (soluble NSF attachment protein receptor) proteins that mark specific target membranes where they are absolutely required for membrane fusion (Sudhof and Rothman, 2009). Syx7/Avl is required for vesicle fusion with early endosomes in *Drosophila* (Lu and Bilder, 2005). In contrast, Syx16, which is located mostly at the Golgi and to some extent on lysosomes (Akbar et al., 2009), exhibits significantly less colocalization with V100 and no mutant accumulation (Figs. 3B and 4B). V100 directly binds to Syntaxin1A (Syx1A), the target SNARE required for synaptic vesicle fusion (Hiesinger et al., 2005). To test a possible interaction of V100 with Syx7/Avl and Syx16, we performed co-immunoprecipitations using the V100 antibody from fly heads. As shown in Fig. 6A some Syx7/Avl, but not Syx16 co-immunoprecipitates with V100. These results indicate that V100 exists in a complex with Syx7/Avl, but not Syx16 in the brain. Conversely, V100 is co-immunoprecipitated with Syx7/Avl from brain extracts (Fig. 6B). The amount of co-immunoprecipitated Syx7 was low compared to Syx1A (Fig.6A). To test the strength and specificity of these interactions we performed a series of pull-down assays. First, we performed pull-downs from fly head extracts with his-tagged V100N (the N-terminal half of V100 that is

unaffected by the R755A mutations) or his-tagged Syx7 and probed for Syx7 and V100, respectively. As shown in Fig. 6C-D, both proteins can pull down each other from brain extract robustly. This pull-down result is specific, as Syx7 and Syx1A, but not Syx16, are pulled down with V100N, corroborating the co-IP results (Fig. 6D). Finally, since V100 is known to directly interact with Syx1A, we tested the direct interaction of bacterially synthesized and purified GST-tagged V100N with His-tagged Syx7. As shown in Fig. 6E, V100 and Syx7 show strong, direct interaction. We conclude that V100 and Syx7/Avl robustly interact *in vitro* and *in vivo*. Note that the R755A mutation resides close to the C-terminus of the 855aa V100 protein, whereas the SNARE-interaction motif resides in the N-terminal 140aa (Hiesinger et al., 2005). As shown here, the unaltered N-terminus is sufficient to bind to Syx7/Avl. Hence, these findings suggest a mechanistic basis for an acidification-independent function of V100 in vesicle fusion with target membranes marked by specific Syntaxins.

2.3.7 Loss of v100 causes slow, adult-onset degeneration

Our data suggest that vesicle fusion with early endosomes in the $v100^{R755A}$ rescue leads to the fast accumulation of enlarged compartments that mature into degradation-incompetent compartments due to lack of acidification (Fig. 5F, G, M). In contrast, in the null mutant we observe a much slower accumulation of degradation-incompetent compartments, as evidenced for example for pHluorin in Fig. 5E and K. If the accumulation of degradation-incompetent compartments is detrimental to cell viability, then the *v100* null mutant might cause slow degeneration.

We previously reported synaptic transmission defects, but no developmental or degenerative defects, in embryos as well as adult *v100* mutant photoreceptors of one day-old flies (Hiesinger et al., 2005). Consistent with the previous findings, the

depolarization of up to one-week old *v100* mutant photoreceptors is indistinguishable from wild type (Figure 7A, B). However, a weak reduction of the depolarization becomes apparent after 3 weeks (Fig. 7E, F) and progressively worsens with 5 weeks (Fig. 7I, J). All flies were raised in a 12h light/12h dark cycle. We also dark-reared a set of control and *v100* mutant flies to investigate whether this reduction of photoreceptor responses is stimulus-dependent. Dark-reared control flies exhibit a significantly increased depolarization (Fig. 7M). The dark-reared mutants do not show this increase, but a depolarization that is not significantly different from 4-5 week old control flies raised in a normal light/dark cycle (Fig. 7N). Figure 7Q summarizes these results quantitatively. Next, we analyzed the morphology of these eyes by immunolabeling with a monoclonal antibody against the transmembrane protein Chaoptin that labels the rhabdomeres, i.e. the light-sensitive membrane organelles. In contrast to control flies, *v100* mutant photoreceptor cell bodies exhibit accumulations of Chaoptin-positive structures, while losing most discernible rhabdomeric structure by 5 weeks (Fig. 7K-L). Again, these phenotypes are progressive (comp. Fig 7C-L). Traditional plastic sections of these eyes further reveal the extent of the degenerative phenotypes with little discernible structures after 5 weeks (Suppl. Fig. 4F, G). In 5 week-old dark-reared mutants aberrant Chaoptin-positive accumulations are also apparent, but the rhabdomeric as well as the overall structure are significantly less disrupted than in mutants after 5 weeks light/dark-cycle (Fig. 7O, P). Together these data show a degenerative phenotype in *v100* mutant neurons that coincides with transmembrane protein accumulation, progresses slowly and can be attenuated by absence of stimulation.

2.3.8 Selective rescue of the acidification-independent function accelerates degeneration by increasing accumulations in Syx7-positive, degradation-incompetent compartments

Our combined data support a model in which the acidification-defective V100^{R755A} rescues vesicle fusion with the presynaptic membrane (via Syx1A interaction) and early endosomes (via Syx7 interaction) (Figure 8A). In this model, rescue with *v100^{R755A}* effectively speeds up cargo overload in degradation-incompetent compartments. Our model predicts that Chaoptin, which accumulates slowly in null mutant photoreceptors (Fig. 7), accumulates faster in Syx7-positive compartments in the *v100^{R755A}* rescue. As shown in Figure 8B-D, in 1-day adult synaptic terminals of the null mutant, Chaoptin exhibits small accumulations that are partially associated with Syx7 accumulations, but mostly Syx7-negative. In contrast, *v100^{R755A}* rescue of the null mutant at the same time point exhibits a dramatic increase of Chaoptin accumulations in large vesicles that are invariably enclosed by large Syx7-positive compartments (arrows in Fig. 8D; see also schematic in Suppl. Fig. 5F-I). This observation supports the idea that V100^{R755A} promotes the fusion of cargo vesicles with Syx7-positive endosomes.

Finally, our model predicts a dominant function of V100^{R755A} that is different from the loss-of-function phenotype, but consistent with the ERG defects shown in Fig. 1B-D. We therefore analyzed the effect of *v100^{R755A}* overexpression on photoreceptor morphology and degeneration in two-week old flies. As shown before, loss of *v100* causes slow neurodegeneration that is accompanied by accumulations of Chaoptin (Figure 7 and Suppl. Fig. 5A). This phenotype is rescued by *v100* expression in mutant photoreceptors (Suppl. Fig. 5B). Overexpression of wild type *v100* causes no obvious defects (Suppl. Fig. 5C). In contrast, overexpression of *v100^{R755A}* in wild type photoreceptors causes the accumulation of Syx7 at the base of rhabdomeres (arrows in Suppl. Fig. 5D), but no apparent accumulation of Chaoptin and no degeneration of the rhabdomeric structure (arrowheads in Suppl. Fig. 5B-D). These observations are consistent with a mild dominant effect of *v100^{R755A}* that is distinct from the null mutant

phenotype (comp. Suppl. Fig. 5G, H). Finally, expression of $v100^{R755A}$ in null mutant photoreceptors causes dramatically 'blown up' accumulations that appear like exacerbated versions of those in the null mutant (Suppl Fig. 5E, I). These data suggest that $v100^{R755A}$ in wild type photoreceptors causes mild intracellular accumulations and no degeneration, whereas $v100^{R755A}$ in mutant photoreceptors greatly exacerbates the null mutant phenotype.

2.4 DISCUSSION

In this paper we characterize an integrated dual function of V100, the neuron-specific V0 ATPase subunit a1 in *Drosophila*. The genetic dissection of two molecularly distinct functions of *v100* suggests one role of V100 in endosomal vesicle fusion, and a second role in acidification downstream of endosomal sorting. Our data support an acidification-independent function in promoting vesicle fusion with target membranes marked by specific Syntaxins that explains both V100's role in endosomes presented here as well as in synaptic vesicle exocytosis reported previously (Fig. 8A) (Hiesinger et al., 2005). Importantly, *v100* is only required in neurons after neuronal differentiation; general cellular functions that require essential endolysosomal trafficking are unaffected. We conclude that V100 provides a neuronal degradation mechanism whose loss leads to neurodegeneration.

2.4.1 Genetic Dissection of the Dual Function

We propose the following model based on V100's dual function (Fig. 8A and Suppl. Fig. 5): In the absence of V100, vesicles with heterogeneous cargo – either endocytosed or ER/Golgi-derived – fail to fuse with Syntaxin7-positive endosomes, resulting in intracellular accumulations (Suppl. Fig. 5F, G). Over time, many of these accumulations are engulfed by AVs. V100-dependent acidification is required, and possibly acts as a trigger, for the subsequent maturation and degradation of MVBs and AVs. Expression of $v100^{R755A}$ does not rescue acidification-dependent degradation in *v100* null mutant neurons, but promotes fusion of cargo vesicles with endosomes that thereby contain acidification-defective v-ATPases. In a wild type background, the

presence of wild type V100 provides some acidification for the degradation of cargo (Suppl. Fig. 5H), whereas in a mutant background this re-routing of cargo leads to dramatically increased MVB and AV formation (Suppl. Fig. 5I).

V0 and V1 sector assembly is thought to be a regulatory mechanism that initiates acidification (Marshansky and Futai, 2008; Nishi and Forgac, 2002). The reversible assembly of the V0/V1 holoenzyme provides an elegant mechanism for the integration of V100's dual function. V100 is the largest component of the V0 membrane complex and its N-terminus is potentially free to interact with Syntaxins when the two sectors are disassembled.

We have no evidence that the acidification function of *v100* is required for neurotransmitter release. In fact, neurotransmitter release in photoreceptors is the only phenotype that is rescued with the acidification-disrupted $V100^{R755A}$. In contrast, the neuron-specific endolysosomal trafficking defects described here can only be explained in the context of two distinct molecular functions. Notably, V100 is localized to both synaptic vesicles and endosomes, but not required for the acidification of either of these organelles (Fig. 8A). In addition, we have previously shown that *Drosophila* V100 can rescue a vesicle trafficking, but not an acidification defect of its ortholog *vph1* in yeast (Hiesinger et al., 2005). It is possible that a conserved acidification-independent function of *vph1* can be rescued in a trans-species experiment with *v100* in yeast, while the V0/V1-holoenzyme-dependent acidification function is not as easily rescued.

What is the mechanism of the acidification-independent function of V100? We report here that V100 specifically interacts with Syntaxins on membranes where its function is most consistent with the promotion of membrane fusion: synaptic vesicle fusion with presynaptic membranes marked by Syntaxin1A and endosomal fusion marked by Syntaxin7. These results suggest a novel role for V100 and its homologs in

targeting or increasing the fusion probability of vesicles marked with different compartment-specific subunit a1-a4 homologs and their respective target membranes. This function would be consistent with a role of V100 before or during SNARE-mediated membrane fusion.

2.4.2 A Neuronal 'Sort-and-Degrade' Mechanism

We show that *v100* is not required for the acidification of compartments in which cargo (e.g. pHluorin or Chaoptin) accumulates. The observation that selective rescue of an acidification-independent sorting function causes more accumulation than the null mutant alone implies that degradation in *v100* mutant neurons is only partly abolished. In other words, loss of *v100* does not affect at least one other v-ATPase (i.e. Bafilomycin-sensitive and a2-a4-dependent) degradation pathway. The presence of at least one other degradation pathway is further supported by the presence of a normal number of strongly acidified degradative (Lysotracker-positive) compartments in the mutant cells prior to neuronal differentiation. Together with the wild type expression data, our results indicate that *v100* only comes into play after a cell has adopted the neuronal cell fate. Finally, the idea that essential endolysosomal function is unaffected in *v100* mutant neurons is also supported by the observation that *v100* mutant neurons lack several hallmarks of general lysosomal degradation mutants, including accumulations of autofluorescent lipofuscin or ceroid (Futerman and van Meer, 2004). Together these data suggest that V100 is not required for all endolysosomal degradation in neurons. The *v100*-dependent mechanism need not be different from the essential endolysosomal pathway in any component other than *v100* itself; V100 promotes fusion with endosomes which it later acidifies for degradation. Taken together these data suggest that *sorting* and *degradation* are tightly balanced.

v100 is required only in neurons in *Drosophila* and is at least strongly enriched in the nervous system of all animals investigated for it. However, the temporally integrated mechanism of *'sort-and-degrade'* that we describe here could be more general. All a1-a4 homologs are highly conserved and acidification-independent roles in secretion have been suggested for a2 in *C. elegans* (Liegeois et al., 2006) and a3 in mouse (Sun-Wada et al., 2006). The zebra fish a1 ortholog has an acidification-independent function in phagosome-lysosome fusion in microglial cells (Peri and Nusslein-Volhard, 2008). Hence, it is possible that the mechanism we describe here for neurons may be employed by other cell types.

2.4.3 Neuronal Endolysosomal Trafficking, Autophagy and Neurodegeneration

Loss of *v100* leads to heterogeneous accumulations of endosomal compartments, MVBs as well as AVs. Autophagy intersects at many levels with the classical endolysosomal pathway: Fusion of AVs with lysosomes, multivesicular bodies and early endosomes are known to form amphisomal compartments and have been shown to be required for autophagic function (Eskelinen, 2005; Filimonenko et al., 2007; Razi et al., 2009). Numerous mutants in endolysosomal and autophagic pathways lead to late onset neurodegeneration (Futerman and van Meer, 2004; Hara et al., 2006; Komatsu et al., 2006). Conversely, induction of autophagy can alleviate neurodegenerative effects (Mizushima et al., 2008; Wang et al., 2009). Similarly, our findings are consistent with the idea that loss of degradation capacity sensitizes neurons to 'cargo overload'. In support of this idea, overexpression of human disease proteins (including Abeta and tau) exhibit significantly accelerated neurodegeneration in *v100* mutant photoreceptors (W.R.W. and P.R.H., unpublished observations). The recognition of a neuronal mechanism that operates in addition to essential degradation mechanisms may be an

important parameter to consider in neuronal diseases associated with undegraded protein accumulations.

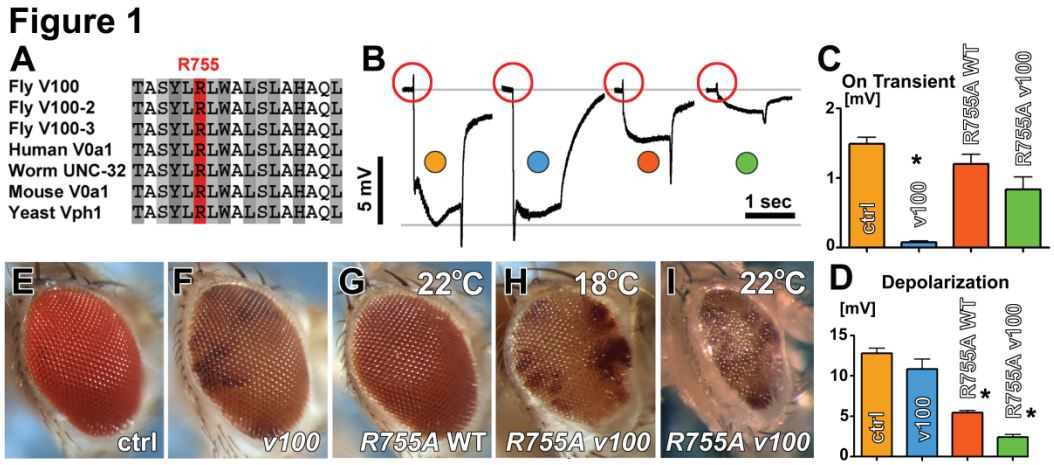

Figure 2.1: A v100 mutant that rescues neurotransmission but causes cell death at high levels

(A) Alignment of 17 amino acids surrounding the Arginine at position 755 (R755) shows 100% conservation across species. (B) Neurotransmitter release rescue experiments: Representative ERG traces from left to right: ctrl (yellow), *v100* null mutant (*ey*FLP eye mosaic, blue), $v100^{R755A}$ expression in wild type photoreceptors (red), and $v100^{R755A}$ expression in *v100* mutant photoreceptors (green). Note that rescue with $v100^{R755A}$ exhibits opposite phenotypes from the null mutant: rescue of the 'on' transient and a strong reduction of the response amplitude (depolarization). (C) Quantification of 'on' transients for all four genotypes. The asterisk denotes pairwise comparisons (all $p<0.001$). (D) Quantification of depolarization for all four genotypes. Asterisks denote pairwise comparisons: $v100^{R755A}$ in a wild type background (red) and $v100^{R755A}$ in a mutant background (green) compared to ctrl (orange) and mutant (blue) ($p<0.001$). (E-I) Eye pictures show dosage-dependent loss of photoreceptors upon $v100^{R755A}$ expression in the mutant (H, I), but not upon $v100^{R755A}$ expression in wild type (G).

Figure 2

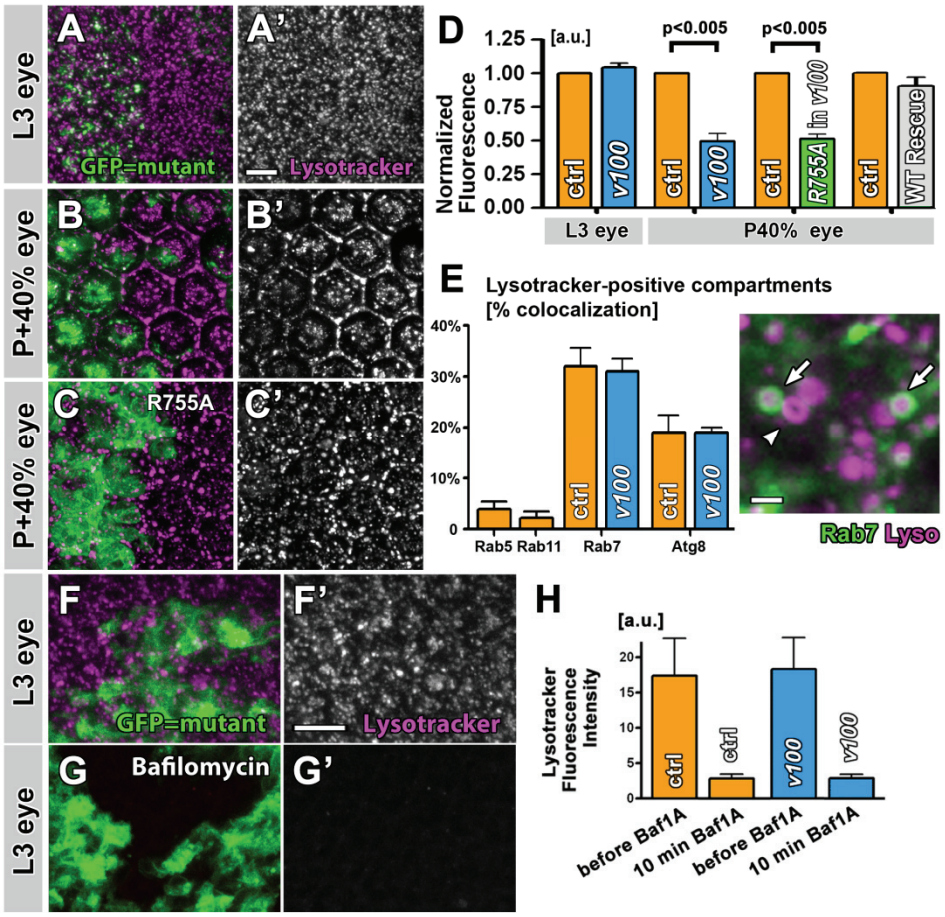

Figure 2.2: V100 is required for the acidification of a subset of neuronal degradative compartments

(A-C) Lysotracker live measurements in eye-brain cultures. (A, B) Representative scans of *v100* MARCM eye discs (mutant cells marked with GFP). (A', B') Only Lysotracker channel. (C) Live scan of a *v100* MARCM eye expressing $v100^{R755A}$ only in the mutant cells marked by GFP. (C') Only Lysotracker channel. (D) Quantification of Lysotracker data in (A-C) shows a significant reduction in Lysotracker signal after photoreceptor differentiation at P+40% (control in orange, mutant in blue). Expression of $v100^{R755A}$ in the mutant (green) does not rescue the Lysotracker signal reduction. Grey: expression of $v100^{WT}$ in mutant photoreceptors. (E) Identification of Lysotracker-positive compartments by live imaging using GFP-Rab5, GFP-Rab11, GFP-Rab7 and Atg8-GFP. Note that the ratio of Rab7/Lysotracker and Atg8/Lysotracker compartments is unaltered in the mutant despite the 50% Lysotracker reduction shown in (D). The inset shows Rab7-positive late endosomes that are filled with Lysotracker (arrows). The arrowhead shows a Rab7-negative, lysotracker-positive ring, presumably a lysosomal or autophagosomal structure. (F-H) Block of all v-ATPase-dependent acidification using Bafilomycin A1 in L3 larval eye discs with mutant *v100* MARCM clones marked by GFP. Scale bar in (A') for (A-C): 10µm; in (F') for (F-G): 10µm. Scale bar in D, inset): 1µm.

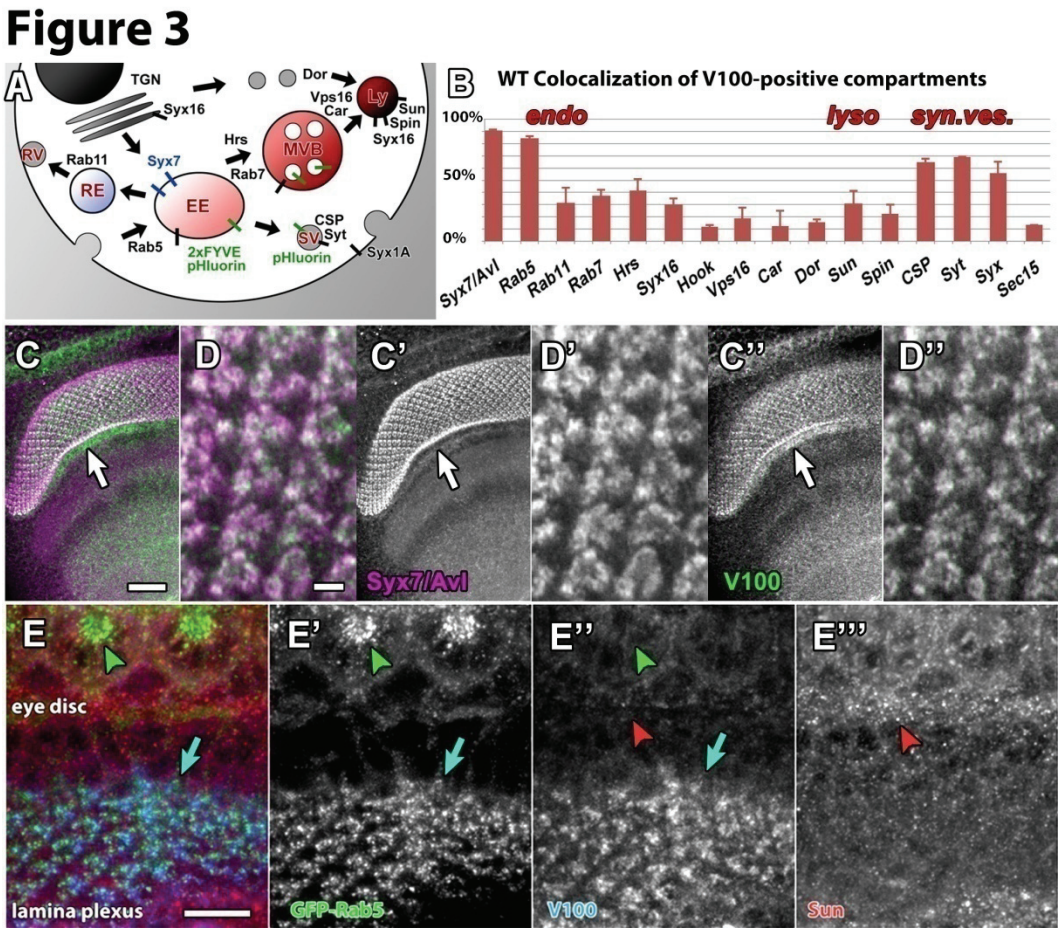

Figure 2.3: V100 is predominantly an early endosomal protein in addition to its localization to synaptic vesicles

(A) Schematic of intracellular localization of markers and compartments in wild type. (B) Wild type colocalization of 16 markers with V100 in developing photoreceptor terminals at ~P+25%. (C, D) Double-labeling of a developing optic lobe for Syx7/Avl (purple) and V100 (green). (D) High-resolution section of the developing lamina. (C'-D'') Single channels from (C, D). (E) Triple-labeling of a developing eye-brain section. Green: Photoreceptor-specific expression of Rab5-GFP; blue: V100; red: Sunglasses/CD63. Note that V100 and Rab5-GFP colocalize at the developing photoreceptor terminals (lamina plexus), whereas Rab5-GFP is also enriched at the developing rhabdomeres in the cell bodies (eye disc). In contrast, the lysosomal marker Sunglasses marks different compartments, mostly in the cell bodies (E'''). Arrows in (C) indicate increased labeling of the lamina, which is shown as higher resolution in (D). Blue arrows in (E) show colocalization of GFP-Rab5 and V100 at synapses; green arrowheads indicate absence of colocalization of GFP-Rab5 and V100 at the rhabdomeres; red arrowheads indicate absence of colocalization of Sun and V100. EE: early endosome; MVB: multivesicular body/late endosome; Ly: Lysosome; SV: synaptic vesicle; RE: recycling endosome; RV: recycling vesicle. Scale bars in (C): 10µm; in (D): 1µm; in (E): 5µm. Error bars are S.E.M.

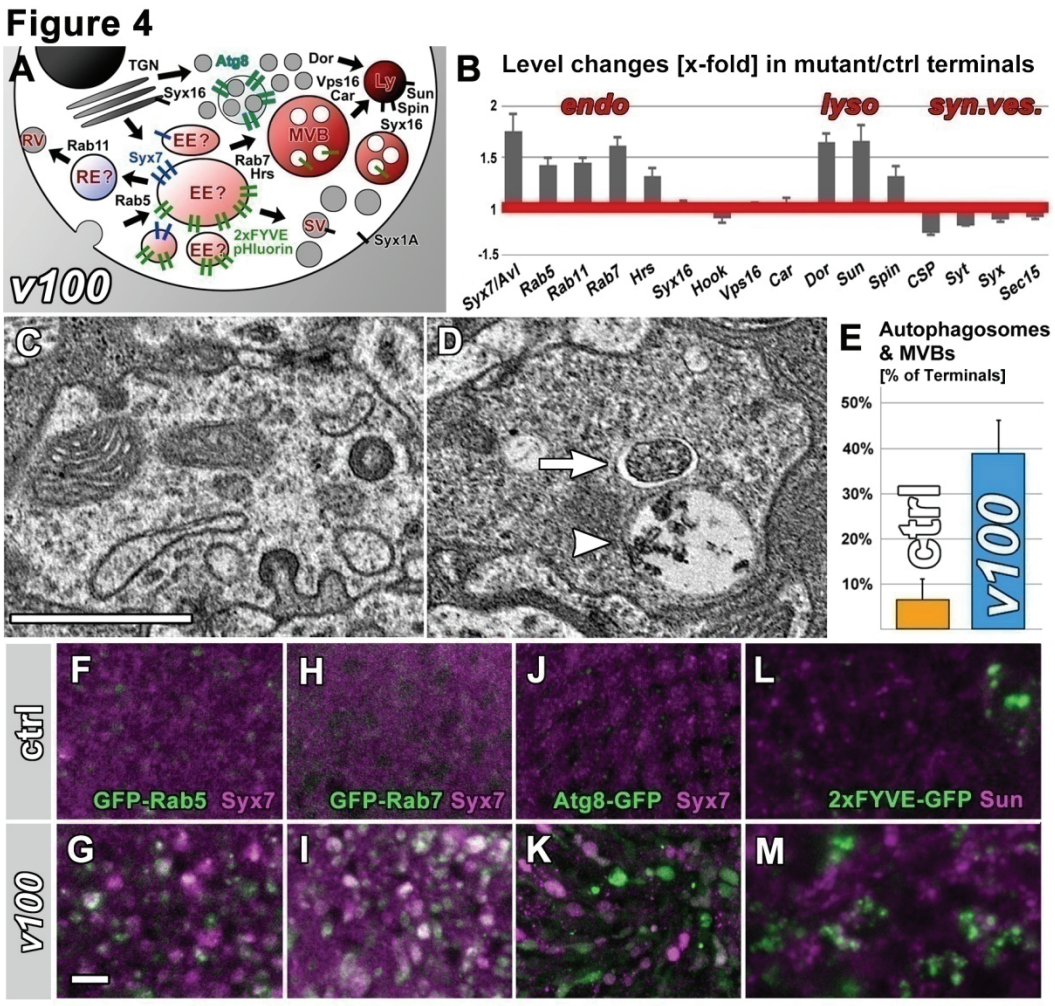

Figure 2.4: Loss of v100 causes endosomal and autophagic accumulations

(A) Schematic of heterogeneous intracellular accumulations in the *v100* mutant. (B) Ratio of expression levels in mutant photoreceptor terminals compared to wild type control in 50% mosaics. The red line represents unaltered levels. Note that numerous endosomal and lysosomal membrane markers are upregulated. (C, D) Representative transmission electron micrographs reveal aberrant multivesicular structures and autophagosomal vacuoles (MVBs, indicated by arrowhead and AVs, indicated by arrow) in *v100* mutant photoreceptor terminals. (E) Quantification of MVB-like (single membrane) and AV-like (double membrane) structures per photoreceptor terminals show a more than 5-fold increase in the mutant ($p<0.01$). (F-G) Co-immunolabeling of early endosomes using Syx7 and Rab5 reveals strong upregulation in mutant cells. (H-I) Co-immunolabeling of Syx7 and Rab7. (J, K) Co-labeling of autophagosomes using Atg8-GFP and anti-Syx7 labeling reveal both makers accumulating in mostly separate compartments. (L, M) Co-labeling of early endosomes using 2xFYVE-GFP and lysosomes using anti-Sunglasses reveals that both markers accumulate in mutually exclusive compartments. EE, MVB, Ly, CV, RE and RV as in Figure 3. Scale bar in (C) for (C-H): 5µm; in J for (J-O): 1µm. Error bars are S.E.M.

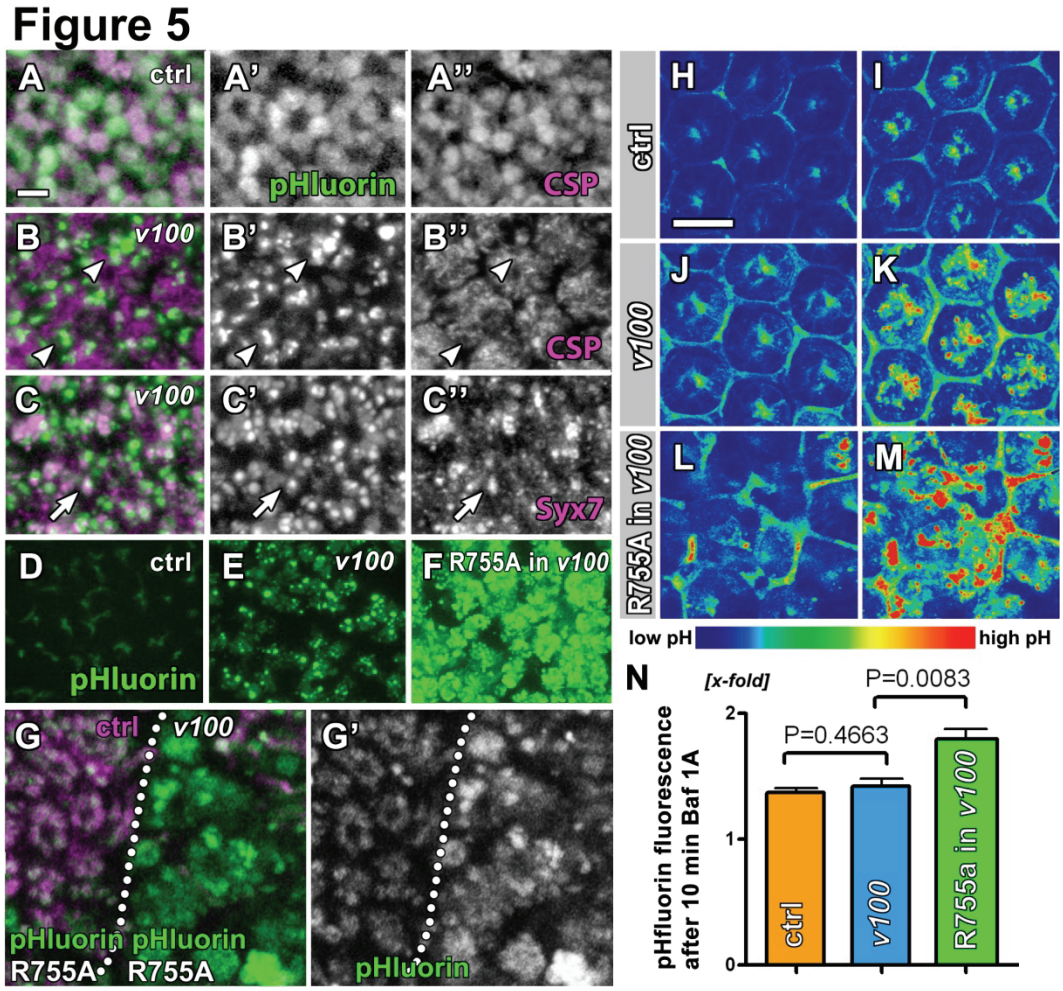

Figure 2.5: V100 exerts an acidification-independent function on early endosomes

(A-C) High-resolution section of wild type (A) and *v100* mutant (B, C) 1-day adult photoreceptor terminals expressing synapto-pHluorin (green) and immunolabeled for CSP or Syx7/Avl (magenta). Note that pHluorin forms accumulations that exclude CSP (arrowheads) but partially colocalize with Syx7 (arrows) in the mutant. (D-F) Levels of pHluorin accumulations in live adult photoreceptor terminals at equal pH for the genotypes indicated. (G) Negatively marked *v100* mutant clone (wild type terminals in magenta). Both mutant and control clone equally overexpress pHluorin and $v100^{R755A}$. Note that $v100^{R755A}$ expression only in the mutant terminals leads to pHluorin accumulations. The dotted line approximates the clonal boundary. (H-M) Live confocal scans of P+20% eye discs before and after 10 minutes incubation with the v-ATPase inhibitor Bafilomycin 1A. (H, I) Control before and after Bafilomycin treatment. (J, K) *v100* mutant before and after Bafilomycin. (L, M) *v100* mutant with $v100^{R755A}$ rescue. (N) Quantification of fluorescence increases after Bafilomycin treatment shows that pHluorin accumulates in compartments that are acidified in a v-ATPase-dependent manner. Scale bar in (H) for (H-M): 10µm.

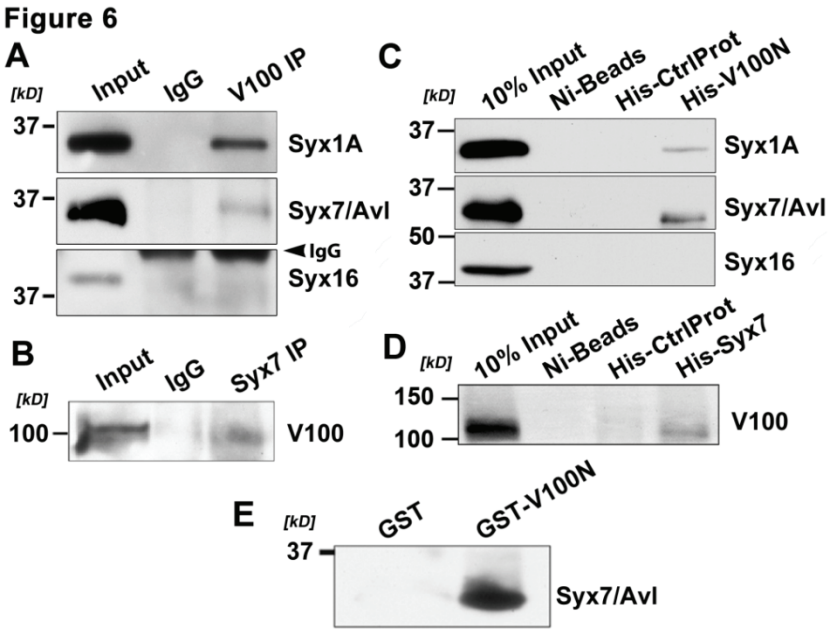

Figure 2.6: V100 interacts with the endosomal Syntaxin7/Avalanche, but not the Golgi/lysosomal Syntaxin16

(A) Immunoblots of co-immunoprecipitation with anti-V100 antibody from adult fly head extract, probed with antibodies against Syx1A, Syx7/Avl and Syx16. IgG: Analogous co-IPs using pre-immunserum instead of anti-V100 serum. (B) Co-immunoprecipitation with anti-Syx7/Avl antibody from adult fly head extract, probed with anti-V100. (C) Pull-down from adult fly head extract using bacterially made His-Syx7. As negative control (His-CtrlProt) we used a bacterially made His-fusion to a fly lipid enzyme (CG8630). Immunoblot probed with anti-V100. (D) Pull-down from adult fly head extract using bacterially made His-V100 N-terminus. Immunoblot probed with anti-Syx1A, anti-Syx7, and anti-Syx16. (E) GST-Pull-down of bacterially made His-Syx7 with bacterially made GST-V100 N-terminus.

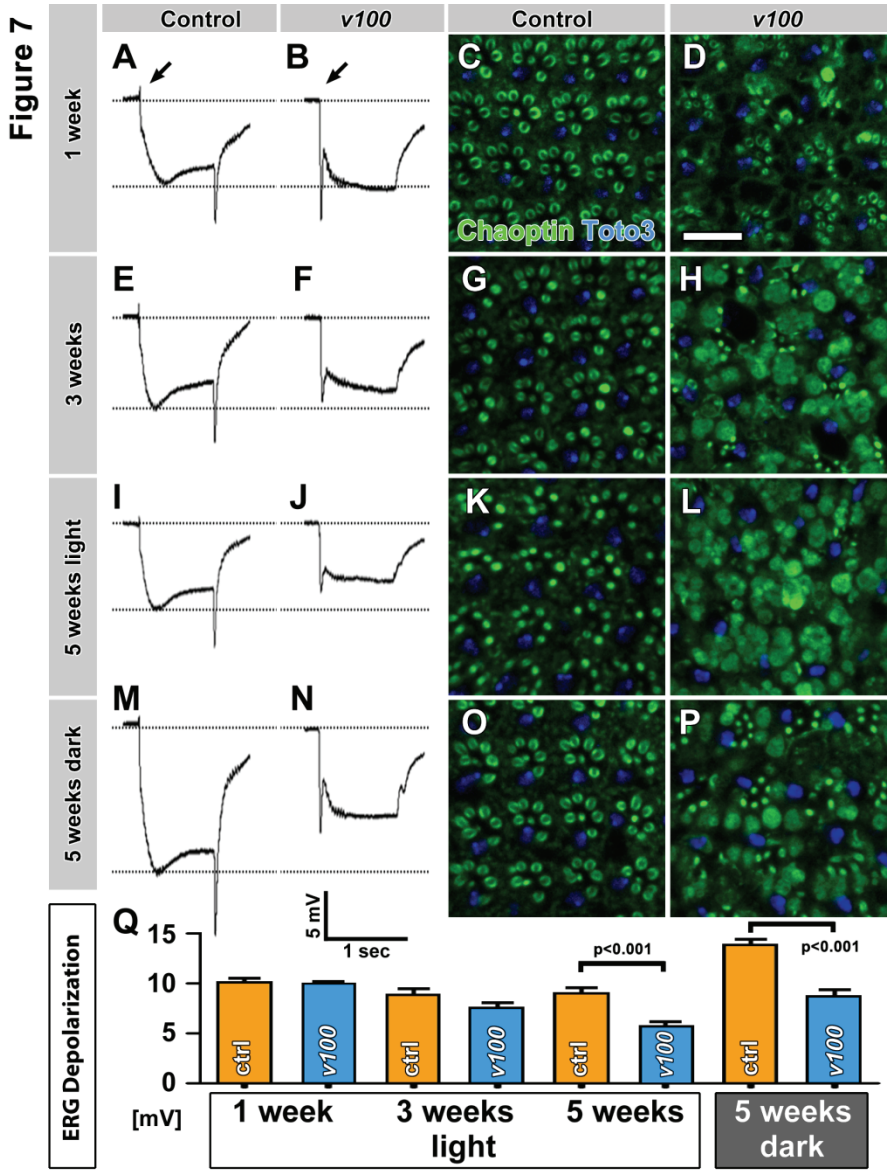

Figure 2.7: Loss of v100 causes slow, adult-onset neurodegeneration

(A, B) ERG recordings of 1-week old flies. Note that mutant ERGs lack the 'on' transient (arrows), but display normal depolarization. (C, D) Eyes from 1-week old wild type and *v100* mutant flies labeled with the photoreceptor-specific rhabdomere marker Chaoptin (green) and the nuclear marker Toto-3 (blue). (E, F) ERG recordings from 2-3 week old flies show a slight reduction in depolarization. (G, H) 2-3 week old wild type and *v100* mutant eyes. (I-L) ERGs and immunolabeling of 5 week-old wild type and mutant eyes reveal progressive degeneration. (M-P) ERG recordings and immunolabelings from 5 week-old flies kept in the dark show attenuated mutant phenotypes. (Q) Quantification for ERG depolarizations. Scale bar in (D) for (C-D, G-H, K-L, O-P): 10µm.

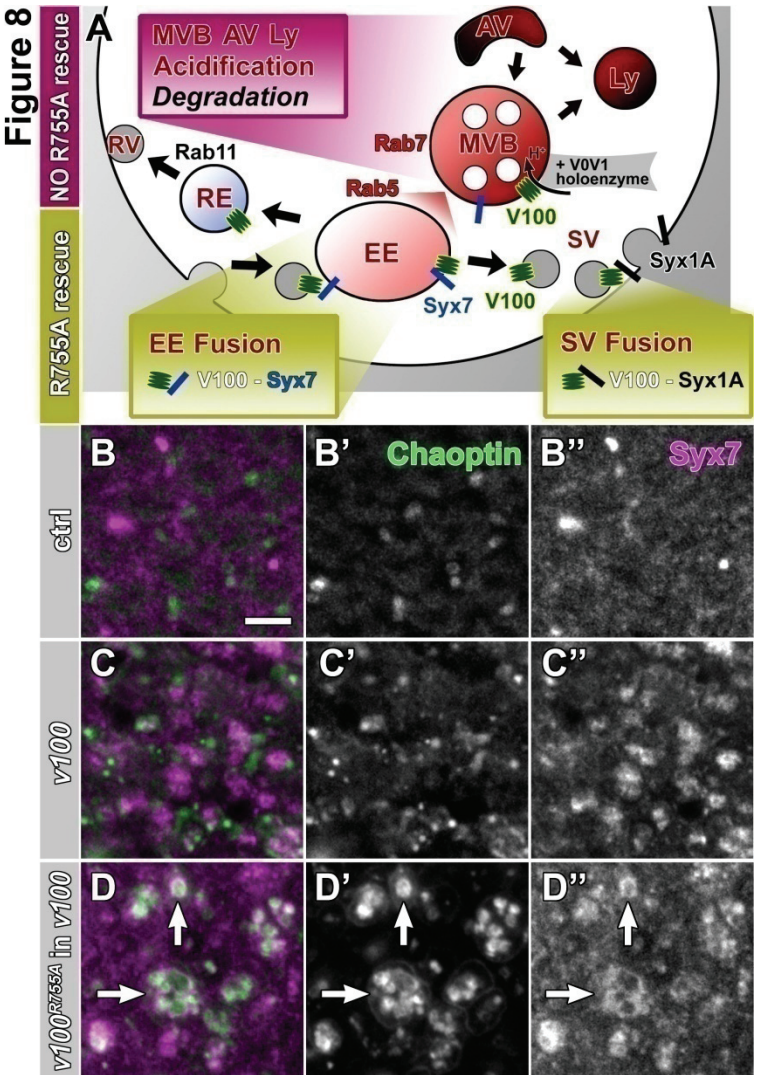

Figure 2.8: Selective rescue of the acidification-independent function accelerates degeneration by increasing accumulations in Syx7-positive, degradation-incompetent compartments

(A) Summary of V100 functions and *v100*^{R755A} rescue data. Our findings indicate two acidification-independent functions that are rescued by *v100*^{R755A}: synaptic vesicle (SV) fusion through Syx1A interaction and early endosomal (EE) fusion through Syx7 interaction. In contrast, V100 has a function as part of the V0/V1 holoenzyme once endosomes mature into degradative compartments that is not rescued by *v100*^{R755A}. Consequently, selective rescue of the acidification-independent function leads to increased accumulations in Syx7-positive, degradation-incompetent compartments. (B-D) 1-day adult photoreceptor terminals for control (B), *v100* null mutant (C) and *v100*^{R755A} rescue in the *v100* mutant. (B'-D') Chaoptin alone (green channel). (B''-D'') Syx7 alone (magenta channel). In the *v100*^{R755A} rescue most Chaoptin accumulates in large, Syx7-encircled MVB-like structures (arrows). RE: recycling endosome; RV: recycling vesicle. Scale bar in (B) for (B-D): 5µm.

2.6 CHAPTER TWO SUPPLEMENTAL FIGURES

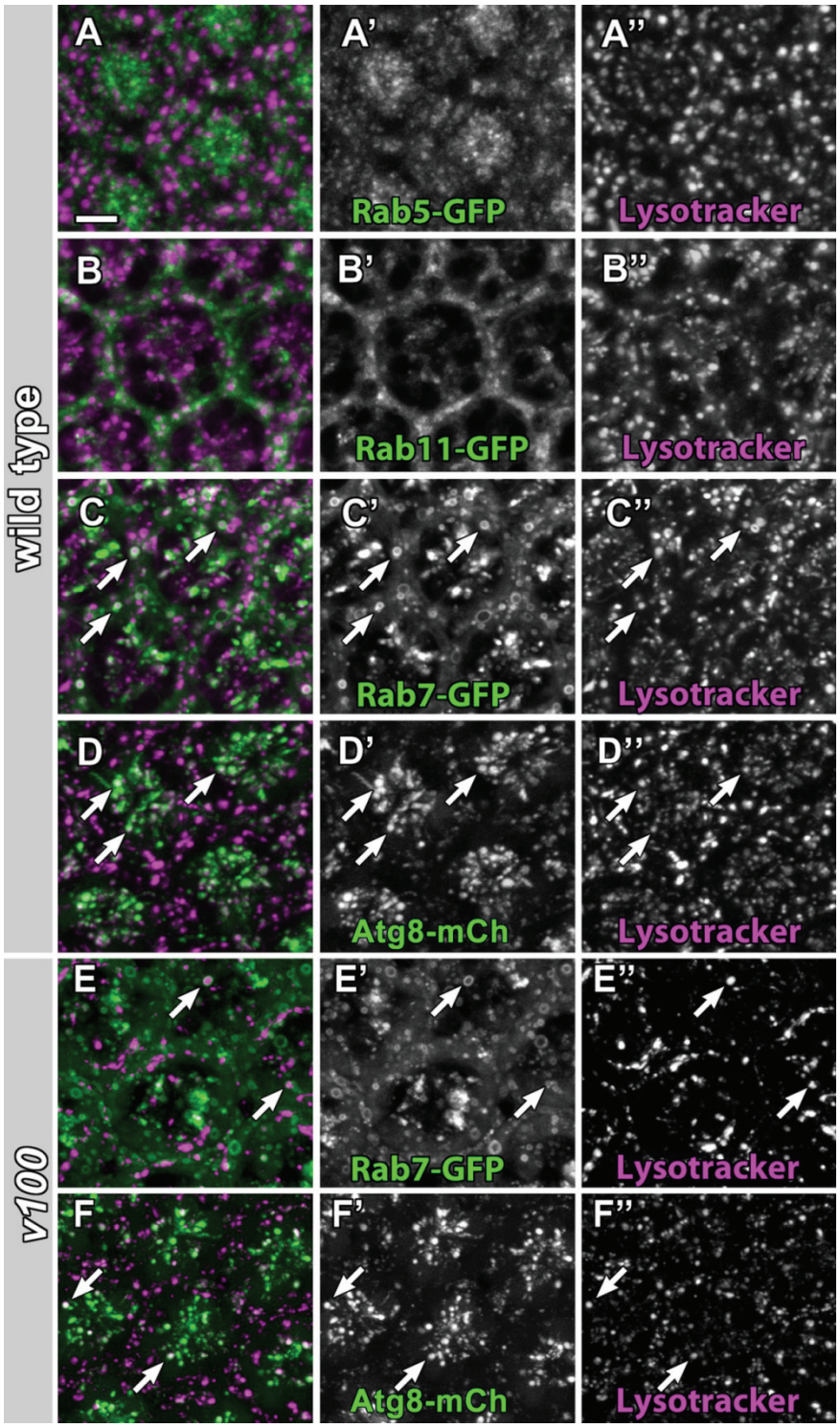

Figure S2.1: Lysotracker labels late endosomal and autophagosomal compartments that are acidified in a v-ATPase-dependent manner.

(A–C’’) Live confocal scans of P + 20% eye discs expressing Rab7-GFP (A), Rab5-GFP (B), or Rab11-GFP (C) labeled with Lysotracker red. (D–D’’) Live confocal scan of P + 20% eye disc expressing Atg8-mCherry labeled with Lysotracker green. (E–F’’) L3 larval eye discs with mutant *v100* MARCM clones marked by GFP. Note that in larval eye discs, mutant cells do not yet exhibit a Lysotracker defect, but 10 min bafilomycin 1A treatment leads to a loss of Lysotracker signal. Arrows show colocalization. Bar, 5 μm.

Suppl. Fig. 2

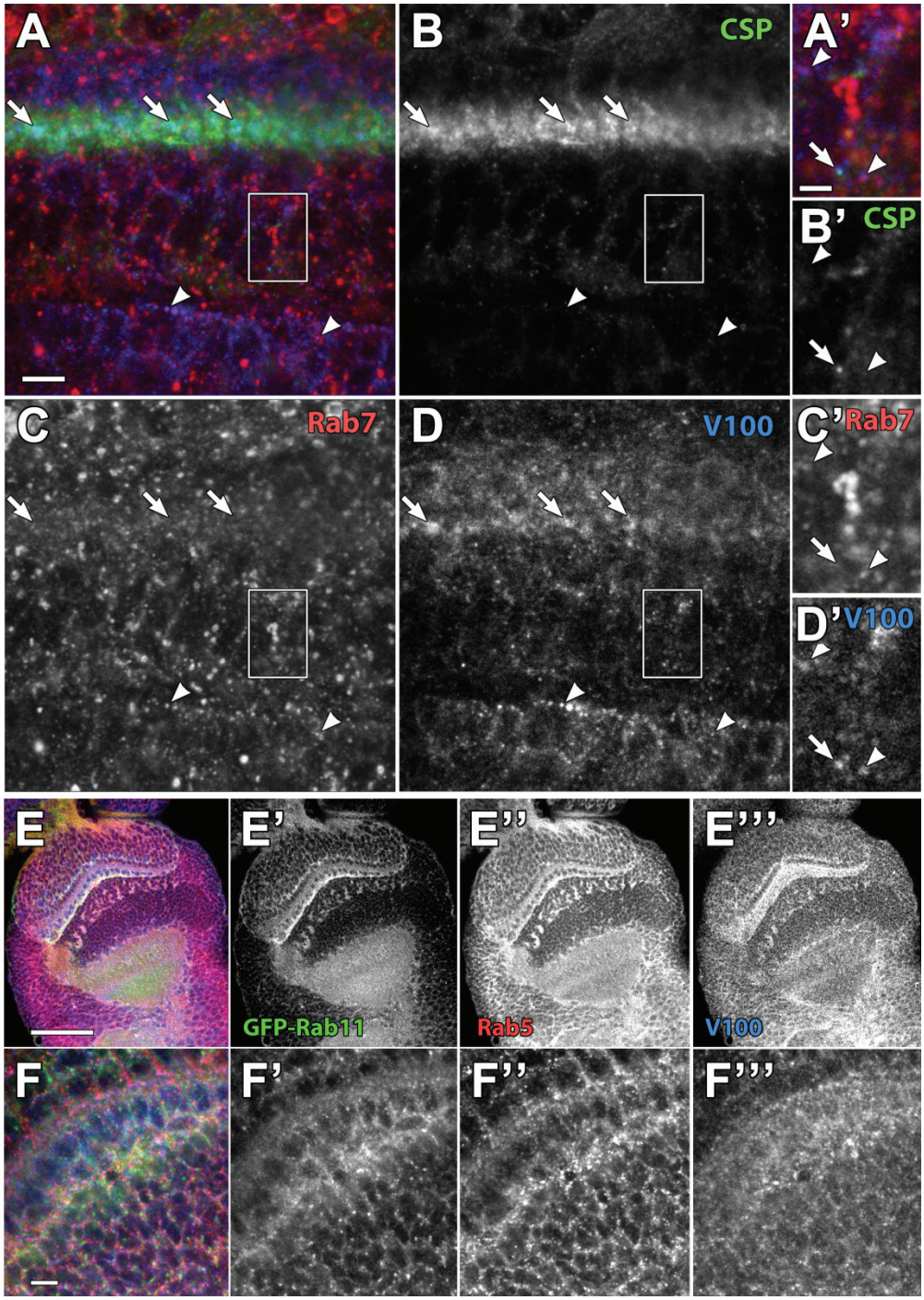
A
B
CSP
A'
B' CSP
C
Rab7
D
V100
C' Rab7
D' V100
E
E'
E''
E'''
GFP-Rab11
Rab5
V100
F
F'
F''
F'''

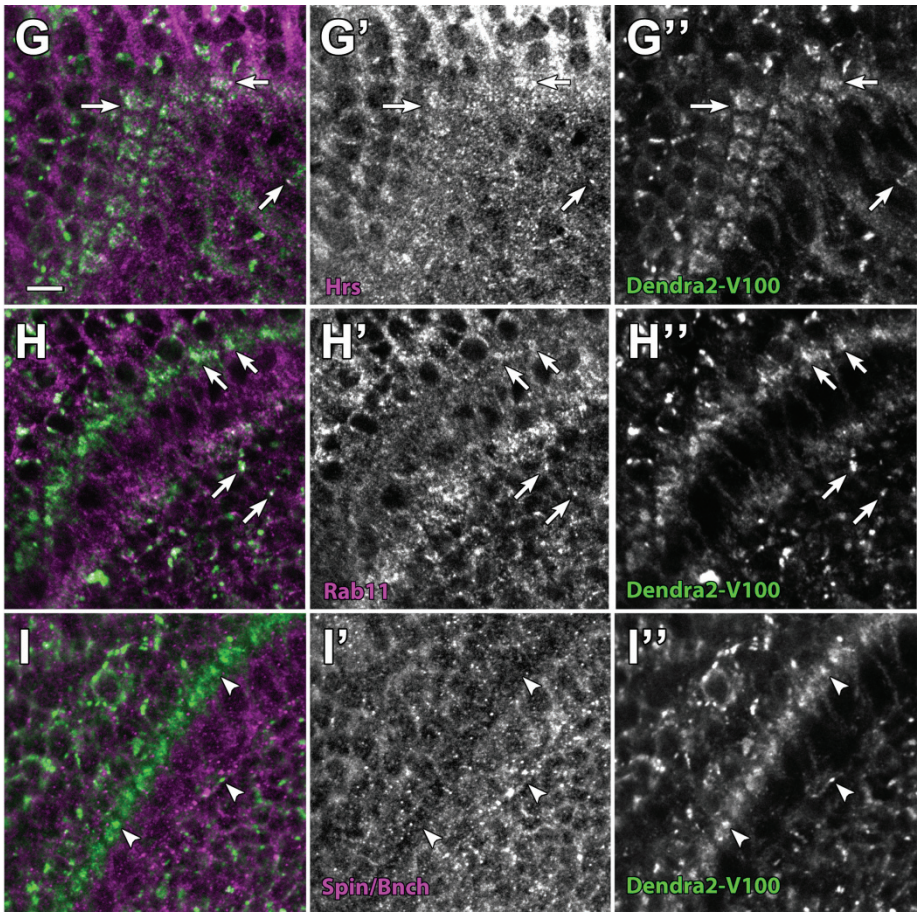

Figure S2.2: High-resolution 3D colocalization studies of intracellular compartment marker colocalization. V100 colocalizes with endosomal markers, but not the lysosomal protein Spin/Bnch.

(A–D) V100 colocalizes with endosomal markers but not the lysosomal protein Spin/Bnch. Confocal section from a 3D dataset of the P30% developing optic lobe immunolabeled for the synaptic vesicle marker CSP (green), the late endosomal marker Rab7 (red), and V100 (blue). CSP most prominently labels the developing synapses of the lamina but also small punctae in the surrounding cell bodies (e.g., boxed region). Arrows show colocalization of CSP with V100, and arrowheads show colocalization of Rab7 with V100. (A'–D') Boxed regions in A–D are shown at higher magnification. Except for the dense developing lamina region, individual intracellular compartments are clearly discernible. (E–F''') P + 5% developing brain hemispheres pan-neuronally expressing GFP-Rab11 colabeled with anti-Rab5 and anti-V100 antibodies show similar localization patterns at low (E) and high resolution (F). (G–I') Pan-neuronal expression of fluorescently (Dendra2) tagged V100 was used for colocalization experiments with antibodies raised in guinea pig and that therefore cannot be used together with guinea pig anti-V100. Although the endosomal markers Hrs and Rab11 exhibit partial colocalization with Dendra2-V100 (C and D), the lysosomal marker Spin/Bnch does not colocalize with V100 (I). Arrows mark colocalization, and arrowheads mark absence of colocalization. Bars: (A and G) 5 μm; (A') 2 μm; (E) 50 μm.

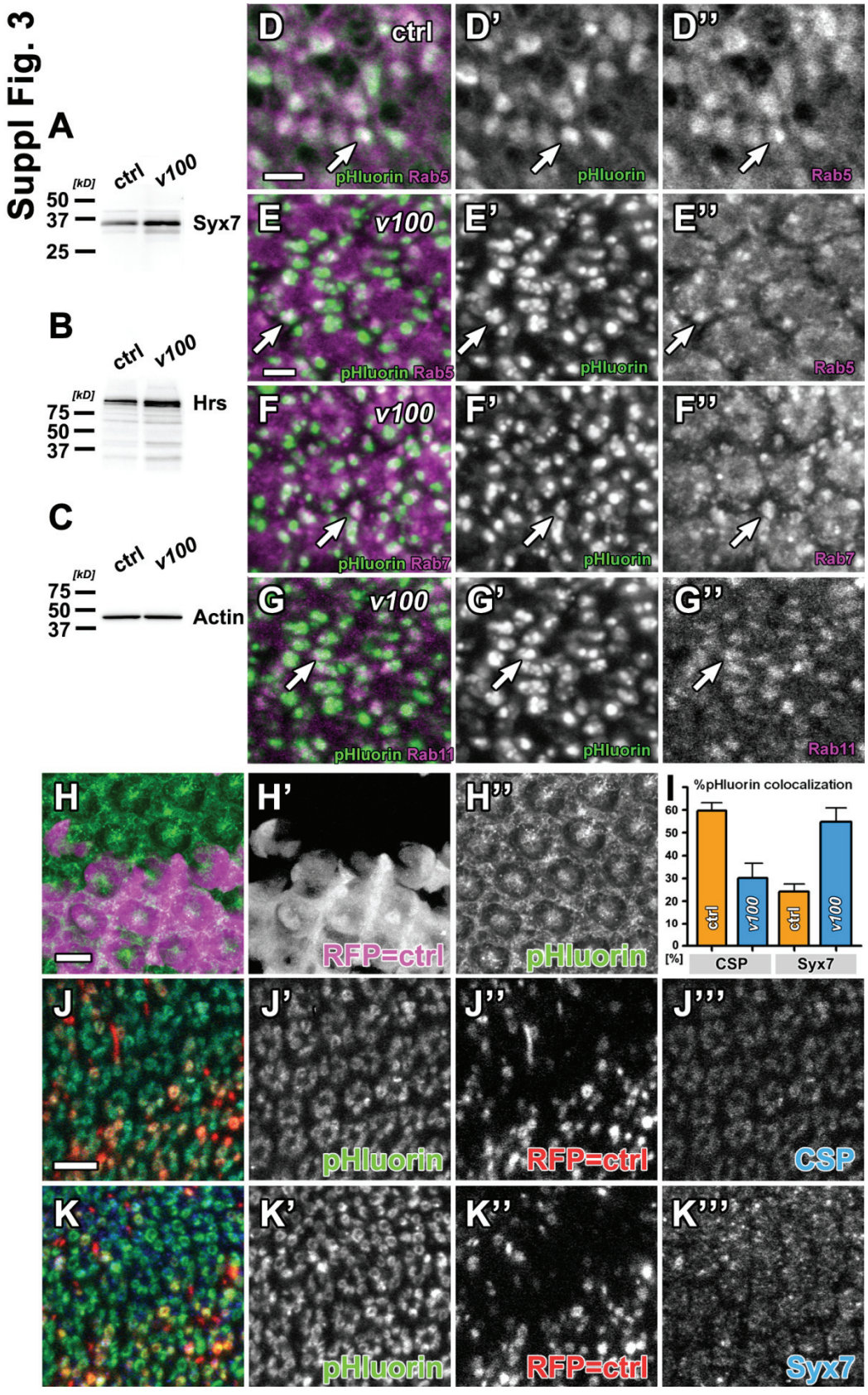
Suppl Fig. 3
A
[kD]
ctrl
v100
50
37
25
Syx7
B
ctrl
v100
[kD]
75
50
37
Hrs
C
ctrl
v100
[kD]
75
50
37
Actin
D
ctrl
pHluorin Rab5
D'
pHluorin
D''
Rab5
E
v100
pHluorin Rab5
E'
pHluorin
E''
Rab5
F
v100
pHluorin Rab7
F'
pHluorin
F''
Rab7
G
v100
pHluorin Rab11
G'
pHluorin
G''
Rab11
H
H'
RFP=ctrl
H''
pHluorin
%pHluorin colocalization
60
50
40
30
20
10
0
[%]
ctrl
v100
ctrl
v100
CSP
Syx7
J
J'
pHluorin
J''
RFP=ctrl
J'''
CSP
K
K'
pHluorin
K''
RFP=ctrl
K'''
Syx7

Figure S2.3: Endosomal defects: The endosomal proteins Syx7 and Hrs exhibit elevated protein levels in v100 mutant eye-lamina complexes and Synapto-pHluorin accumulates in endosomal compartments.

(A–C) Western blot analysis of *ey*FLP *v100* mutant 2-d-old eye–lamina complexes probed for Syx7 (A), Hrs (B), and actin (C). (D–D') Expression of pHluorin in WT photoreceptors shows partial colocalization with Rab5 at adult terminals. (E–G') In *v100* mutant photoreceptor terminals, pHluorin accumulates in more distinct compartments that partially colocalize with Rab5 (E), Rab7 (F), or Rab11 (G). (H–K) Expression of WT *v100* in *v100* mutant photoreceptors rescues pHluorin localization to synaptic vesicles. (H) P + 30% developing mosaic eye with *v100* mutant cells marked by absence of RFP. All cells express $v100^{WT}$ and pHluorin. Note that pHluorin localization is identical across clonal boundaries. (I) Quantification of J–K' is shown. Error bars indicate SEM. (J–K') Adult photoreceptor terminals in the lamina labeled with CSP (J) or Syx7 (K). As in H, *v100* mutant photoreceptors are marked by the absence of RFP, and both the rescuing *v100WT* and pHluorin are expressed in all cells. ctrl, control. Arrows indicate colocalization. Bars: (D and E): 2 μm; (H and J) 10 μm.

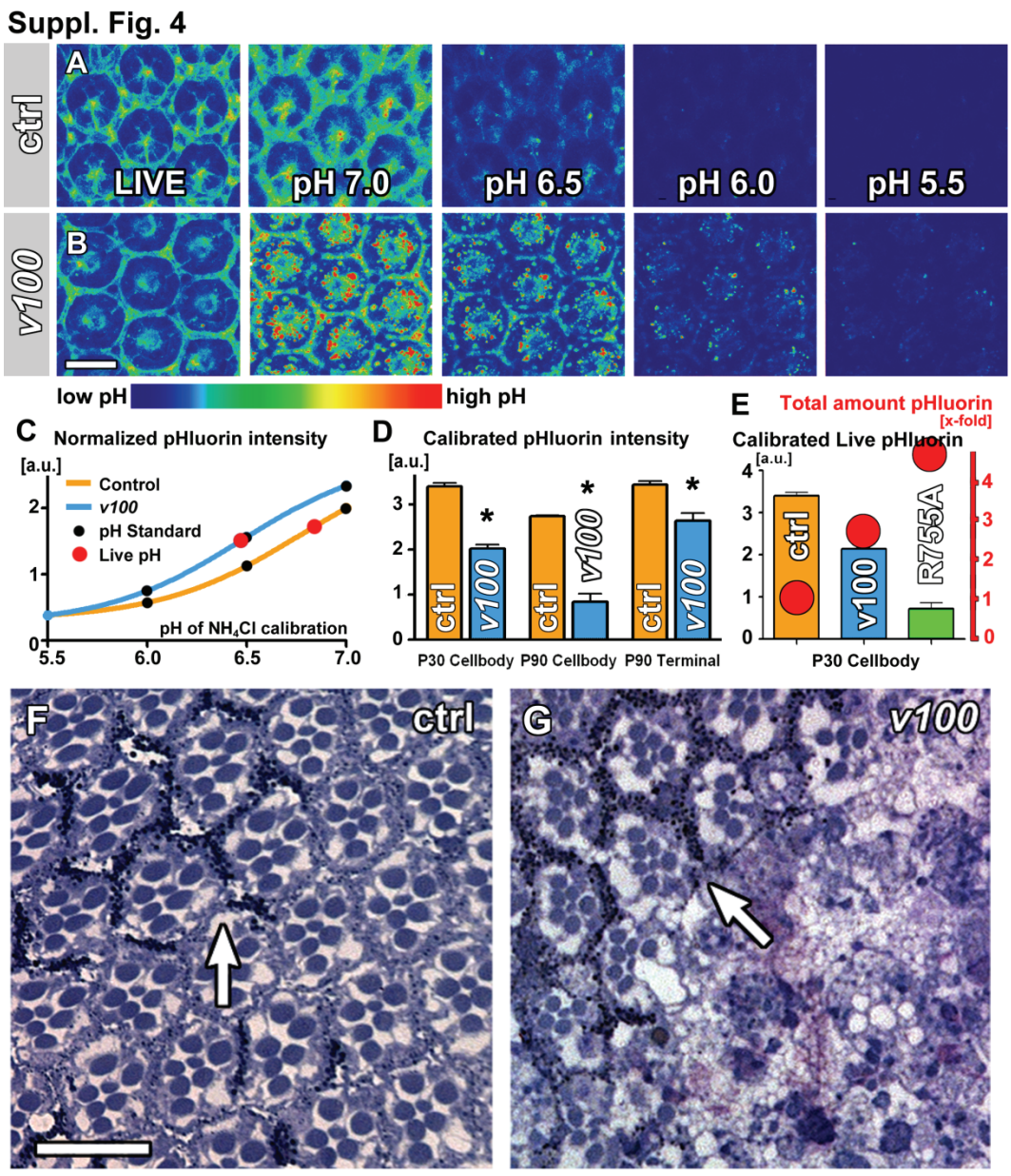

Figure S2.4: Eye defects: Calibrated NH_4Cl washes reveal pHluorin accumulations in acidified endosomes. 5-week old v100 mutant eyes display almost complete loss of discernible structure.

(A and B) Representative live scans of pHluorin fluorescence measurements. (C) Calibration curves were established for individual preparations by successive NH4Cl washes at decreasing pH (see Materials and methods). (D) Overall quantification of 22 pH measurements based on calibrated pHluorin fluorescence in live and *v100* mutant photoreceptor cell bodies at P + 30% and P + 90% as well as synaptic terminals at P + 90%. Asterisks indicate $P < 0.05$. (E) pHluorin measurement at photoreceptor terminals (P + 90%). Colored bars show calibrated live pH measurements that reveal increasing

amounts of pHluorin (red circles; quantification of data shown in Fig. 5, D–F) accumulate in acidified compartments in *v100*-null mutant and $v100^{R755A}$ rescue. (F) Plastic section of a 5-wk-old mosaic eye for a WT chromosome (*ey*FLP). The pigmented area (arrow) is heterozygous. The rhabdomere structure and overall morphology are intact in both heterozygous and homozygous eye tissue. (G) Section of a 5-wk-old *ey*FLP *v100* mosaic eye. Again, a small pigmented heterozygous area is shown in the top left corner (arrow). The homozygous mutant eye tissue exhibits almost complete loss of discernible structure. Ctrl, control. Error bars indicate SEM. Bars, 10 µm.

Suppl. Fig. 5

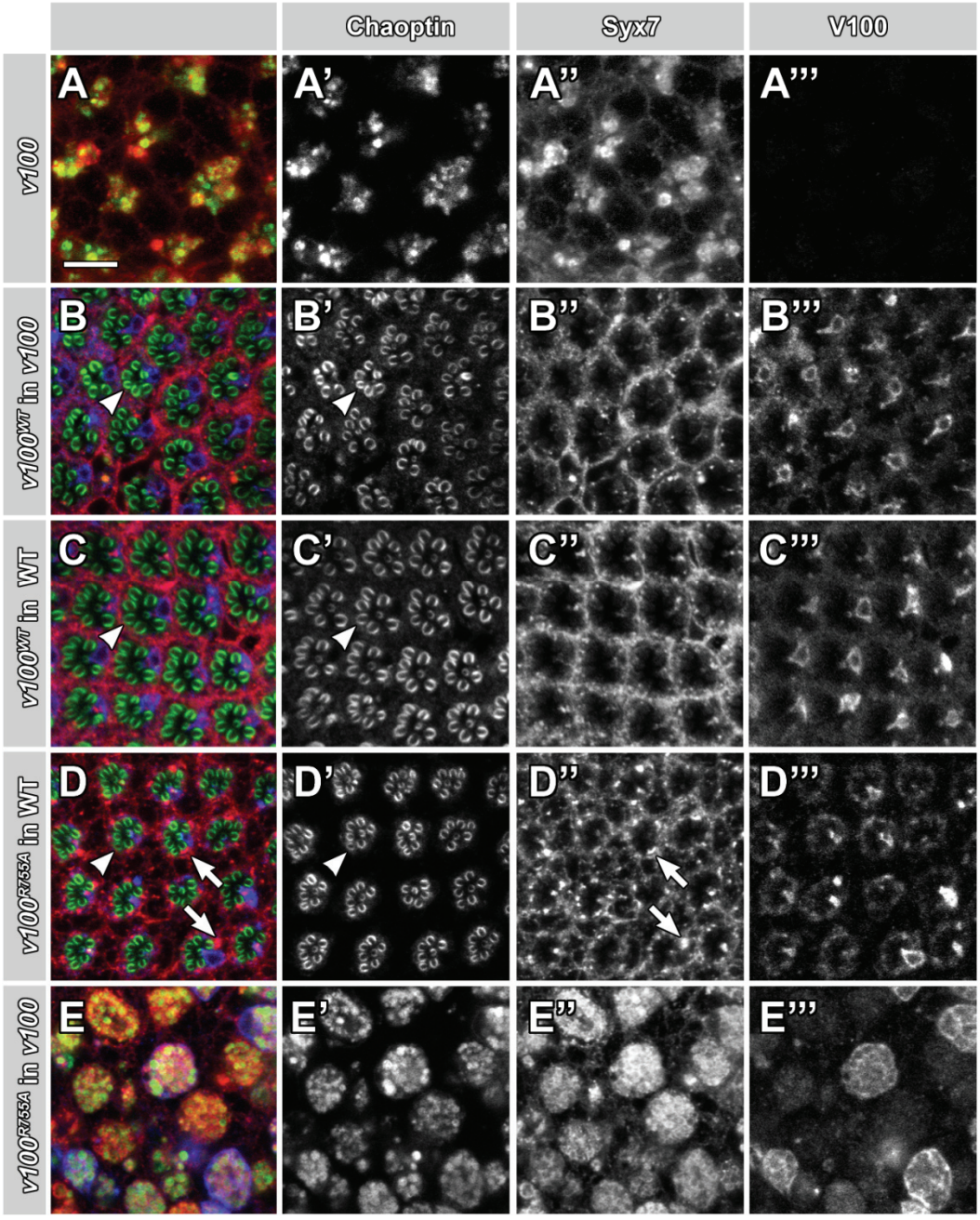
Chaoptin
Syx7
V100
v100
v100WT in v100
v100WT in WT
v100R755A in WT
v100R755A in v100
A
A'
A''
A'''
B
B'
B''
B'''
C
C'
C''
C'''
D
D'
D''
D'''
E
E'
E''
E'''

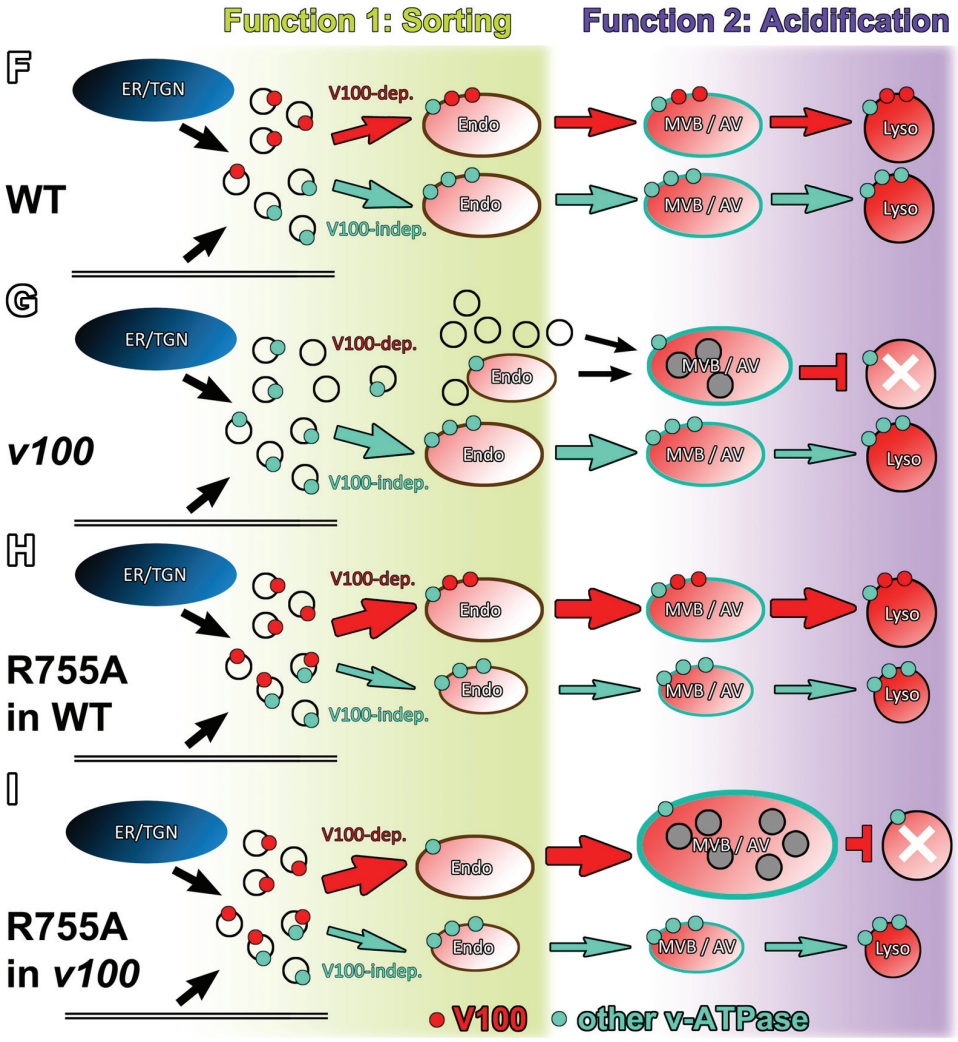

Figure S2.5: $V100^{R755A}$ expression causes a dominant defect that is different from the null mutant.

Confocal eye sections from 2-wk-old flies immunolabeled with anti-chaoptin (green), anti-Syx7 (red), and anti-V100 (blue) are shown. (A–A’’’) *v100* mutant eyes exhibit a loss of rhabdomeric structure and chaoptin as well as Syx7 accumulations that are partly overlapping. (B–B’’’) Expression of $v100^{WT}$ in mutant photoreceptors rescues this phenotype and restores the rhabdomere structure (arrowheads). (C–C’’’) Overexpression of $v100^{WT}$ in WT photoreceptors causes no obvious defects (arrowheads show rhabdomere structure). (D–D’’’) Overexpression of $v100^{R755A}$ in WT photoreceptors causes some accumulations of Syx7 at the rhabdomere base (arrows), but does not cause chaoptin accumulations and does not affect rhabdomere structure (arrowheads). (E–E’’’) Overexpression of $v100^{R755A}$ in *v100* mutant photoreceptors causes huge accumulations of all markers. Note that this section is at the same scale as the mutant in A. (F) V100-dependent (red) and -independent (turquoise) endolysosomal pathways that receive vesicles from the ER/TGN and/or the plasma membrane are depicted. Shades of red

indicate increasing acidification along the degradation pathways. (G) In the *v100* mutant, a heterogeneous population of vesicles accumulates in degradation-incompetent MVBs and AVs. A V100-independent lysosomal pathway must exist (turquoise pathway) because lysosomal degradation still occurs, as indicated by (1) a normal number of Lysotracker-positive and bafilomycin-sensitive degradative compartments before neuronal differentiation, (2) the absence of classical lysosomal degradation phenotypes like accumulations of lipofuscin, and (3) the observation that expression of an acidification-defective V100 leads to substantially larger amounts of membrane proteins that fail to degrade. This is because, as shown in I, $V100^{R775A}$ still functions in sorting vesicles into a V100-dependent pathway, where V100-dependent acidification does not occur. This leads to dramatically increased MVB and AV accumulations selectively in a *v100* mutant background. In contrast, as shown in H, $V100^{R775A}$ expression in WT neurons rescues vesicle sorting into thereby V100-containing endosomes but does not lead to dramatic accumulations because WT V100 is still present to provide acidification required for degradation. Bar, 10 μm.

CHAPTER THREE

Guidance receptor degradation is required for neuronal connectivity in the *Drosophila* nervous system

Previously published in: **Williamson, W.R.**, Yang, T., Terman, J., and Hiesinger, P.R. (2010). Guidance Receptor degradation is required for neuronal connectivity in the *Drosophila* nervous system. PLoS Biology 8(12): e1000553.

3.1 ABSTRACT

Axon pathfinding and synapse formation rely on precise spatiotemporal localization of guidance receptors. However, little is known about the neuron-specific intracellular trafficking mechanisms that underlie the sorting and activity of these receptors. Here we show that loss of the neuron-specific v-ATPase subunit a1 leads to progressive endosomal guidance receptor accumulations after neuronal differentiation. In the embryo and in adult photoreceptors, these accumulations occur after axon pathfinding and synapse formation is complete. In contrast, receptor missorting occurs sufficiently early in neurons of the adult central nervous system to cause connectivity defects. An increase of guidance receptors, but not of membrane proteins without signaling function, causes specific gain-of-function phenotypes. A point mutant that promotes sorting but prevents degradation reveals spatiotemporally specific guidance receptor turnover and accelerates developmental defects in photoreceptors and embryonic motorneurons. Our findings indicate that a neuron-specific endolysosomal degradation mechanism is part of the cell biological machinery that regulates guidance receptor turnover and signaling.

3.2 INTRODUCTION

Axon guidance, target selection and synapse formation determine the neuronal connectivity of the brain and rely on the spatially and temporally controlled localization of guidance receptors (Chen and Cheng, 2009; Dickson, 2002). The dynamic localization of these receptors is at least partly regulated at the level of vesicular membrane trafficking through the secretory pathway, endosomal recycling, and endolysosomal degradation (O'Donnell et al., 2009; Sann et al., 2009). Endosomal routing is also a means of receptor activation and inactivation: receptors may signal from the plasma membrane or endosomal compartments, and receptor signaling can be turned off by endolysosomal degradation (O'Donnell et al., 2009; Seto et al., 2002). A growth cone may reuse a number of guidance receptors through cycles of endo- and exocytosis. Alternatively, constitutive synthesis and degradation may provide a constant stream of receptors that can be sorted to exert spatiotemporally defined roles. However, for most cell types it is unknown which mode of receptor trafficking prevails to regulate receptor (de-) activation during development and function. Similarly, surprisingly little is known about the neuron-specific molecular mechanisms that underlie guidance receptor trafficking for either strategy during brain wiring.

The *Drosophila* nervous system has proven to be a powerful system for the characterization of the molecules that guide axons along their pathways and enable correct target selection (Araujo and Tear, 2003; Broadie et al., 1993; Mast et al., 2006; Ting and Lee, 2007). The visual system has been particularly useful, because both photoreceptors and visual interneurons are dispensible for viability and are easily genetically manipulated in otherwise wild type flies. Genetic screens based on methods that generate mutant visual neurons in heterozygous flies led to the discovery of

numerous important secreted and membrane-associated guidance molecules and receptors, their regulators and signal transducing proteins (Clandinin et al., 2001; Lee et al., 2001; Stowers and Schwarz, 1999). Amongst the many known guidance molecules and receptors implicated in visual system development are the cadherins N-Cadherin and Flamingo (Lee et al., 2001; Lee et al., 2003; Senti et al., 2003), the tyrosine phosphatases PTP69D and Dlar (Clandinin et al., 2001; Garrity et al., 1999; Maurel-Zaffran et al., 2001), and the immunoglobulin superfamily cell adhesion molecules Fasciclin II and Roughest (Kaphingst and Kunes, 1994; Lin et al., 1994; Schneider et al., 1995). Although spatiotemporally dynamic expression has been shown for most of these receptors, almost nothing is known about their intracellular trafficking, activation, turnover and degradation.

Genetic mosaic screens in the *Drosophila* visual system have also led to the discovery of numerous mutants with membrane and organelle trafficking defects (Hiesinger et al., 2006; Stowers et al., 2002; Verstreken et al., 2003). The *Drosophila* gene *v100* was originally identified in a screen for mutants that affect synapse formation, specification or function (Hiesinger et al., 2005; Hiesinger et al., 2006). *v100* encodes subunit a1 of the V0 complex, the membrane-bound sector of the two-sector vesicular (v-) ATPase (Marshansky and Futai, 2008; Nishi and Forgac, 2002). V100 is a neuron-specific subunit of the v-ATPase that is required for neurotransmitter release (Hiesinger et al., 2005) and provides a neuronal degradation mechanism in photoreceptors. This degradation mechanism is created by a dual function: V100 sorts vesicles into endosomal compartments and subsequently acidifies degradative compartments as part of the v-ATPase holoenzyme. Loss of *v100*-dependent degradation leads to adult-onset degeneration, but no developmental or synaptic specification defects in photoreceptors

(Williamson et al., 2010b). Similarly, *v100* mutant embryos exhibit normal nervous system morphology (Hiesinger et al., 2005).

In this study, we report that a neuron-specific, *v100*-dependent membrane sorting and degradation mechanism is required for brain wiring in *Drosophila*. Loss of *v100* results in missorting and intracellular accumulation of guidance receptors at the time and place where they are subject to active turnover. These accumulations precede axon mistargeting. We further show that guidance receptors aggregate on endolysosomal compartments and cause exacerbated gain-of-function phenotypes in *v100* mutant photoreceptors as well as in the embryonic nervous system. Our findings show that *v100* reveals spatiotemporally regulated receptor trafficking and turnover during neuronal development. Specifically, our findings reveal that continuous receptor turnover and degradation by a neuron-specific mechanism is a general mode of guidance receptor trafficking. Our data suggest that a *v100*-dependent neuronal degradation mechanism underlies a regulatory strategy that depends on a constant turnover of receptors that can be sorted to exert spatiotemporally defined roles.

3.3 RESULTS

3.3.1 V100 is required for neuronal connectivity in the developing adult central nervous system, but not in photoreceptors or any embryonic or larval neurons

Several genetic mosaic methods have been developed that render visual system neurons homozygous mutant in heterozygous flies (Chotard et al., 2005; Newsome et al., 2000; Stowers and Schwarz, 1999). In our previous studies of *v100* function in photoreceptors, we used the '*ey3.5Flp*' system developed by Salecker and colleagues, which renders only photoreceptors mutant (Chotard et al., 2005; Mehta et al., 2005). Our studies on *v100* in photoreceptors uncovered defects in neurotransmission (Hiesinger et al., 2005) and neurodegeneration (Williamson et al., 2010b), but no developmental defects. In contrast to this photoreceptor-specific method, the original *eyFLP* system (Newsome et al., 2000) generates thousands of homozygous mutant neurons in the central nervous system (CNS) in addition to photoreceptors. Importantly, *eyFLP* only affects CNS neurons of the visual and olfactory systems that are not required for viability of the organism under laboratory conditions and thereby allows the investigation of *v100* mutant central brain neurons in a living fly (Suppl. Fig. 1) (Mehta et al., 2005). Surprisingly, we found severe axon pathfinding and targeting defects in these *eyFLP v100* brains that were not present in our previous experiments when only photoreceptors were mutant (Fig. 1A-D). Further analysis of the *eyFLP v100* brain with the active zone marker Brp (nc82) revealed severe structural defects in the arrangement of synaptic neuropils resulting from defective axon pathfinding during pupal development prior to synaptogenesis (Fig. 1E-F). For clarity we will hereafter refer to the photoreceptor-

specific system as *eyFLP*^{PRonly} and the original *eyFLP* system that additionally renders CNS neurons mutant as *eyFLP*^{CNS}.

Neuron-specific expression of *v100* with the *elav*^{c155}-Gal4 driver is sufficient to rescue viability in *Drosophila* (Hiesinger et al., 2005). However, Peri and Nusslein-Volhard (2008) recently reported a function for the zebrafish ortholog of *v100* in phagosomal/lysosomal fusion in microglial cells (Peri and Nusslein-Volhard, 2008). The zebrafish *v100* (atp6v0a1) is a true ortholog because the protein is more closely related to *Drosophila* V100 (61% identical) and the human subunit a1 (82% identical) than it is to the closest paralog in zebrafish (V0 subunit a2, 54% identical). We therefore wondered whether the developmental CNS defects described here could be attributed to a non-neuronal cell type. We analyzed *v100* mutant brains rescued with only neuronal *v100* expression. As shown in Figure 1D, neuronal expression of *v100* rescues the wiring defect of an *eyFLP*^{CNS} brain. Hence, *v100* is required in CNS neurons for brain wiring in *Drosophila*.

We have recently shown that V100 is expressed in the pupal and adult visual system (Williamson et al., 2010b). To determine the onset of V100 expression in the developing CNS, we performed co-labeling experiments with the developing synapse marker N-Cadherin (N-Cad) and the active synapse marker Synaptotagmin (Syt). As shown in Fig. 1G-I, anti-V100 labeling of a larval brain hemisphere reveals strong enrichment in the synaptic neuropils of the functional larval brain (arrows). In contrast, regions of neuronal and glial differentiation are only labeled at background levels, suggesting no prominent role during early brain development. However, at the time of axon targeting at 20% of pupal development (P+20%), V100 is strongly enriched in the developing first synaptic neuropil in the optic lobe, the lamina plexus, where axon terminals are actively sorting to generate a precise visual map (arrows in Fig. 1J-L).

V100 labeling at this time is most prominent in the lamina plexus, but increases in all neuropils throughout development (Fig. 1M-O). Note that V100 labeling, although enriched in the synaptic neuropils, appears distinctly different from the synaptic vesicle marker Synaptotagmin (Syt; Fig. 1M-O). These data show that V100 is enriched in specific synaptic regions of the visual system prior to synaptogenesis. Taken together our data indicate that *v100* plays a hitherto unrecognized developmental role in CNS neurons of the adult brain.

Next, we asked whether the observed brain wiring defects are caused by early cell death. Immunolabeling of activated Caspase-3 (Yu et al., 2002) in $eyFLP^{CNS}$ brains reveals no significant difference in the number of cells undergoing programmed cell death between mutant and wild type during development (Suppl. Fig. 2A-B; $eyFLP^{CNS}$ *v100*: 34 +/- 10 apoptotic cells per confocal optic lobe section; ctrl: 31+/-9) or in 10-day old optic lobes (mutant neurons marked in green, control unmarked; Suppl. Fig. 2C). This is consistent with the previously documented finding of slow adult-onset degeneration in photoreceptors, which causes cells to become unhealthy long after development is complete (Williamson et al., 2010b). These data indicate that the brain wiring defects are not the result of premature cell death.

3.3.2 Loss of v100 causes guidance receptor accumulations in CNS neurons in the optic lobe

Our previous characterization of V100 function revealed roles in synaptic vesicle exocytosis (Hiesinger et al., 2005) and endolysosomal degradation in neurons (Williamson and Hiesinger, 2010). The brain wiring defects described in this study are unlikely to be caused by defects in neurotransmitter release, since we and others have previously shown that neuronal activity, including synaptic vesicle release, is not

required for photoreceptor or optic lobe development (Clandinin and Zipursky, 2002; Hiesinger et al., 2006). In contrast, *v100*'s role in neuronal endolysosomal degradation could potentially be required for development since many signaling molecules are regulated through the endolysosomal pathway. This idea raises the question how a defect in endolysosomal trafficking could lead specifically to neuronal connectivity defects in the brain without affecting earlier stages of neuronal development.

Cell adhesion molecules that function as guidance receptors are key proteins directing axon pathfinding and targeting. To investigate a possible link between *v100* and the observed brain wiring defects, we analyzed several guidance receptors known to play roles during optic lobe development and visual map formation in the *Drosophila* brain. First, we investigated the localization patterns of the five guidance receptors Dlar, N-Cadherin, Flamingo, Fasciclin II and Roughest (Clandinin et al., 2001; Lee et al., 2001; Lee et al., 2003; Lin et al., 1994; Ramos et al., 1993) in 1-day old control and *eyFLP*^{CNS} brains. All five guidance receptors exhibit a similar phenotype of aberrant accumulations in synaptic neuropils and cell bodies of the *eyFLP*^{CNS} optic lobe (Fig. 2A-J). This phenotype is most pronounced for Dlar and N-Cadherin, whose wild type expression patterns in the optic lobe are restricted to synaptic neuropils (Fig. 2A-B,I-J). (Clandinin et al., 2001; Lee et al., 2003). While these findings show that guidance receptor localization is indeed affected in *v100* mutant neurons, they also indicate that the underlying intracellular trafficking defect is not specific to a particular guidance receptor. Hence, our results suggest that the developmental defects are a cumulative effect of the mislocalization of many receptors.

3.3.3 Guidance receptors accumulate on endosomal compartments in v100 CNS neurons

v100 mutant photoreceptors exhibit a slow accumulation of endolysosomal compartments (Williamson et al., 2010b). Intracellular accumulation of guidance receptors might cause developmental defects in CNS neurons by at least two mechanisms: First, receptors might fail to be transported to the plasma membrane, leading to loss-of-function phenotypes. Second, receptors might fail to endocytose or accumulate on signaling-active endosomal compartments, leading to gain-of-function phenotypes. In contrast to such loss or gain of function effects, accumulation of receptors in signaling-inactive lysosomal compartments should not lead to any receptor-specific defects. We therefore analyzed guidance receptor localization on intracellular compartment using an *eyFLP*^{CNS} -based approach where only mutant cells are fluorescently marked (MARCM, (Lee and Luo, 1999)). First, we confirmed that v100 mutant CNS neurons have the same endolysosomal accumulations as photoreceptors. As shown in Figure 3A-B, both the early endosomal marker 2xFYVE-GFP and the late endosomal marker Rab7 accumulate in v100 mutant neurons. 2xFYVE-GFP is a cytosolic probe that predominantly marks early endosomal compartments by associating with PI(3)P-rich membranes (Wucherpfennig et al., 2003). Note that in this experiment only 50% of CNS neurons are mutant and these cells are marked with 2xFYVE-GFP expression. As shown in Figure 3A, 2xFYVE-GFP only exhibits low levels of labeling in wild type clones. In contrast, *v100* mutant CNS neurons exhibit substantial accumulations (arrows in Figure 3B). Rab7-positive compartments exhibit similar accumulations. However, PI(3)P-rich endosomal accumulations are even more apparent than Rab7 accumulations (compare green and red labeling in Figure 3B). These results are consistent with our previous characterization of endolysosomal accumulations in photoreceptors and indicate that v100 mutant CNS neurons exhibit the same

endolysosomal trafficking problem. As in photoreceptors, early endosomal markers are upregulated strongest (Williamson et al., 2010b).

Next, we analyzed subcellular guidance receptor localization. As shown in high-resolution confocal images in Figure 3C, the receptor Dlar accumulates in highly heterogeneous compartments in CNS neuronal cell bodies. In this experiment, we marked the mutant cells with the lysosomal marker lamp-GFP, a transmembrane protein that traffics through the endolysosomal pathway and is quickly degraded in wild type (Pulipparacharuvil et al., 2005). Co-labeling with the early endosomal marker Syx7 reveals that 68.7% of all Dlar accumulations are Syx7-positive (arrows), but only 29.4% are lamp-GFP positive. We observed similar results for all guidance receptors (Fig 3D-E and data not shown). Amongst these receptors, Fasciclin 2 exhibited the strongest colocalization with the early endosomal marker Syx7 in both cell bodies of CNS neurons in the medulla cortex (arrows in Fig. 3D) and at photoreceptor synapses in the lamina (arrows in Fig. 3E). Interestingly, our high-resolution analyses of subcellular localization revealed a pattern of increased guidance receptor accumulations on the outside of large (up to 5μm) Syx7-positive compartments, as shown in Figure 3E for Fasciclin 2. We made similar observations for guidance receptor accumulations using two additional genetic manipulations, namely increased sorting into endosomal compartments and receptor overexpression in *v100* mutant neurons, as described below. In summary, our findings indicate that guidance receptors accumulate after endocytosis in compartments most prominently labeled by early endosomal markers.

3.3.4 Differential onset of guidance receptor accumulations in CNS neurons versus photoreceptors correlates with the occurrence of developmental defects

Why do *eyFLP*^{PRonly} adult photoreceptors lack a developmental defect?

Photoreceptors conclude axon pathfinding less than 48 hours after differentiation while many adult CNS neurons adopt the neural fate many days before brain connectivity is established (Truman et al., 1993). *v100* mutant neurons exhibit a progressive increase of intracellular accumulations due to lack of degradation (Williamson et al., 2010b). We reasoned that in CNS neurons, disruptive intracellular accumulations might occur sufficiently early during neuronal development to cause developmental defects. In contrast, in photoreceptors such defects might occur only after the critical developmental time periods of axon pathfinding and target recognition. To compare the time course of intracellular trafficking defects in *eyFLP*^{PRonly} and *eyFLP*^{CNS}, we investigated guidance receptor localization in developing and adult brains. As shown in Figure 4A-B, optic lobes of *eyFLP*^{CNS} *v100* brains at P+30% exhibit Dlar accumulations that are absent in *eyFLP*^{CNS} control brains. To identify even small changes of Dlar levels in photoreceptors, we analyzed mutant and neighboring control terminals in MARCM clones. As shown in Figure 4C, mutant photoreceptors exhibit indistinguishable Dlar levels compared to control. In 1-day adult *eyFLP*^{CNS} optic lobes, Dlar accumulations are further increased (Fig. 4D-E) while mutant photoreceptor terminals are just beginning to show receptor accumulations (Fig. 4F). We observed similar temporal dynamics for the other guidance receptors, although with varying onset, localization and severity of accumulations as discussed in the next section. Our data show that guidance receptor accumulations occur in both CNS neurons and photoreceptors. However, the photoreceptor defects are delayed and seem to occur sufficiently late to allow normal development. These observations are consistent with the idea that cell-specific axonal targeting defects depend on the dynamics of a progressive degradation and intracellular accumulation defect.

Next, we tested whether the differential onset of Dlar accumulations in CNS neurons vs. photoreceptors reflects a general degradation problem of transmembrane proteins that traffic through the endolysosomal system. We analyzed the time course of lamp-GFP accumulations in developing optic lobe neurons (*eyFLP*^{CNS}). In late 3rd instar larvae, lamp-GFP exhibits a prominent degradation and accumulation phenotype in the *v100* mutant CNS (Fig. 4 G-H), while mutant photoreceptors show almost no lamp-GFP accumulations at this stage (Fig. 4I) However, accumulations do become apparent in photoreceptors at 30% pupal development, i.e. even before Dlar accumulations become discernible (Fig. 4J; comp Fig. 4C). In summary, accumulations of lamp-GFP, like Dlar, reveal a progressive intracellular degradation defect that occurs earlier in mutant CNS neurons than photoreceptors.

We have previously shown that *v100* mutant photoreceptors have an acidification defect as evidenced by lysotracker labeling experiments (Williamson et al., 2010b). Lysotracker is a membrane-permeable dye that accumulates in highly acidified compartments in cells, i.e. lysosomes, late endosomes, and autophagosomes. Larval eye discs show no difference in lysotracker uptake in mutant versus control cells while pupal eye discs show a 50% reduction in lysotracker signal in mutant cells (Williamson et al., 2010b). To characterize the onset of acidification defects in optic lobe CNS neurons, we generated GFP-labeled *v100* mutant clones as before (*eyFLP*^{CNS} MARCM). In control experiments, we used the same approach, except both the marked and unmarked cells were wild type. As shown in Fig 4K-M, we found a significant reduction of Lysotracker signal in mutant CNS neurons of the 3rd instar larva, i.e. at the same time when photoreceptors are differentiating and do not yet exhibit Lysotracker defects. Furthermore, the strength of the larval CNS defect is reminiscent of photoreceptors at P+40%, i.e. approximately 2 days later. Like Dlar and Lamp-GFP accumulations, the

observed reduction of Lysotracker-positive compartments in optic lobe CNS neurons is sufficiently early to account for the brain wiring defects. In contrast, a similar reduction of strongly acidified compartments in photoreceptors is only observed after axon pathfinding and visual map formation are concluded.

3.3.5 Selective rescue of v100-dependent sorting into degradation-incompetent compartments accelerates developmental defects

Our data show that both the accumulation of membrane proteins as well as the loss of Lysotracker-positive degradative compartments precede the onset of developmental defects in CNS neurons. In contrast, our results argue that *v100* mutant photoreceptors lack a developmental defect because endolysosomal defects are delayed. To test the causality of this correlation, we designed an experiment to accelerate *v100* endolysosomal trafficking defects and assay the effect on photoreceptor development. We have previously generated a mutant version of *v100* that accelerates and thereby exacerbates null mutant phenotypes by selectively rescuing the sorting of cargo into degradation-incompetent compartments. Selective rescue of the endosomal sorting function, but not the acidification function of *v100* is achieved by expressing the mutant $v100^{R755A}$ in *v100* null mutant neurons. In contrast, $v100^{R755A}$ expression in wild type neurons has almost no effect since the wild-type protein is present to acidify degradative compartments (Williamson et al., 2010b).

As shown in Figure 5A-B, $v100^{R755A}$ expression in *v100* mutant photoreceptors ($eyFLP^{PRonly}$) leads to axon targeting defects (arrows in Fig. 5A) that are completely absent when $v100^{R755A}$ is expressed in wild type neurons, consistent with our previous report that $v100^{R755A}$ does not act as a dominant-negative (Williamson et al., 2010b). Similarly, these developmental defects are not observed in *v100* null mutant

photoreceptors or in mutant photoreceptors that are rescued with wild type *v100* (Fig. 1B, D). In addition, large amounts of the photoreceptor-specific transmembrane protein Chaoptin accumulate when $v100^{R755A}$ is expressed in mutant neurons (arrowhead in Fig. 5A). These data suggest that $v100^{R755A}$ expression in mutant neurons accelerates intracellular accumulations and causes developmental defects in photoreceptors. Next, we assessed the effect of $v100^{R755A}$ expression on the wiring defect in *v100* mutant optic lobe CNS neurons (Fig. 5E). Strikingly, $v100^{R755A}$ causes a dramatically worse wiring defect than the null mutant and affects a total loss of recognizable neuropil structure (Fig. 5C, E). Neuronal expression of wild type *v100* fully rescues this defect (Fig. 5D), and no such defect is observed when $v100^{R755A}$ is expressed in wild type neurons (Fig. 5F).

Where do guidance receptors accumulate in neurons with developmental defects due to $v100^{R755A}$-accelerated sorting? Figure 5G-H shows cross-sections through photoreceptor cell bodies of 1-day old eyes in which the cell on the right side of the clonal boundaries are both *v100* mutant and express $v100^{R755A}$, while the neighboring clones on the left side are wild type. In this experiment the mutant cells are marked with synapto-pHluorin (green, MARCM), which accumulates in endosomal compartments (Williamson et al., 2010b). As shown for Dlar and Fas2 in Figure 5G-H, guidance receptors exhibits strong accumulations in mutant photoreceptor cell bodies containing synapto-pHluorin aggregates. Interestingly, a substantial amount of both Dlar and Fas2 encircles Syx7 labeling and is found on the plasma membrane of the dramatically enlarged cell bodies (arrow heads in Figure5G-H) as well as Syx7-positive compartments (arrows). Very similar cell body membrane accumulations are observed for the other guidance receptors (data for Dlar, Rst and Fas2 in Suppl. Fig. 3A, C, E). These observations suggest an endocytic defect of membrane receptors. While it is at this point unclear whether these endocytic defects are primary or secondary to an accelerated clog-

up or recycling problem in the endocytic pathway, these observations clearly show that guidance receptors do not only accumulate in signaling-incompetent lysosomal compartments. In summary, our data indicate that accelerated endolysosomal sorting into degradation-incompetent compartments causes guidance receptor accumulations on plasma and/or endosomal membranes and accelerates the onset and severity of developmental defects in both photoreceptors and CNS neurons.

3.3.6 Sorting into degradation-incompetent compartments reveals different guidance receptor turnover rates

Our observations suggest that accelerated sorting by $v100^{R755A}$ expression in *v100* mutant neurons during brain wiring accelerates the accumulation of guidance receptors. To test this idea we analyzed Dlar, N-Cad, Flamingo, Fas2 and Rst in *v100* mutant photoreceptors ($eyFLP^{PRonly}$) with or without $v100^{R755A}$ expression at P+30%. As shown in Figure 6, none of the guidance receptors exhibit obvious receptor accumulations in either the developing eye or at photoreceptor synapses at this developmental time point in the *v100* null mutant (also compare Fig. 4C). Very mild increases are only just discernible for Rst in the developing eye and Flamingo at synapses (arrows in Fig. 6J', M'). In comparison, accelerated sorting into degradation incompetent compartments ($v100^{R755A}$ in *v100)* leads to increased accumulations with highly variable severity and in different parts of the neuron for these five receptors at P+30%. As shown in Figure 6O, Rst accumulations are strongly increased in the eye, while N-Cad and Fas2 exhibit comparably mild increases (Fig. 6G, S) and Dlar and Flamingo are apparently unaffected in cell bodies in the eye (Fig. 6C,K). In contrast, at photoreceptor synapses in the same brains, Flamingo is strongly increased (Fig. 6L), whereas Rst, Dlar, N-Cad and Fas2 show mild or no increased accumulations (Fig. 6D, H, P, T). Since all five guidance

receptors analyzed here as well as other transmembrane proteins including lamp-GFP and CD8-GFP accumulate in *v100* mutant neurons over time (comp. Figures 2 & 4), we conclude that only receptors that are in the endolysosmal system at a given time in the cell body or at the synapse are subject to $v100^{R755A}$-accelerated sorting *and v100*-dependent degradation. This interpretation is consistent with the two strongest effects shown here: Rst plays a key role in membrane sorting during eye development at P+30%, but is not yet strongly expressed at synapses (Reiter et al., 1996; Schneider et al., 1995), whereas Flamingo plays a key role in photoreceptor targeting at P+30% (Lee et al., 2003). Co-labeling of the $v100^{R755A}$-accelerated accumulations of Rst in the eye and Fmi at synapses with Syx7 reveals many co-localizing accumulations (Suppl Fig. 4). The colocalization with the early endosomal marker are consistent with the findings for both *v100* mutant photoreceptors and CNS neurons (Figs. 3C-E and 5G-H). In summary, specifically restoring the sorting function of *v100* accelerates the rate of guidance receptor accumulations in developing neurons.

3.3.7 Guidance receptors accumulate in signaling-competent compartments in v100 mutant photoreceptors

Our findings in both photoreceptors and CNS neurons indicate that guidance receptors accumulate on membranes where they could potentially exert increased signaling. In particular, the $v100^{R755A}$-accelerated sorting leads to accumulations of receptors both on endosomal compartments and the plasma membrane. These findings are not consistent with the idea of accumulations in signaling-incompetent lysosomal compartments or failed exocytic membrane delivery. Rather, our data strongly suggest defects along the endocytic pathway. To directly test the activity of missorted guidance receptors in *v100* mutant neurons, we designed an experiment to challenge *v100* mutant

photoreceptors (*eyFLP*^{PRonly}) with overexpression of guidance receptors and other transmembrane cargo. We reasoned that increased numbers of guidance receptors should lead to receptor-specific gain-of-function phenotypes that are exacerbated when *v100*-dependent sorting and degradation are removed. In contrast, membrane proteins without signaling function should not cause developmental defects, even though they may still accumulate in the same intracellular compartments. As control transmembrane cargo, we selected lamp-GFP and myristoylated RFP (myrRFP). Overexpression of both lamp-GFP and myrRFP leads to pronounced accumulations in synaptic terminals of *eyFLP*^{PRonly} *v100* mutants, but not in the synaptic terminals of wild type photoreceptor neurons (Fig. 7A,B). However, even co-overexpression of both transmembrane-anchored fluorescent probes in *v100* mutant photoreceptors causes no appreciable developmental defects (Fig. 7C-D). We conclude that accumulations of membrane proteins without signaling function are not sufficient to cause developmental defects. In contrast, overexpression of Roughest, Fas2 or N-Cadherin in *v100* mutant photoreceptors causes well-defined, strong axon pathfinding or visual map formation defects. Specifically, overexpression of Roughest causes distinct axon fasciculation and pathfinding defects, a phenotype that is dramatically worsened in a *v100* mutant background (Fig. 7E, F). In contrast, overexpression of N-Cadherin in wild type photoreceptors does not cause any appreciable developmental defect, whereas overexpression of N-Cadherin in *v100* mutant photoreceptors causes distinct defects in visual map formation in the lamina (Fig. 7G-J). This phenotype is very different from the misrouted axon bundles caused by increased Roughest function. Whereas the Roughest-specific fasciculation and pathfinding defects are best shown in the 3D visualizations of axon projections in the brain, the visual map formation defect in the lamina is best demonstrated by the lamina cross-sections shown in Fig. 7G-J. Similarly, overexpression of Fas2 in wild type photoreceptors causes no

pathfinding defects, but a highly specific sorting defect of synaptic terminals in the lamina (i.e. a specific visual map formation defect; 11% of synaptic cartridges contain more than 8 or less than 4 terminals, compared to <1% in wild type) and this FasII-dependent phenotype is substantially worsened in a *v100* mutant background (23% of synaptic cartridges contain <4 or >8 terminals; Fig. 7K-L). In contrast, loss of Fas2 in photoreceptors causes no obvious defects in axon targeting or visual map formation (data not shown). These results show that overexpression of guidance receptors, but not membrane-tagged fluorescent probes without signaling function, causes specific developmental defects that strongly suggest exacerbated gain-of-function phenotypes. Our findings are consistent with the idea that both guidance receptor overexpression and increased receptor sorting into degradation-incompetent compartments lead to developmental defects due to increased guidance receptor activity. Indeed, both genetic manipulations lead to increased colocalization of guidance receptors with the early endosomal Syx7, as shown for Fas2 in Suppl. Fig. 5. Taken together with the finding of early accumulations of guidance receptors on endosomal compartments in *v100* mutant CNS neurons, our findings support the idea that brain wiring defects in the adult CNS result at least partially from increased guidance receptor activity.

3.3.8 V100-dependent guidance receptor accumulations cause gain-of-function defects in the embryo

To further test the idea that *v100*-dependent accumulations of guidance receptors lead to increased receptor signaling we turned to the *Drosophila* embryonic nervous system. *Drosophila* embryonic motor axons have long provided a simple *in vivo* model for characterizing axon guidance molecules (Araujo and Tear, 2003; Van Vactor, 1998) since individual axons can be followed to their targets and phenotypes that result from

increased signaling can often be differentiated from loss-of-function defects (e.g., (Hung et al., 2010; Lin et al., 1994; Lin and Goodman, 1994; Terman et al., 2002)). The discovery of the progressive *v100*-dependent neuronal degradation mechanism makes clear predictions for guidance receptor sorting in the embryonic nervous system. Specifically, we propose that 24 hours of embryonic development are not sufficient to lead to aberrant receptor function. However, both accelerated sorting into degradation-incompetent compartments ($v100^{R755A}$ in *v100*) as well as guidance receptor overexpression in *v100* mutant neurons should accelerate the occurrence of receptor-specific phenotypes similar to the effects shown for photoreceptors. To test this hypothesis, we analyzed axon pathfinding and guidance receptor sorting in the embryo. The guidance receptor Fas2 not only plays a critical role in axon pathfinding, but is also one of the most commonly used markers to analyze pathfinding, branching and fasciculation defects in the embryonic nervous system (Van Vactor, 1998). Furthermore, the *Drosophila* embryonic nervous system has been used as a model to differentiate the effects of increased vs. decreased Fas2 signaling (Grenningloh et al., 1991; Lin et al., 1994; Lin and Goodman, 1994). As shown in Figure 8A-B, Fas2-positive ISNb axons reveal no statistically significant guidance defects in null mutant embryos (blue bar in Fig. 8D). In contrast, accelerated sorting into degradation-incompetent compartments ($v100^{R755A}$ in *v100*) leads to statistically significant axon guidance defects (Fig. 8C; red bar in Fig. 8D). Interestingly, these phenotypes are indicative of increased axon-axon fasciculation, a phenotype that is known to result from increased Fas2 signaling in axons (Lin et al., 1994). As shown in Fig. 8H, Fas2 immunolabeling is significantly increased in $v100R^{755A}$-'rescued' embryos. Furthermore, co-labeling with the early endosomal marker Syx7 reveals increased accumulations of Fas2 in degradation-incompetent compartments ($v100^{R755A}$ in *v100*) of embryonic neurons (Suppl. Fig. 6A-C, G-H).

Similar to *v100*^{R755A} expression in *v100* mutant neurons, overexpression of Fas2 in *v100* mutant neurons leads to significantly enhanced gain-of-function fasciculation defects compared to Fas2 overexpression in *v100* heterozygous or wild type neurons (Figure 8E-G). These results reveal that the V100-dependent degradation pathway regulates the levels of Fas2 in neurons in both the *Drosophila* visual and embryonic systems and strongly argues that these *v100*-dependent accumulations lead to increased Fas2 signaling. Interestingly, certain aspects of embryonic nervous system development and axon pathfinding remain largely unaffected. For example, midline crossing, which is partly regulated by the Slit-Robo system (Spitzweck et al., 2010), is mostly resistant to *v100*^{R755A}-accelerated receptor sorting (with only low penetrance defects). Similarly, *v100*^{R755A}-accelerated receptor sorting does not enhance Sema-1a/PlexA–mediated repulsive signaling at the midline (data not shown; (He et al., 2009)). However, analysis of Robo1 receptor expression reveals mild accumulations in the ventral ganglion that are increased by *v100*^{R755A} expression (Suppl. Fig. 6E-F, I-J). These findings are consistent with our observation that *v100*^{R755A} expression in *v100* mutant neurons reveals spatiotemporally specific turn-over rates of guidance receptors. A straightforward explanation for the lack of midline crossing defects is that loss of degradation does not lead to aberrant Robo signaling within the timeframe of embryonic development.

Finally, the embryonic nervous system allows to directly test our observation that there is no obvious defect in guidance receptor trafficking to the membrane surface through the secretory pathway. We made embryonic filet preparations in which axons are directly accessible to antibody washing solutions in the absence of detergent. Since the Fas2 immunohistochemistry antibody is specific to the intracellular domain, we tested this idea with an antibody against the extracellular domain of the guidance receptor DPTP69D, which also functions in ISNb axon pathfinding similar to Fas2 at the same

time and place (Desai et al., 1996). As shown in Figure 8I and Suppl. Fig. 7, this receptor exhibits slightly increased levels of expression on the axon membrane surface in *v100* mutant and $v100^{R755A}$- 'rescued' neurons compared to control. Taken together, our analysis of *v100*-dependent receptor sorting in the embryonic nervous system fully supports our results in photoreceptors and adult brain CNS neurons. Specifically, these results highlight that numerous guidance receptors are subject to the *v100*-dependent *'sort-and-degrade'* mechanism, that receptor trafficking defects are downstream of receptor secretion in the endosomal pathway and that increased levels of guidance receptors lead to exacerbated gain-of-function defects.

3.4 DISCUSSION

In this paper, we show that loss of a neuron-specific v-ATPase-dependent degradation mechanism leads to brain wiring defects in *Drosophila*. Neurons mutant for the v-ATPase V0 subunit a1, *v100*, progressively accumulate degradation-incompetent compartments that contain multiple classes of guidance receptors. Both accelerated sorting into degradation-incompetent compartments and overexpression of guidance receptors in *v100* mutant neurons lead to increased receptor accumulations on signaling-competent membranes and accelerate developmental defects in photoreceptors and embryonic motorneurons. However, only accumulations of guidance receptors, but not transmembrane proteins without signaling function, lead to specifically exacerbated gain-of-function defects. Hence, our results indicate that block of *v100*-dependent degradation can lead to the accumulation of guidance receptors in signaling-competent compartments. We conclude that in the *Drosophila* CNS, *v100*-dependent receptor degradation is required during development for the cell to spatiotemporally control guidance receptor signaling, which is in turn necessary for neuronal connectivity in the brain. Our findings suggest that continuous turnover and degradation is a general mode of guidance receptor regulation which sets the stage for other trafficking mechanisms that instructively regulate guidance receptor localization and signaling.

3.4.1 The role of v100-dependent intracellular trafficking in neuronal development

Membrane trafficking underlies the growth and remodeling of axonal and dendritic branches. However, the loss of *v100*-dependent endolysosomal trafficking presented here has no apparent effect on membrane addition and remodeling. Instead, we

identified a role for *v100* in intracellular receptor trafficking. Intracellular trafficking and the v-ATPase are known to play critical roles in the dynamic localization and signaling of a plethora of transmembrane receptors (Vaccari et al., 2010; Yan et al., 2009). Receptors may signal from the plasma membrane or may be endocytosed to exert a signaling function (Seto et al., 2002). A prominent example in neuronal development is the regulation of cellular differentiation by endocytosis of the Notch ligand Delta (Chitnis, 2006). However, loss of *v100* causes no early developmental defects and is therefore not required for the regulation of receptor-mediated signaling that governs cellular differentiation and early tissue patterning. In contrast, we report that CNS neurons of the developing adult brain exhibit axon pathfinding and synaptic specification defects. Our findings indicate that V100 has a specialized task in neurons and has no function in the essential endolysosomal machinery required for early development. In contrast, the loss of key subunits of the V1 complex of the v-ATPase (which is probably required for all v-ATPase function) cause cell lethality. Specifically, *ey*FLP *vha55* and *ey*FLP *vha68* lead, in stark contrast to *ey*FLP *v100*, to an abolishment of the eye (P.R.H, unpublished observations).

The *v100* mutant phenotypes are most similar to two other intracellular trafficking mutants that we have described before. First, loss of *n-syb*, the gene that encodes the vesicle SNARE *neuronal Synaptobrevin*, leads to guidance receptor accumulations and synaptic specificity defects in the *Drosophila* visual system (Hiesinger et al., 1999). Second, *sec15* encodes a component of the Exocyst complex required for neuronal targeting or secretion functions other than neurotransmitter release. Similar to loss of *n-syb*, loss of *sec15* leads to mislocalization of guidance receptors and photoreceptor targeting defects (Mehta et al., 2005). These findings represent mounting evidence for the employment of neuronal intracellular trafficking machinery during brain

wiring. However, the neuronal degradation function presented here for *v100* differs from the earlier findings on *n-syb* and *sec15*, in that loss of *v100* does not lead to targeting or 'tiling' defects in the photoreceptor terminal field. Curiously, the guidance receptors most prominently affected by loss of either *n-syb* or *sec15* are Fas2 and Dlar, while N-cadherin and Flamingo are not affected in *sec15* mutant photoreceptors (Mehta et al., 2005). In contrast, all these guidance receptors are affected by loss of *v100* in CNS neurons. We interpret these differences in the context of differing molecular functions: While loss of *sec15* may lead to targeting defects of a subpopulation of neuronal vesicles required for guidance receptor localization, loss of *v100* disrupts general receptor turnover downstream of the secretory pathway in neurons. This disruption could be partly due to 'clog-up' of the endolysosomal pathway or due to defective endosomal recycling.

Our challenge experiments using guidance receptor overexpression in *v100* mutant photoreceptors and embryonic motorneurons are similar to wingless overexpression experiments in intracellular degradation mutants. Dubois et al. (2001) showed that Wingless is targeted to lysosomes and is continuously and specifically degraded posterior to each stripe of Wingless transcription. Disruption of lysosomal degradation leads to the Wingless accumulations and, together with Wingless overexpression, ectopic signaling (Dubois et al., 2001). Similarly, we find that guidance receptors undergo constant turnover (see discussion in the next section) and their overexpression in *v100* mutant neurons leads to ectopic signaling. For example, N-Cadherin overexpression in wild type photoreceptors, analogous to the wingless experiments, does not cause obvious defects. In contrast, N-Cadherin overexpression in *v100* mutant photoreceptors causes gain-of-function phenotypes. Similarly, overexpression of low levels (one copy) of Fasciclin 2 causes only very mild

fasciculation defects in embryonic motorneurons (Lin et al., 1994). In contrast, the same level of Fasciclin 2 overexpression in *v100* mutant neurons causes a phenotype very similar to high levels of Fasciclin 2 overexpression (two copies) (Lin et al., 1994). These observations strongly suggest increased gain-of-function phenotypes and are not consistent with loss-of-function phenotypes for these receptors. However, these findings do not exclude the possibility that parts of the compound brain wiring defects in *eyFLP*^{CNS} *v100* mutants are due to loss of function for other proteins affected by *v100*-dependent sorting.

Importantly, *v100* is a neuron-specific gene and its loss does not lead to hallmark phenotypes of general lysosomal degradation mutants, including autofluorescent lipofuscin or ceroid accumulations or aberrant multilamellar lysosomal organelles (Dermaut et al., 2005; Futerman and van Meer, 2004; Williamson et al., 2010b). Hence, V100 provides a neuronal degradation mechanism specifically required after differentiation for late brain development and neuronal maintenance.

3.4.2 The role of receptor turnover during the establishment of synaptic specificity

How guidance receptors are dynamically localized is unknown for most receptors. Several guidance receptors are known to be regulated by intracellular trafficking. Sema3A-induced endocytosis of Neuropilin-1 has been shown to be required for growth cone collapse during axon guidance (Castellani et al., 2004). Similarly, internalization of UNC-5A prevents UNC-5A-mediated growth cone collapse in hippocampal axon guidance (Bartoe et al., 2006). One of the best characterized examples for intracellular dynamic sorting is the guidance receptor Robo (Keleman et al., 2002; Keleman et al., 2005; Spitzweck et al., 2010). During embryonic nervous system development certain axons are prevented from crossing the midline by a repellent

guidance cue that binds to the Robo receptor. During a short time window, Robo is removed from the plasma membrane and the axon crosses the midline exactly once. Thereafter, Robo receptors return to the membrane and prevent the axon from crossing again. Remarkably, this dynamic relocalization of the Robo receptor is achieved by diverting a continuous supply of receptors from the ER/Golgi temporarily into the endolysosomal pathway for degradation by means of the intracellular sorting receptor Comm. Hence, the dynamic membrane presentation of Robo receptors on the growth cone is not regulated by endo- and exocytosis of a fixed amount of receptors. Instead, the regulation occurs via an intracellular sorting receptor, revealing a strategy that relies on constitutive synthesis and degradation of receptors that can be sorted to exert spatiotemporally defined functions. Notably, the proposed diversion of Robo receptors into degradative compartments is only very short. Indeed, we observe a mild increase of Robo accumulations in embryonic neurons. However, the lack of developmental defects suggests that these accumulations are not sufficient to cause aberrant signaling. We propose that loss of *v100*-dependent degradation only leads to slow build-up of undegraded receptors, and 24 hours of embryo development are not sufficient to lead to neuronal connectivity defects.

The role of *v100* in guidance receptor turnover is most strikingly highlighted by the selective rescue of *v100*-dependent sorting into degradation incompetent compartments. Rescue of the sorting function, without rescue of acidification-dependent degradation, leads to a dramatically accelerated accumulation of endogenously expressed guidance receptors. Interestingly, these accumulations are increased compared to the *v100* null mutant. Hence, V100 actively promotes vesicle sorting into endosomal compartments destined for degradation. In addition we observe accumulations of guidance receptors on the plasma membrane. While we cannot exclude a primary defect

in endocytosis, a secondary effect due to clog-up of the endolysosomal system or endosomal recycling defects seem more likely. In either case, these observations clearly show that guidance receptors do not exclusively accumulate in signaling-incompetent compartments. In addition, the absence of early developmental defects indicates and our staining of DPTP69D in the embryo demonstrates functional guidance receptor exocytosis.

Our findings reveal several key features of *v100*-dependent *'sort-and-degrade'*: First, in the complete absence of *v100*-dependent sorting and degradation this turnover is at least partially taken over by a *v100*-independent degradation pathway. This interpretation is consistent with our previous model that V100 acts in parallel to an essential endolysosomal pathway that ensures cellular differentiation and viability (Williamson et al., 2010b). Second, the progressive nature of the *'sort-and-degrade'* mechanism is similar in all different types of neurons analyzed here. We conclude that the occurrence of neuronal connectivity defects is a function of the duration between neuronal differentiation and synaptic specification. Third, these experiments reveal that guidance receptors are subject to a constant turnover. Indeed, combined measurement of guidance receptor accumulation in *v100* mutant neurons and $v100^{R755A}$-'rescued' neurons is a tool to assess the turnover rate of different guidance receptors. This is supported by the observation of different accumulation kinetics of several guidance receptors investigated here. For example, our experiments at P+30% reveal high Rst turnover in the developing eye but not at synapses, high Flamingo turnover at synapses, but not in the eye and very little Dlar turnover at this developmental time point. Taken together, our findings suggest that *v100*-dependent *'sort-and-degrade'* is required for guidance receptor turnover, and its manipulation is a method to assess receptor turnover at different time points.

3.5 CHAPTER THREE FIGURES

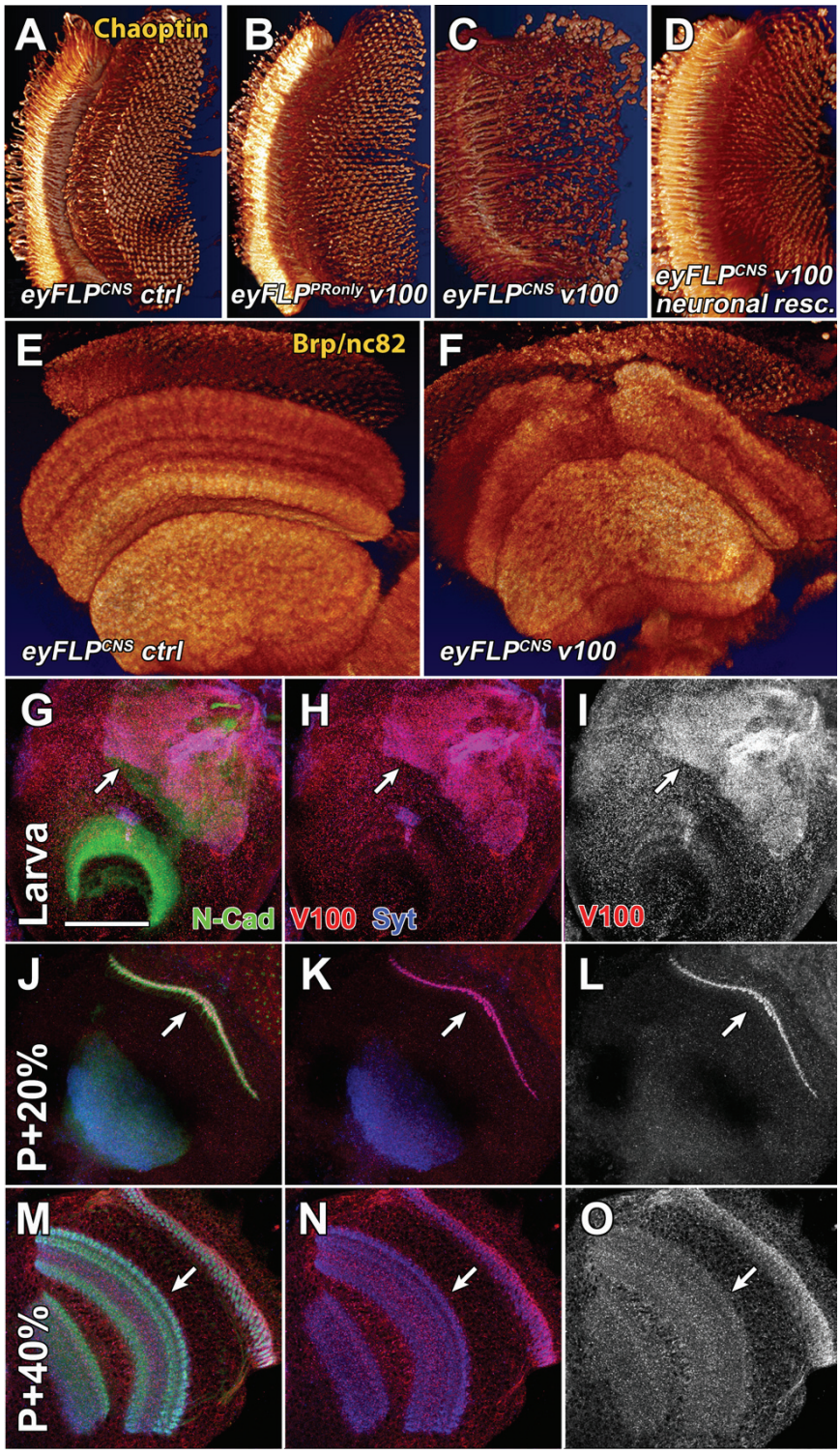

Figure 3.1: V100 is required for neuronal connectivity in the adult brain.

(A-D) 3D visualizations of photoreceptor projections in the adult brain immunolabeled for Chaoptin (distal to the left). (A, B) Both control and *v100* mutant photoreceptors *(eyFLP^{PRonly} v100)* exhibit wild type axon targeting patterns. (C, D) In contrast, photoreceptor targeting is disrupted in optic lobes with mutant CNS neurons *(eyFLP^{CNS} v100)* and rescued with pan-neuronal expression of WT *v100* cDNA using elav-Gal4. (E, F) Three-dimensional visualizations of optic lobe neuropils immunolabeled with Brp/nc82 in control (E) and *eyFLP^{CNS} v100* (F). See also the schematic of optic lobe structure in Suppl. Fig. 1C. (G-O) Characterization of wild type V100 expression dynamics in the developing optic lobe. (G-I) Wild type L3 larval brain hemisphere. Developing synapses are immunolabeled with anti-N-Cadherin (N-Cad, green); active synapses are labeled with anti-Synaptotagmin (Syt, blue); anti-V100 in red. Note that V100 mostly localizes to active neuropil regions in the larval brain (arrows). (J-L) At 20% pupal development (P+20%), V100 is strongly enriched in the lamina plexus, i.e. the developing first optic neuropil. (M-O) At 40% pupal development, V100 is enriched in all synaptic neuropils of the developing optic lobe (arrows), where it remains throughout adulthood. Scale bar in (G) for (G-O): 50µm.

Figure 2

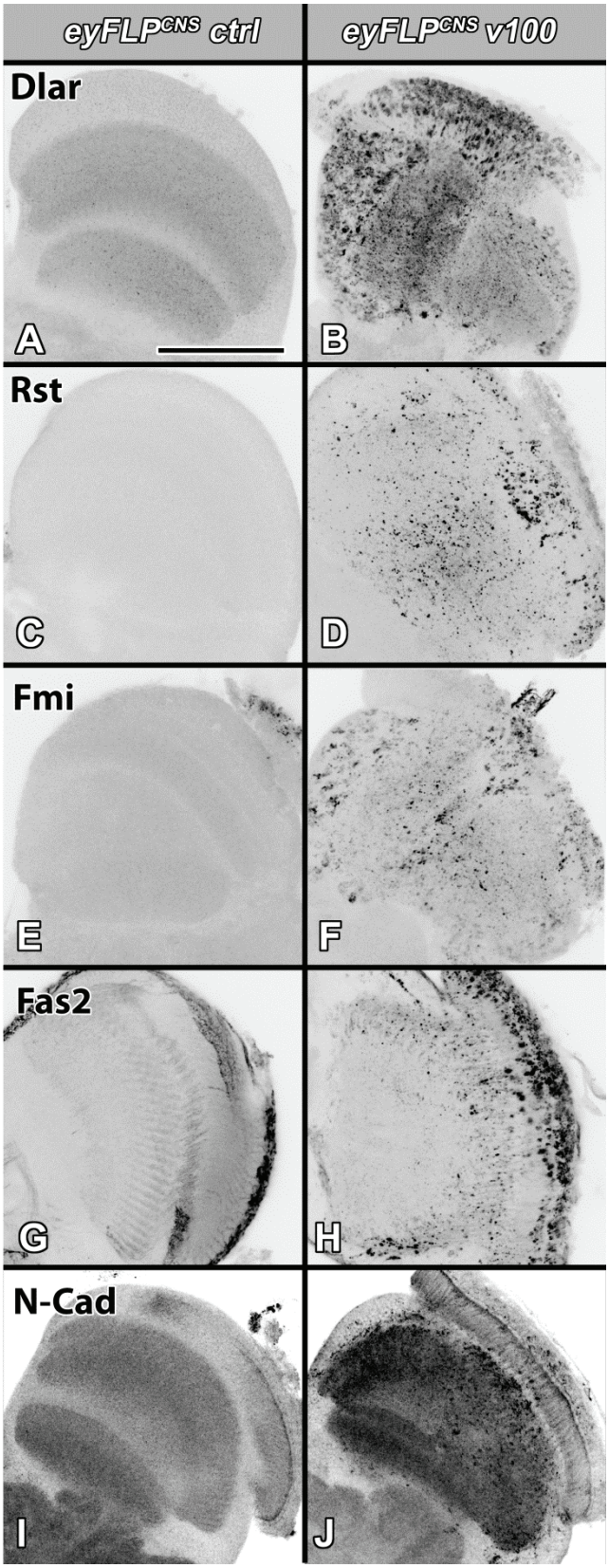
eyFLP^CNS ctrl
eyFLP^CNS v100
Dlar
A
B
Rst
C
D
Fmi
E
F
Fas2
G
H
N-Cad
I
J

Figure 3.2: Loss of v100 causes guidance receptor accumulations in CNS neurons in the optic lobe.

(A-J) Confocal images of 1-day old *Drosophila* optic lobe sections labeled with antibodies against the guidance receptors Dlar, Rst, Fmi, Fas2, and N-Cad. All five guidance receptors accumulate in cell bodies and at synapses of *eyFLP*^{CNS} *v100* optic lobes, while accumulations are absent in control brains. Scale bar in (A) for (A-J): 50μm.

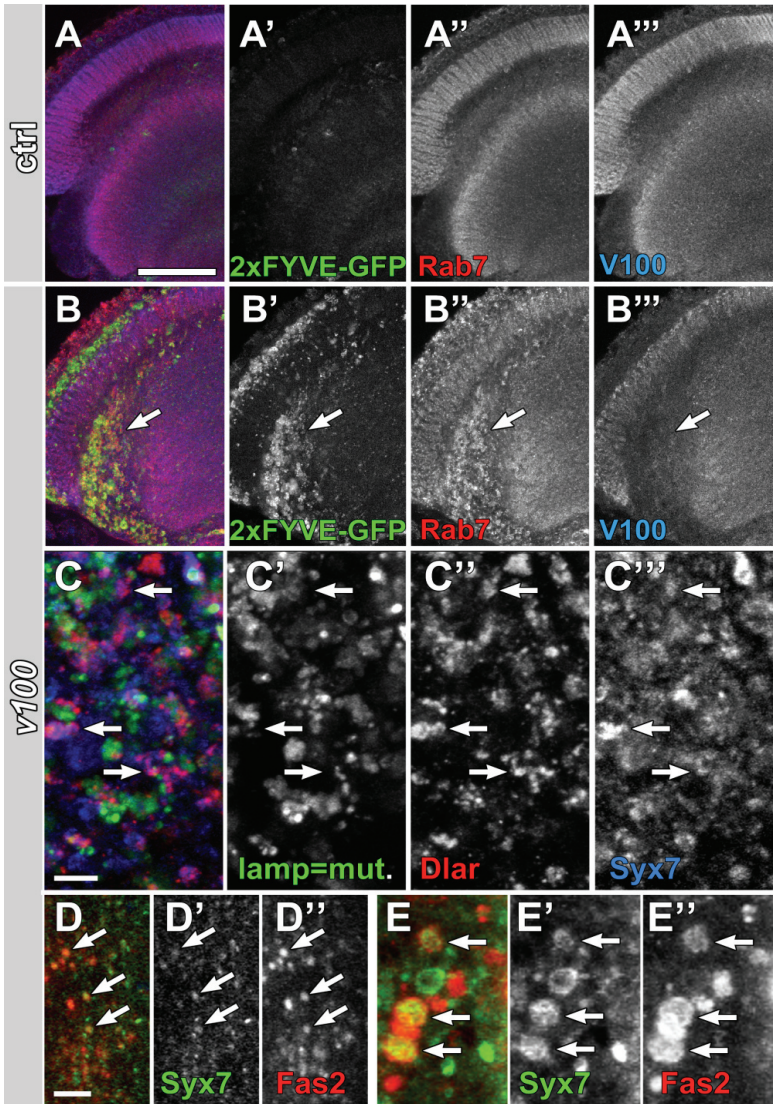

Figure 3.3: Loss of v100 in CNS neurons causes endosomal guidance receptor accumulations.

(A-B) Confocal sections of adult *eyFLP*^{CNS} ctrl (A) and *v100* (B) optic lobes with 50% of all *eyFLP*^{CNS} cells labeled with 2xFYVE-GFP. Expression of 2xFYVE-GFP in control cells results in weak 2xFYVE-GFP (A) but strong accumulations in *v100* mutant CNS neurons (B). Similarly, immunolableling of the late endosomal marker Rab7 (red) reveals increased accumulations in *v100* mutant CNS neurons. 2xFYVE-GFP only shown in (A' and B'), Rab7 only in (A'' and B''), V100 only in (A''' and B'''). (C) High-resolution confocal section of adult *eyFLP*^{CNS} *v100* optic lobe with 50% of all *eyFLP*^{CNS} cells labeled with lamp-GFP. Similar to 2xFYVE-GFP and Rab7, the lysosomal marker lamp-GFP accumulates. However, Dlar accumulations colocalize more with the early endosomal marker Syx (arrows, blue) than lamp-GFP. (D-E) High-resolution confocal sections of *eyFLP*^{CNS} *v100* mutant CNS neuron cell bodies in the medulla cortex (D) and photoreceptor synapses in the lamina (E). Scale bars: in (A) for (A-B): 50µm; in (C): 5µm. In (D) for (D-E): 5µm.

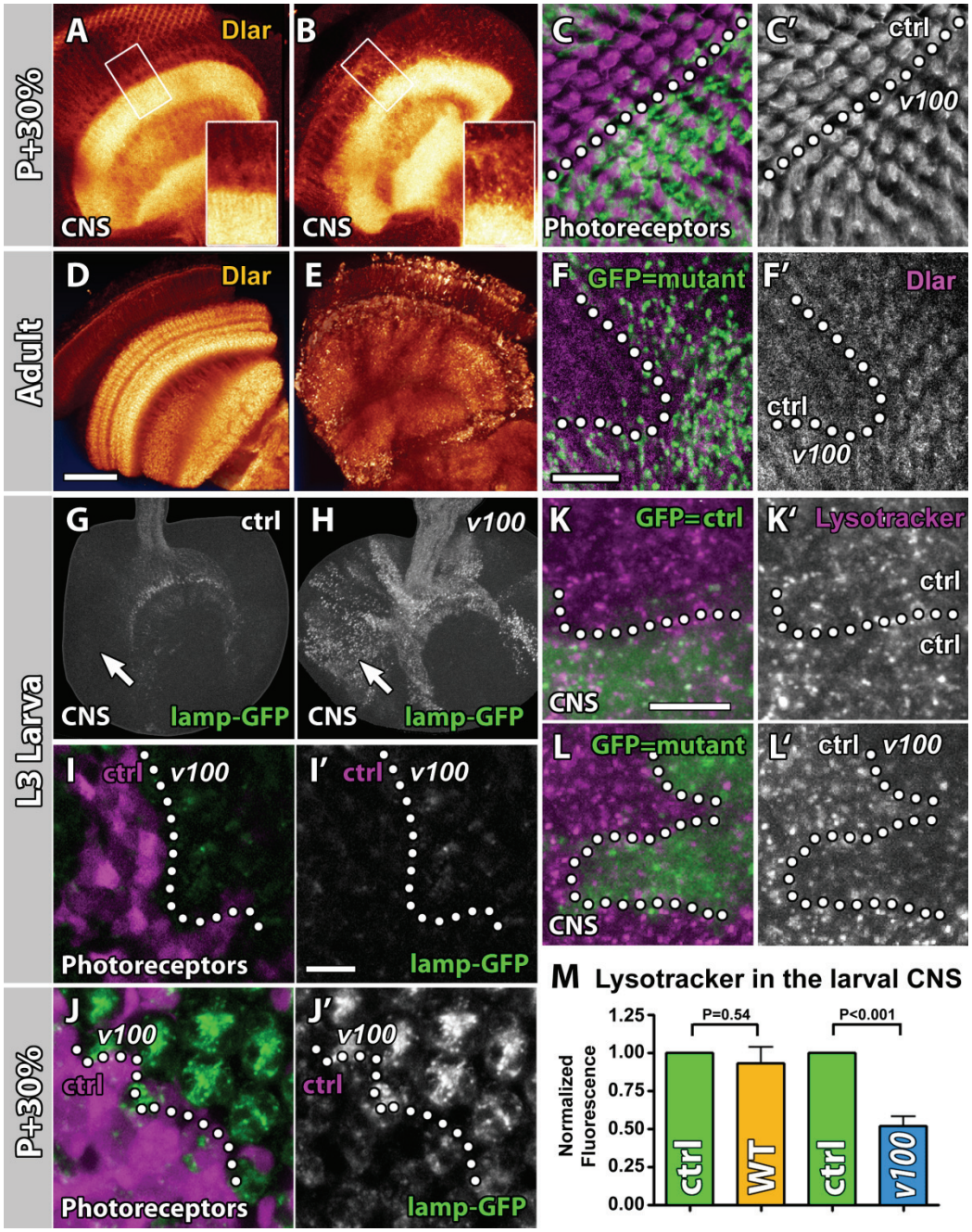

Figure 3.4: Differential onset of guidance receptor accumulations in CNS neurons versus photoreceptors correlates with the occurrence of developmental defects.

(A, B) Confocal sections of P+30% optic lobes immunolabeled with Dlar. (A) ctrl. (B) *eyFLP*^{CNS} *v100*. Insets are magnifications of the boxed regions and reveal Dlar accumulations in the mutant neurons that are absent in control. (C) P+30% photoreceptor terminals in the first optic neuropil (lamin plexus). 50% of photoreceptors are mutant

and marked with GFP (*eyFLP*^{PRonly} *MARCM*). Note that Dlar (magenta, single channel in C') is indistinguishable in mutant and control terminals. (D-E) Confocal sections of adult optic lobes immunolabeled with Dlar. (D) ctrl. (E) *eyFLP*^{CNS} *v100*. (F) *eyFLP*^{PRonly} *MARCM* as in (C) reveals mildly increased Dlar levels in mutant terminals (single channel in F'). (G-H) L3 larval hemispheres of *eyFLP*^{CNS} ctrl *MARCM* (G) and *eyFLP*^{CNS} *v100 MARCM* (H). Only cells rendered homozygous for a wild type chromosome (G) or the v100 mutant chromosome (H) express lamp-GFP. Note the strong accumulation of lamp-GFP in mutant CNS neurons (arrow). (I) Clone of *v100* mutant cells in the larval eye disc (wild type cells marked with RFP (magenta)). Single lamp-GFP channel in (I') and clonal boundary marked with a dotted line. Note that the mutant cells in the eye disc show only very mild lamp-GFP accumulations. (J) Same as in (I) at P+30%. Lamp-GFP accumulations are now prominent. (K-L) Live lysotracker labeling of CNS neurons *eyFLP*^{CNS} *MARCM* optic lobes. Cell homozygous for a wild type chromosome in (K) and mutant for v100 (L) are marked with GFP. Dotted lines mark clonal boundaries. Note the reduction on lysotracker signal in the mutant larval CNS neurons. (M) Quantification of Lysotracker measurements. Error bars are S.E.M.; n=6. Scale bars in (D) for (A-B, D-E, G-H): 50 μm; in (F) for (C, F): 10 μm; in (I') for (I, J): 10μm; in (K) for (K, L): 10 μm.

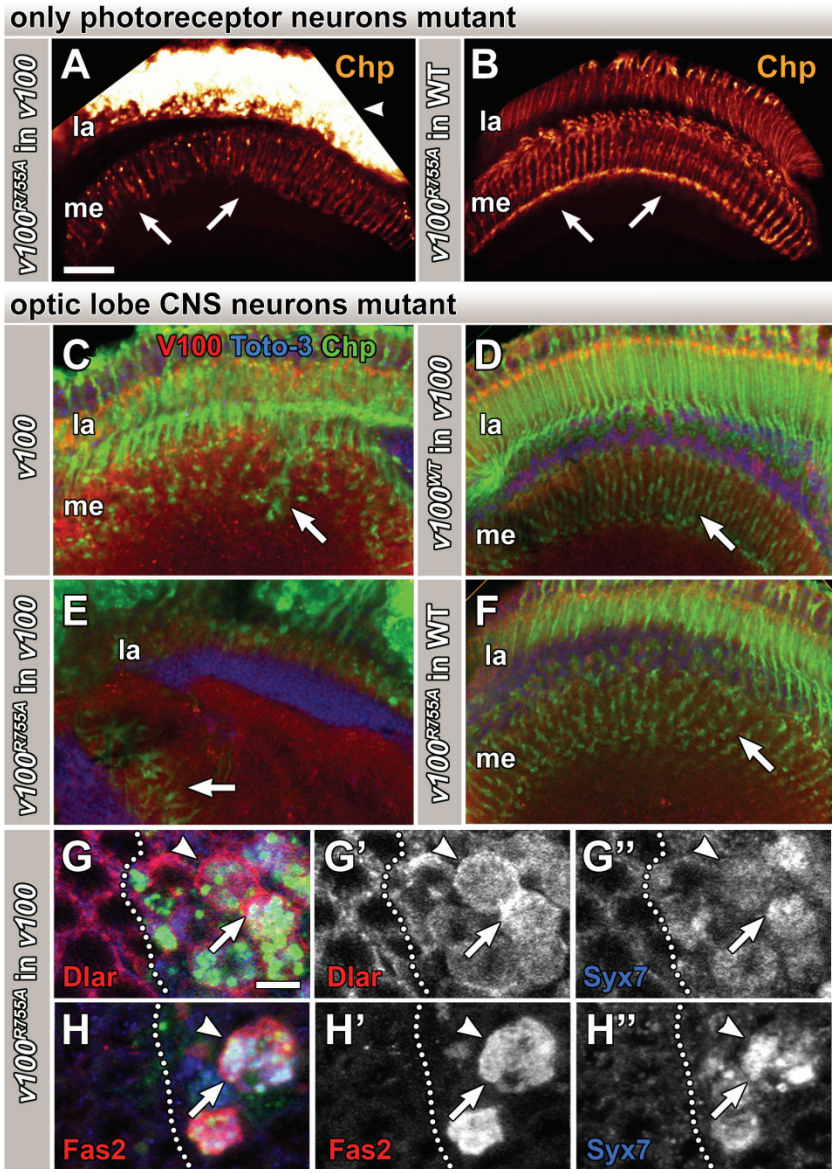

Figure 3.5: Selective rescue of v100-dependent sorting into degradation-incompetent compartments accelerates developmental defects.

(A, B) Chaoptin immunolabeling of photoreceptor projections in adult optic lobes. Expression of *v100*^{R755A} in *eyFLP*^{PRonly} *v100* photoreceptors (A) causes targeting defects (arrows) and chaoptin accumulations (arrowhead) that are absent when v100^{R755A} is expressed in WT photoreceptors (B). (C-F) Confocal images of *Drosophila* optic lobe sections showing a longitudinal section through the first optic neuropil (lamina) on top and deeper photoreceptor projection below. Green: Chaoptin (photoreceptors); red: V100; Blue: Toto-3 (nuclei). Note the targeting defects in eyFLP^{CNS} *v100* in (C), which are dramatically worsened by v100^{R755A} expression in v100 mutant neurons (E). In contrast, pan-neuronal expression of v100 show full rescues (D) and v100^{R755A} expression

in wild type CNS neurons causes little or no defect (F). (G-H) High-resolution confocal sections of 1-day adult mosaic eye with wild type cells to the left and v100R755A expression in v100 mutant cells to the right (using MARCM). Shown are the boxed regions of the data shown at lower resolution in Suppl. Fig. 3A, C. Note that the guidance receptors Dlar and Fas2 accumulate both on Syx7-positive compartments (arrows) as well as on the outer membrane (arrowheads). Scale bar in (A) for (A-F): 20 µm, in (G) for (G-H): 5µm. la: lamina; me: medulla.

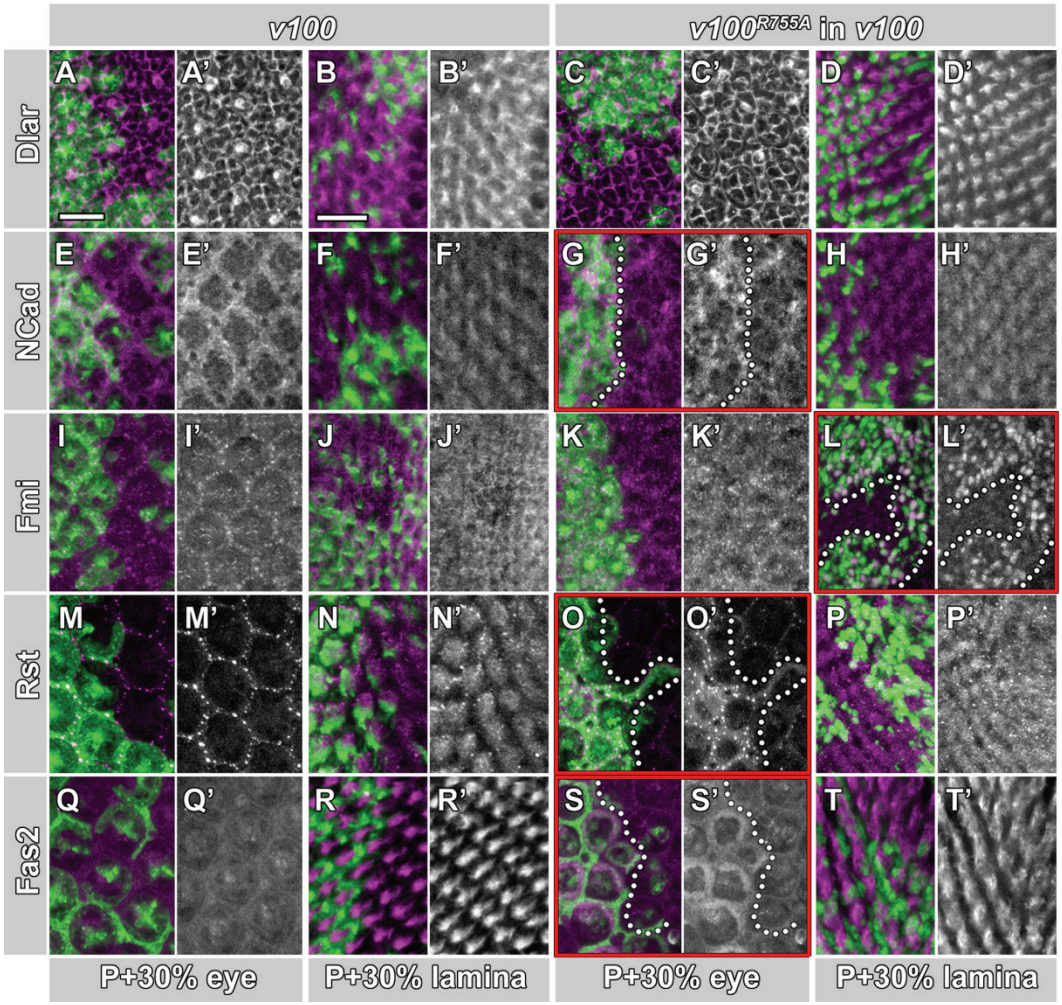

Figure 3.6: Sorting into degradation-incompetent compartments reveals guidance receptor-specific turnover rates.

Confocal images of developing eye discs and laminae at P+30% using *eyFLP*^{PRonly} *MARCM*. GFP marked cells in the four left columns are mutant for *v100*. GFP-labeled cells in the four columns on the right express *v100*^{R755A} in a *v100* mutant background. Unlabeled cells are wild type control in all panels. (A-D) Immunolabeling of Dlar (magenta). Neither loss of v100 (A-B) nor accelerated sorting in degradation-incompetent compartments (C-D) causes obvious Dlar accumulations at P+30% in either the eye (A, C) or at photoreceptor terminals (B, D). Single channels of Dlar immunolabeling shown in (A', B', C', D'). (E-H) Same as (A-D), except immunolabeling of N-Cadherin (magenta). Note that accelerated sorting into degradation-incompetent compartments with *v100*^{R755A} leads to mild N-Cad accumulations in the developing photoreceptor cell bodies (G). (I-L). Immunolabeling of Flamingo; genotypes as before. Note the strong accumulation of Flamingo selectively at photoreceptor terminals expressing *v100*^{R755A} in mutant photoreceptors (L). (M-P) Immunolabeling of Roughest; genotypes as before. Note the strong accumulation of

Roughest selectively in the cell bodies of the developing eye (O). (Q-T) Immunolabeling of Fas2; genotypes as before. Note the strong accumulation of Fas2 selectively in the cell bodies expressing $v100^{R755A}$ in (S). Quantification for experiments marked with red boxes in (G) for NCad show a 1.24-fold increase (+/- 0.04), in (L) for Fmi show a 1.47-fold increase (+/-0.25), in (O) for Rst show a 2.18-fold increase (+/-0.50), and in (S) for Fas2 show a 1.81-fold increase (+/-0.11). Scale bar in (A) for all eye sections in (A-S): 10 μm; in (B) for all lamina sections in (B-T): 10 μm.

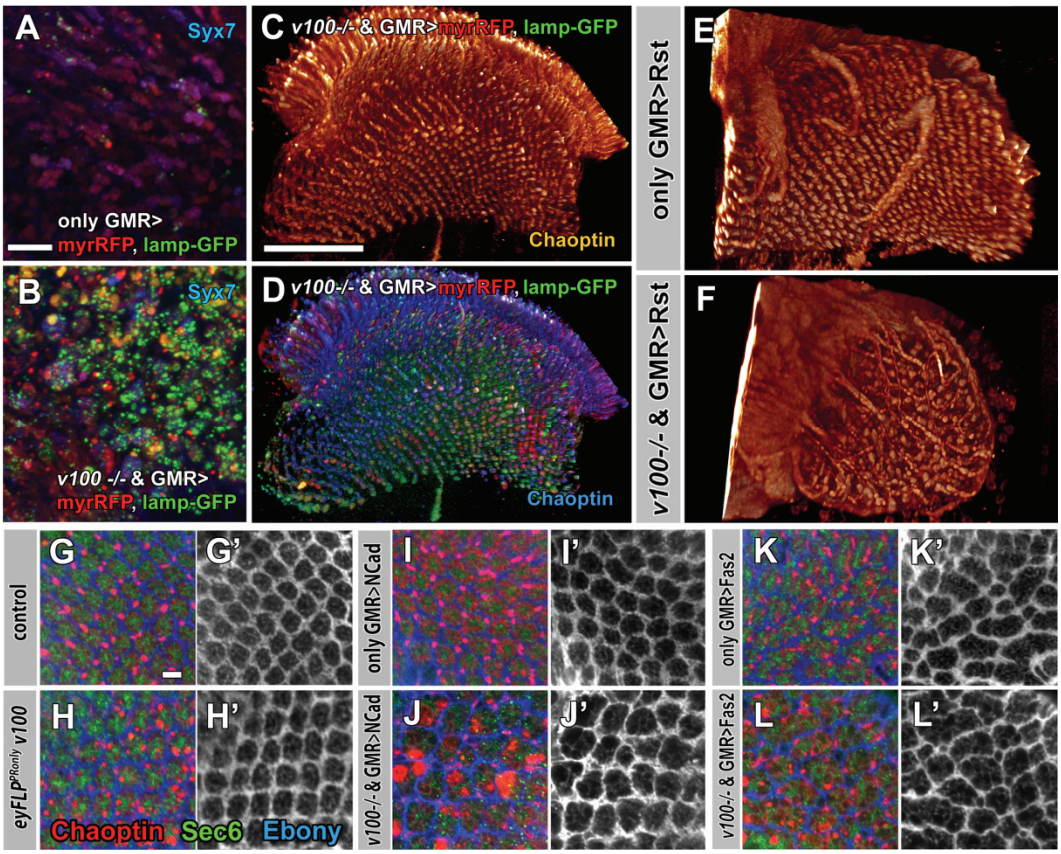

Figure 3.7: Guidance receptors accumulate in signaling-competent compartments in v100 mutant photoreceptors.

(A, B) Adult lamina cross-sections (R1-R6 photoreceptor terminals) of control (A) and *eyFLP*^{PRonly} *v100* photoreceptors terminals. (B) Photoreceptor-specific expression of myristylated RFP (red) and lamp-GFP (green); Blue: Syx7. (C-D) 3D visualizations of R7 and R8 axonal projections of Chaoptin-labeled photoreceptors mutant for *v100* and co-overexpressing both myrRFP and lamp-GFP. Note that both proteins strongly accumulate, but do not cause developmental defects. Single channel in (C). (E-F) 3D visualization of photoreceptor projections expressing the guidance receptor Rst in wild type photoreceptors (E) and *v100* mutant photoreceptors (F). The increase in axon fasciculations and pathfinding defects is a specific exacerbation of the Rst gain-of-function phenotype. (G-L) Confocal images of adult lamina cross sections labeled with Chaoptin (R1-R6 photoreceptors, green), Sec6 (interneurons, red) and Ebony (glia, blue). Control (G) and *eyFLP*^{PRonly} *v100* (H) show normal lamina structure. (I-J) Photoreceptor-specific expression of the guidance receptor NCad has no effect in control (I) but disrupts pattern formation in *v100* mutant photoreceptors (J). Fas2 expression causes mild developmental defects in control (K) that worsen in the mutant (L). Scale bars: in (A) for (A, B): 10µm; in (C) for (C-F): 50µm; in (G) for (G-L): 5µm.

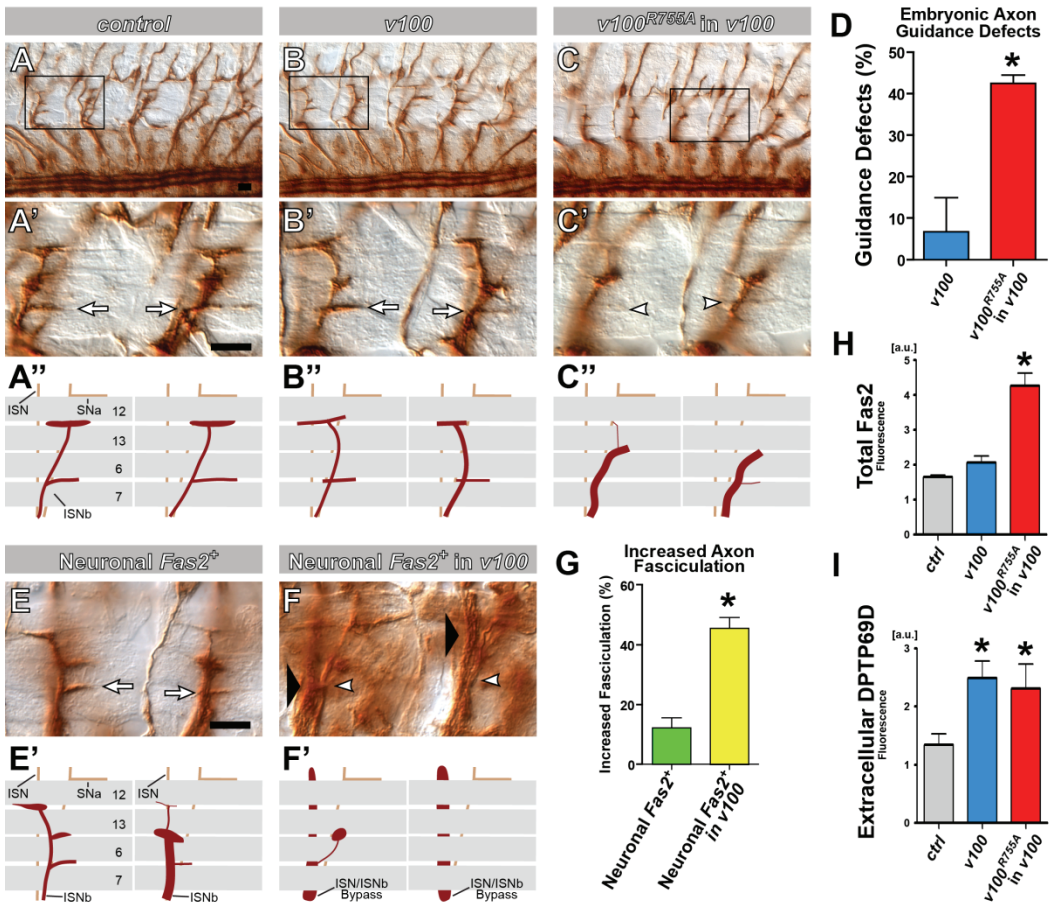

Figure 3.8: V100-dependent guidance receptor accumulations cause gain-of-function defects in the embryo.

(A-C, E-F) Photomicrographs of filleted *Drosophila* embryos stained with the motor axon marker 1D4 (anti-Fas2) where normal innervation (arrows), abnormal innervation (white arrowheads), and increased axon-axon fasciculation "by-pass" defects (large black arrowheads) are demarcated. (A-C) Motor axons within the ISNb axon pathway innervate muscles 6 and 7 normally in control (elav-Gal4 only; A) and in *v100* (B) embryos but show abnormal guidance and targeting in elav> $v100^{R775A}$; *v100* (C) embryos. Boxed regions are shown at higher magnification (A'-C') and are also depicted schematically (A''-C''). (D) The percentage (%) of abnormal muscle 6/7 innervation is shown (normalized to control levels; n>60 hemisegments/genotype) and reveals a statistically significant increase in guidance defects when there is accelerated sorting into degradation-incompetent compartments ($v100^{R775A}$ is expressed in the *v100* mutant background). (E-G) ISNb motor axons were examined in embryos expressing one copy of the Fas2 transgene in all neurons in either a wild-type (E) or a *V100* mutant background (F) and the results reveal that loss of *v100* increases the percentage (%) of abnormal Fas2-mediated ISNb axonal fasciculation events (bypass with the ISN or stall

phenotypes; [(Lin et al., 1994); n>140 hemisegments/genotype). (H) Quantification of Fas2 fluorescence in the embryo for the data shown in Suppl. Fig. 6A-C. Note that this panel is identical to the one in Suppl. Fig. 6G. (I) Quantification of detergent-free immunolabeling of extracellular guidance receptor DPTP69D at the neuromuscular junction. See also images in Suppl. Fig. 7. Asterisks denote statistical significance with P-values <0.01. Scale bars are 10 μm in (A-C, A'-C', E-F). Error bars are SEM; p-value by Student's t-test.

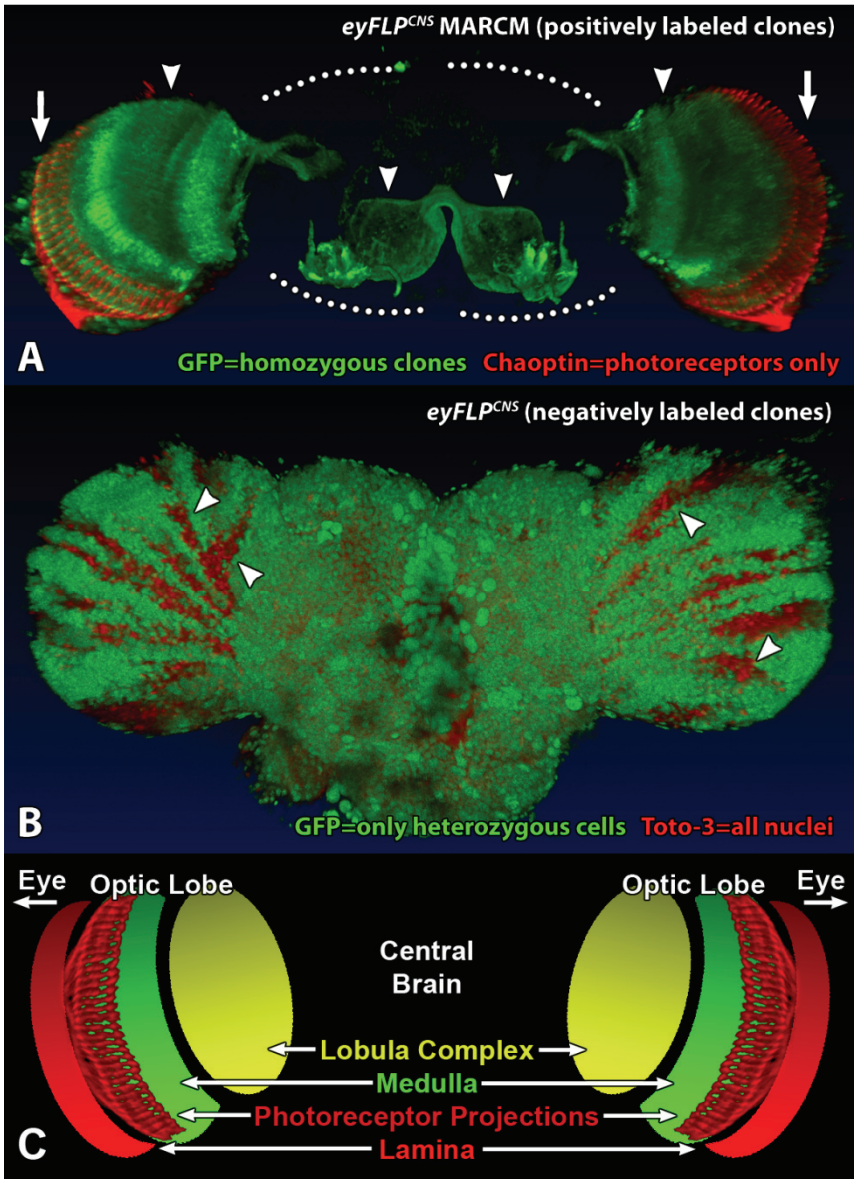

Figure S3.1: The eyFLP system generates mutant CNS neurons selectively in the visual and olfactory systems.

(A) Wholemount adult brain. MARCM analysis labeling 50% of all cells affected by *eyFLP* (Newsome et al., 2000) with GFP (arrowheads). Red: Chaoptin immunolabeling of only the photoreceptors (arrows). These are the cells rendered mutant by the *ey3.5FLP* method (Chotard et al., 2005; Mehta et al., 2005). (B) P+40% pupal *eyFLP* brain in which heterozygous cells are negatively marked with GFP. Note that the nuclear label Toto-3 (red) is only visible in the absence of GFP (arrowheads). (C) Schematic of the optic lobes in th *Drosophila* brain. Lamina and photoreceptor projections are shown in red, medulla in green and the lobula complex (comprised of lobula and lobula plate) in yellow.

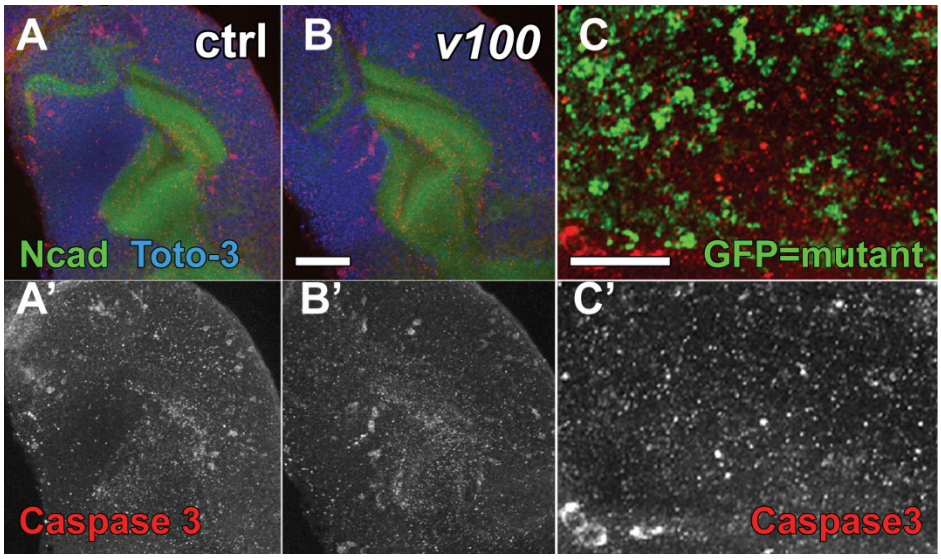

Figure S3.2: Loss of v100 does not cause apoptosis during development or early adulthood.

(A-C) Activated Caspase3 labeling of developing (A, B) and 10-day old (C) optic lobes. (A-B) Immunolabeling of Caspase 3 (red) in P+15% wild type (A) and *eyFLP*^{CNS} *v100* (B) optic lobes reveals no difference in cell death between mutant and control. Green: N-Cadherin (developing neuropil); Blue: Toto-3 (all nuclei). (A' and B' show Caspase 3 channel only). (C) Confocal section of the optic lobe cell bodies of a 10-day old *eyFLP*^{CNS} *v100* MARCM brain. Mutant cell are marked with GFP, Caspase 3 immunolabeling in red; single channel in (C'). Scale bars in (B) for (A-B): 20µm. In (C): 5µm

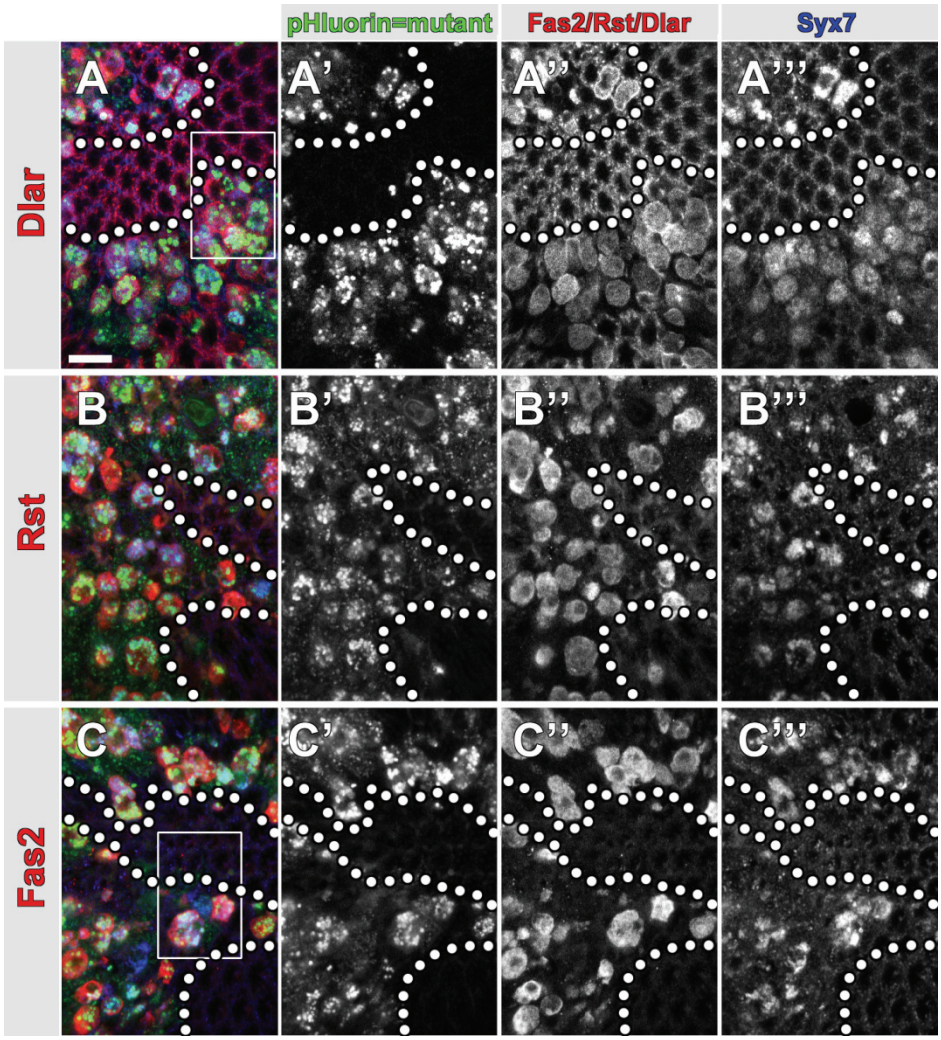

Figure S3.3: $v100^{R755A}$ expression causes heterogeneous guidance receptor accumulations with Syx7-positive membranes and the plasma membrane.

(A-C) Confocal sections of 1-day old mosaic eyes in which 50% are mutant for *v100* and express $v100^{R755A}$ (MARCM), while the other 50% remain wild type. Approximate clonal boundaries are shown with dotted lines. Immunolabeling for the guidance receptor Dlar is shown in (A), for Rst in (B) and Fas2 in (C). The boxed regions in (A) and (C) are shown at higher resolution in Figure 5G-H. Scale Bar in (A) for (A-C): 10µm.

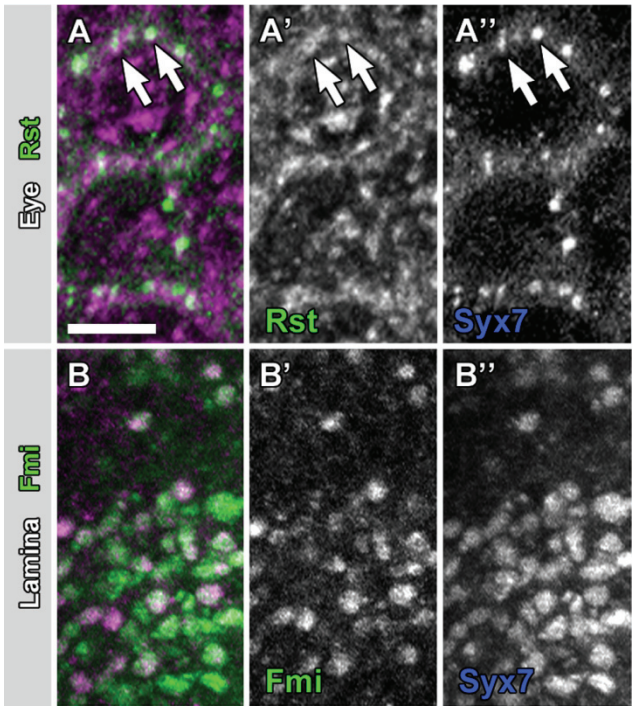

Figure S3.4: Overexpression of guidance receptors in v100 mutant photoreceptors leads to accumulations that partly colocalize with Syx7-positive compartments.

As shown in Figure 6, at P+30% the guidance receptor Rst exhibits the most prominent accumulations in the developing eye, whereas the guidance receptor Flamingo exhibits the most prominent accumulations in photoreceptor terminals. (A) Rst accumulations in the developing eye often partially colocalize with accumulations of the endosomal proteins Syx7 (arrows). (B) Accumulations of Fmi in developing photoreceptor terminals also often partially colocalize with Syx7. Scale Bar in (A) for (A-B): 5µm.

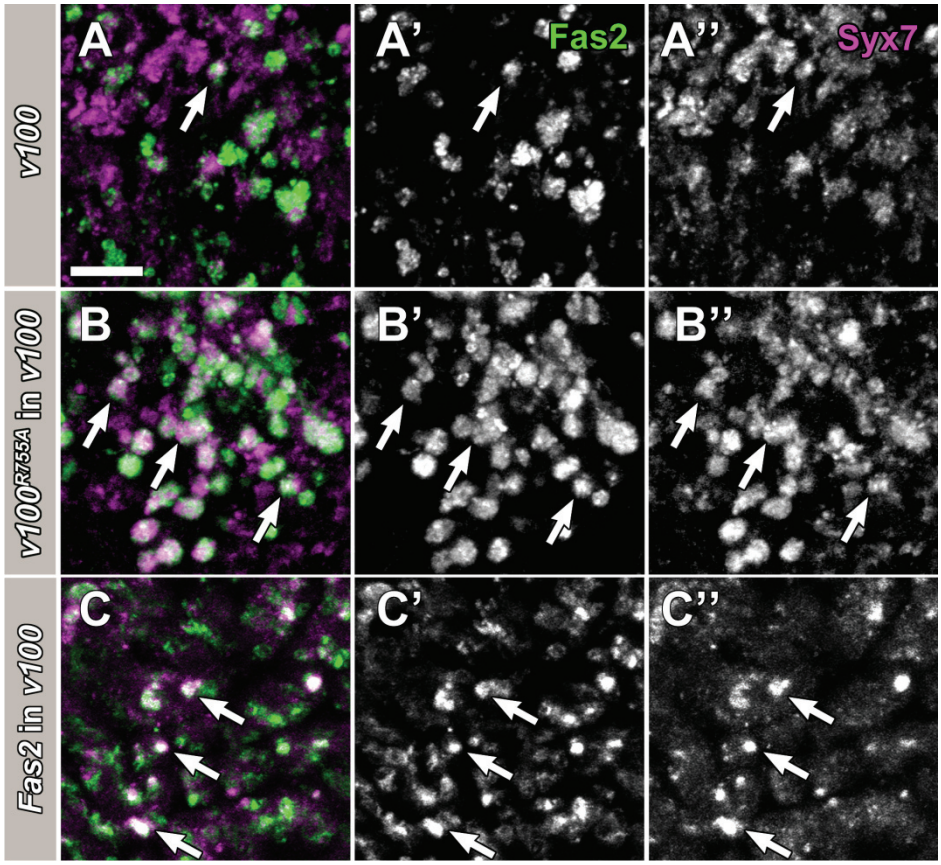

Figure S3.5: Overexpression of $v100^{R755A}$ or the guidance receptor Fas2 cause a similar increase of Fas2 accumulations that colocalize with Syx7-positive endosomal accumulations.

Confocal cross-sections of 1-day photoreceptor terminals in the lamina are shown. Genotypes are shown on the left. (A) Loss of *v100* leads to heterogeneous accumulations of Fas2 that partially colocalize with the endosomal marker Syx7, albeit rarely. (B) Selective rescue of endosomal sorting with $v100^{R755A}$ expression in *v100* mutant neurons leads to an increase of Fas2 accumulations that colocalize with Syx7-positive accumulations. (C) Overexpression of Fas2 in v100 mutant neurons leads to an increase of Fas2 accumulations that colocalize with Syx7-positive accumulations. Scale bar in (A) for (A-C): 5µm.

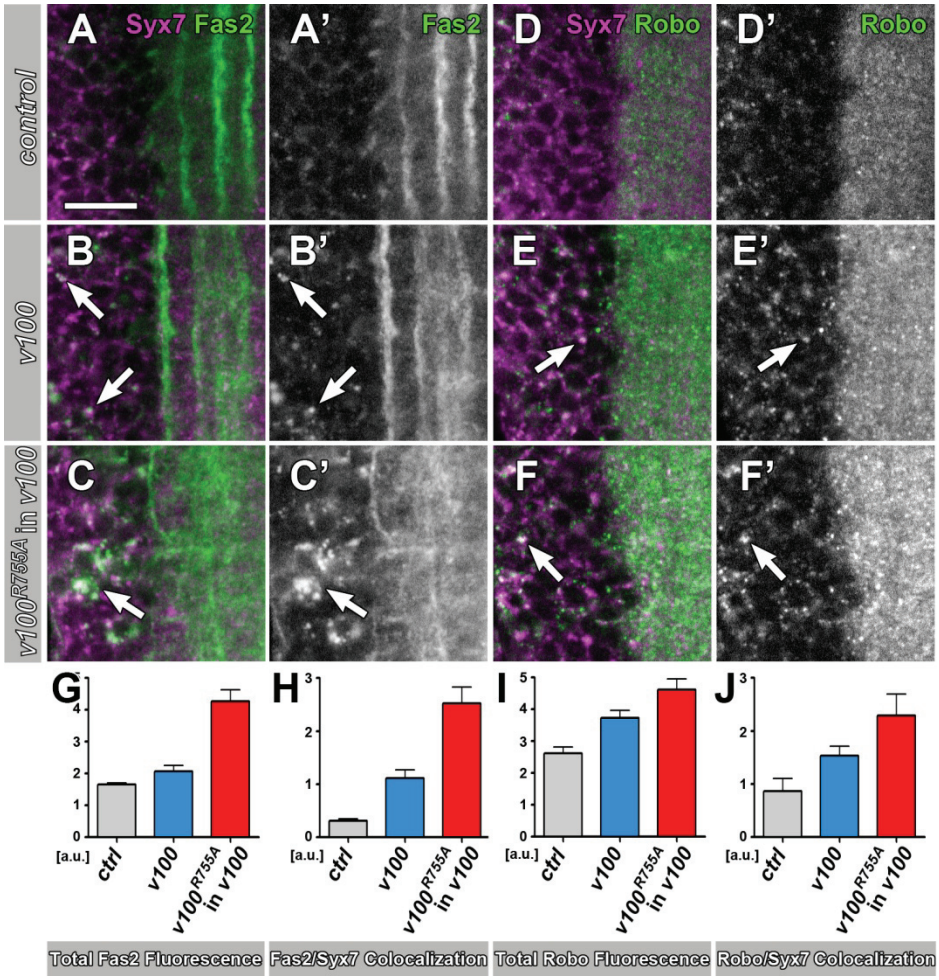

Figure S3.6: Guidance receptors accumulate in Syx7-positive compartments in the embryonic nervous system.

(A-C) Co-immunolabeling for Fas2 and Syx7 of the ventral ganglion with cell bodies to the left. Control is *elav-Gal4* only (A), *v100* null mutant ($v100^{4}/Def$) in (B) and *elav-Gal4>v100R755A;v100/Def* in (C). (D-F) is the same except for Robo immunolabeling instead of Fas2. (G) Total Fas2 immunofluorescence; same panel as in Fig. 8H. (H) Number of co-localizing pixels for Fas2 and Syx7 for all three genotypes. (I-J) same as (G-H) but for Robo immunolabeling. In all cases three independent 3D confocal datasets were quantified. Scale bar in (A) for (A-F) 1µm.

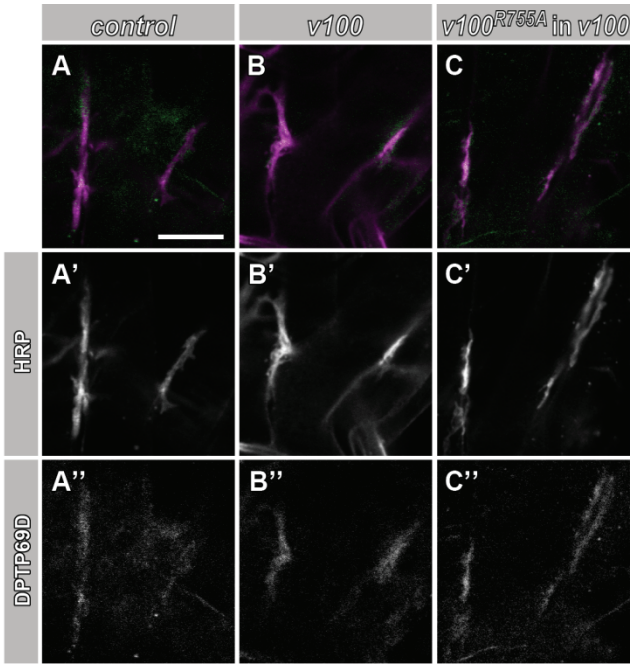

Figure S3.7: Immunolabeling of extracellular DPTP69D reveals no defect in receptor exocytosis.

Confocal sections of embryonic neuromuscular junctions are shown for control (A, elav-Gal4), v100 mutant (B) , and neuronal v100R755A expression in v100 mutant embryos (C). (A', B', C') HRP co-labeling to identify neuromuscular junctions. (A'', B'', C'') DPTP69D channel only. The quantification of this data is shown in Figure 8I. Scale Bar in (A) for (A-C).

CHAPTER FOUR

V0-ATPase subunit a1 regulates vesicle sorting through t-SNARE acceptor complex binding

Dong Wang*, W. Ryan Williamson*, Sankaranarayanan Srinivasan, Daniel Epstein, Florante A. Quiocho, P. Robin Hiesinger * equal contribution

4.1 ABSTRACT

The vesicular ATPase is a multi-subunit proton pump that targets specific membranes via the SNARE-interacting N-terminus of V0a. Here we show that a SNARE-binding deficient variant of the neuronal V0a subunit V100 exhibits defects in neurotransmission and intracellular vesicle sorting. In neurons, V100 binds to the target SNAREs Syntaxin and SNAP25, excluding the vesicle SNARE Synaptobrevin. The V100 N-terminus preferentially binds *in vitro* the helical bundles formed by 'closed' Syntaxin as well as a Syntaxin/SNAP-25 acceptor complex. Binding to this t-SNARE acceptor complex is reduced when Synaptobrevin is present. V100 has a low t-SNARE binding affinity and restricts n-Syb function *in vivo*, suggesting a function prior to v-/t-SNARE complex formation. We propose that the SNARE interaction of V100 exerts an intracellular sorting function, and we show that the V100 N-terminus fused to the C-terminus of the v-SNARE Synaptobrevin is sufficient to execute this function *in vivo*. Taken together, these findings suggest that V100 stabilizes t-SNARE acceptor complexes prior to membrane fusion, a function similar to a growing and heterogeneous group of proteins that includes the Sec1/Munc18-like (SM), Synaptotagmin, and the HOPS complex.

4.2 INTRODUCTION

Spatial and temporal control of neurotransmitter release is accomplished by a series of distinct preparatory events at a neuronal synapse that minimize both the frequency of erroneous release and the activation energy required to induce this energetically unfavorable membrane fusion event (Chen et al., 2001; Sudhof, 2004). Although the core molecular machinery required for membrane fusion is common to other fusion events in cell biology (Jahn and Scheller, 2006a), this high degree of regulation is peculiar to the neuronal synapse and involves highly-conserved molecules that have been intensely studied due to the direct relevance to human neural physiology and ultimately to brain function in general.

The force that results in a single occurrence of synaptic vesicle fusion is generated by complexes of SNARE proteins that form around a point where the synaptic vesicle membrane is in close apposition with the pre-synaptic or 'target' membrane (Sollner et al., 1993). Each SNARE complex must be comprised of SNARE proteins that are anchored in both the synaptic vesicle and the target membrane to form a so-called 'trans'-SNARE complex (Nichols et al., 1997). A SNARE complex contains four coiled-coil 'SNARE motifs,' functional domains that define SNARE proteins. In a trans-SNARE complex, one SNARE motif is donated by the vesicle- (v-) SNARE Synaptobrevin, one from the target- (t-) SNARE Syntaxin1 and two from the t-SNARE SNAP-25, associating to form a trimeric, four-helical bundle with the appropriate topology for synaptic vesicle fusion (Toonen and Verhage, 2007). Following the fusion event, the SNARE complexes are now highly stable in 'cis' on the pre-synaptic membrane. In preparation for another round of vesicle fusion, t-SNAREs must be

dissociated from the 'cis'-SNARE complex and transferred to Synaptobrevin on a synaptic vesicle to form a new 'trans'-SNARE complex with the correct topology (Nichols et al., 1997; Sudhof, 2004). This essential preparatory process involves a growing list of diverse molecules including the Sec1/Munc18-like (SM) proteins, which have the common feature of preferentially binding one or more SNARE proteins prior to trans-SNARE complex formation (Carr and Rizo, 2010; Sudhof and Rothman, 2009).

Syntaxin1 is found in two conformations, 'open' and 'closed' (Chen et al., 2008; Richmond et al., 2001). In its closed conformation, the Habc domain of Syx1 is bound to its SNARE motif and inhibits SNARE complex formation (Dulubova et al., 1999). Physiological evidence suggests that the SM protein Munc18 *promotes* trans-SNARE complex formation, yet it preferentially binds the closed form of Syx1 *in vitro* (Toonen and Verhage, 2007). This molecular data would seem to suggest an inhibitory function. However, a mechanistic explanation was recently proposed, based on a study in mice showing that Munc13 weakly binds the Syx1 SNARE motif and promotes the transition from a closed Syx1/Munc18 complex to a SNARE complex containing open Syx1 (Ma et al., 2011b). Further, it was shown in C. elegans that expression of a constitutively open Syx partially overcomes the impaired synaptic function observed in the Munc13 homolog null (Richmond et al., 2001). Thus, the opening of Syx is required for trans-SNARE complex formation and despite the preferential binding of Munc18 to the closed conformation of Syx1, Munc18 functionally promotes trans-SNARE complex formation. It is known that there are at least two modes of synaptic vesicle release in most CNS and motor neurons: those 'evoked' by an action-potential and 'spontaneous.' Although Syx1 is required for both modes, it is currently not known whether the Munc13/Munc18-mediated opening of Syx1 is sufficient to explain trans-SNARE complex formation for all modes of synaptic vesicle release.

In a forward genetic screen for synaptic function mutants in *Drosophila*, a null allele for the a subunit of the synaptic vesicle V-ATPase was isolated and named v100 (Hiesinger et al., 2005). The V-ATPase is traditionally known to acidify the lumen of synaptic vesicles, generating the proton gradient that drives neurotransmitter antiporters (Forgac, 2007). While loss of v100 does not impair the acidification-dependent process of loading a vesicle with neurotransmitter, Hiesinger et al. demonstrate that loss of v100 does block the acidification-independent exocytosis of neurotransmitter. Additionally, v100 has the acidification-independent role in neuronal cell biology of sorting protein cargo into a neuron-specific endo/lysosomal pathway on which v100 is also required for the acidification-dependent maturation of degradation-competent organelles (Williamson et al., 2010b). Key evidence for these acidification-independent roles in synaptic vesicle exocytosis and endosomal sorting comes from experiments using a mutant form of v100 that specifically disrupts the proton-pumping function of the v100-containing V-ATPase. The targeted mutation of the conserved Arginine-755 to Alanine, 'R755A,' specifically blocks proton translocation without affecting the acidification-independent role in synaptic vesicle exocytosis or in endosomal sorting (Williamson et al., 2010b). The WT V100 protein and the R755A mutant both have two coiled-coil domains in the N-terminus, domains known to interact with SNARE motifs (Fig 1a, Jahn and Scheller, 2006a). Although direct interactions have been demonstrated between the N-terminus of V100 and both the synaptic vesicle target SNARE Syntaxin1 (Hiesinger et al., 2005) as well as the endosomal target SNARE Syntaxin7 (Williamson et al., 2010b), it is not known whether the interactions are functionally relevant or whether the coiled-coil domains mediate the interaction. Additionally, there is currently no mechanistic insight into how the a subunit participates in membrane fusion on a molecular level. Finally, the

lack of structural data on the a subunit adds to the challenge of understanding the molecular mechanism of v100 in membrane fusion.

In this study, we show that mutations in the second of two coiled-coil domains disrupt SNARE interactions in vitro. Identical mutations in vivo produce phenotypes attributable to sorting defects. We show that the N-terminus preferentially forms a complex together with Syntaxin 1A and SNAP-25, excluding Synaptobrevin. Additionally, we find that the V100 N-terminus binds to the closed form of Syntaxin 1A but not the open form. Finally, the N-terminus of V100 is sufficient to confer the acidification-independent function of full-length V100 in vivo. Taken together, these results suggest that V100 plays a role in directly stabilizing SNAREs immediately prior to docking in a fashion similar to known SM proteins.

4.3 RESULTS

4.3.1 Identification of V100's SNARE binding domain and requirement for neurotransmission

We have recently generated a V100 variant that specifically disrupts proton translocation, yet functions in synaptic vesicle exocytosis and endosomal sorting (Williamson et al., 2010a). Based on these results and V100's ability to interact with SNARE proteins, we proposed an acidification-independent function of V100 that is based on N-terminal SNARE interaction. To test this idea we now generated a *v100* mutant that specifically disrupts SNARE binding.

An N-terminal fragment containing two coiled-coil domains is sufficient to bind the t-SNARE Syntaxin1A (Hiesinger et al., 2005) (Figure 4.1a,b). To disrupt potential SNARE interactions mediated by these domains while minimizing the possibility of protein instability, we exchanged the central and most-conserved seven amino acids of each coiled-coil domain to Alanines (Figure 4.1c). We generated three versions of a soluble, His-tagged 180 amino acid N-terminal fragment of V100: WT and two with the coiled coil domains mutated singly (termed V100N-*cc1* and V100N-*cc2* in Figure 4.1d). All proteins are stably expressed in bacteria and are recognized by our V100 antibody (Figure 4.1d). Next, we performed pull-down assays using GST-tagged Syntaxin1A. As sown in Fig. 1d, V100N-*cc1* exhibits mildly reduced binding to Syntaxin1A, while binding of V100N-*cc2* is strongly reduced. This finding suggests that coiled-coil 2 is the Syntaxin1A binding domain.

Next we generated transgenic flies expressing full length V100 proteins with coiled-coil mutations identical to those used *in vitro*, here termed $v100^{cc1}$ and $v100^{cc2}$.

We have previously shown that loss of *v100* causes defects in both neurotransmission and endolysosomal degradation. Expression of the acidification-defective $V100^{R755A}$ partially rescues neurotransmitter release, but not endolysosomal degradation in fly photoreceptor neurons (Williamson et al., 2010a). *Drosophila* photoreceptors are well-suited for the study of both functions *in vivo*, because they are not required for viability, whereas a homozygous mutant central nervous system results in embryonic lethality within hours (Hiesinger et al., 2005). We therefore generated genetic mosaics in which only the photoreceptor neurons are rendered mutant in an otherwise wild type (heterozygous) fly (Mehta et al., 2005; Newsome et al., 2000) (Figure 4.1e) in order to compare the ability of $v100^{cc1}$ and $v100^{cc2}$ to rescue *v100* loss of function defects. As a functional read-out for neurotransmitter release, we performed electroretinogram (ERG) recordings. In this assay, expression of $v100^{cc1}$ fully rescues neurotransmission as assessed by the ERG 'On' transient, while expression of $v100^{cc2}$ exhibits only a very mild rescue. In comparison, the acidification defective $v100^{R755A}$ rescues the 'On' transient by about 50% in the same experiment (Figure 4.1f,g; note that R755A is a C-terminal transmembrane mutation that leaves the V100 N-terminus unaffected). These results indicate that a mutated coiled-coil 2 disrupts V100 function in a manner different from the acidification mutant $v100^{R755A}$. However, these experiments do not directly show a role for V100-SNARE binding at the synapse.

4.3.2 SNARE-binding is required for sorting to synaptic and endosomal membranes

We have previously proposed that V100 functions in endosomal sorting through its interaction with the endosomal Syntaxin7, indicating a role for V100 in neuronal cell biology in addition to its known role on synaptic vesicles (Williamson et al., 2010a). To begin the process of determining the functional relevance of SNARE binding for V100 *in vivo*, we analyzed the subcellular localization of the SNARE-binding deficient V100 and observed reduced labeling at synapses (Figure 4.2 e-g). However, immunolabeling of cell bodies reveals robust V100-cc2 expression and accumulation (FigureS4.1). The study of *v100* function must take into consideration that loss of *v100* causes defects in the endo/lysosomal pathway independently of neurotransmitter release (Williamson et al., 2010a). To determine the effect of the coiled-coil mutations on the previously reported Syntaxin-7 interaction, we performed pull-down experiments with GST-Syx7 in a fashion analogous to those shown in Figure 4.1 for GST-Syx1A. As shown in Figure 4.2a, V100N-*cc1* binds Syx7 at or above wild type levels, whereas V100N-*cc2* exhibits reduced, but not abolished, Syx7 binding *in vitro*.

To assess potential consequences of defective Syx7 binding in comparison with loss of v100-dependent acidification in endosomal trafficking *in vivo* we compared expression of the SNARE-binding defective $v100^{cc2}$ and the acidification-defective $v100^{R755A}$ in mutant photoreceptors. We carried out a quadruple labeling of synaptic terminals in mosaic flies in which 50% of photoreceptors are mutant, positively marked and express either $v100^{R755A}$ or $v100^{cc2}$, while neighboring synaptic terminals remain wild type and express no transgenes, thereby providing a consistent experimental control for all genotypes shown (MARCM technique) (Lee and Luo, 1999). As shown in Figure 4.2b-d, both $v100^{R755A}$ and $v100^{cc2}$expression cause increased accumulations of Syx7 and Chaoptin, an abundant transmembrane cargo protein in photoreceptors, compared to the

v100 loss of function alone (Figure 4.2b'-d''). Since both Chaoptin and Syx7 are transmembrane proteins that traffic through the endo/lysosomal system, these accumulations do not reveal the stage at which their trafficking is blocked. We therefore expressed the cytosolic probe 2xFYVE-GFP which binds to PI3P-rich early endosomal membranes (Wucherpfennig et al., 2003). In *v100* mutant terminals, we observed very few 2xFYVE-positive compartments (Figure 4.2b'''), while expression of $v100^{cc2}$ caused a substantial increase of 2xFYVE-positive early endosomes. In contrast to $v100^{cc2}$, expression of $v100^{R755A}$ has the opposite effect and indicates a complete absence of such early endosomal membranes (Figure 4.2c'''-d'''). The effect is even more striking in cell bodies (Figure S4.1g,l). The loss of early endosomal membranes is consistent with our previous interpretation that $v100^{R755A}$ leads to the accumulation of late-stage, degradation-incompetent compartments. The large numbers of early endosomal PI3P-positive compartments in the $v100^{cc2}$ rescue, however, suggest a defect early in endolysosomal progression that is strikingly distinct from the defects caused by acidification-defective $v100^{R755A}$.

While we detect no V100-CC2 protein at synapses marked by Syx7 and Chaoptin accumulations (arrow in Figure 4.2e-g), levels of V100-R755A in the $v100^{R755A}$ rescue are significantly increased at synapses. Despite the increase in labeling at the cell bodies, V100-CC2 is diffusely distributed in the cytoplasm and does not localize to Syntaxin7 and Chaoptin accumulations (Figure S4.1f-j). In contrast, V100-R755A encircles together with Syntaxin7 large Chaoptin accumulations (Figure S4.1k-o). In the context of the *v100* null and $v100^{R755A}$ phenotypes, these findings suggest that the consequences of the mutations induced in the second coiled-coil include defective Syntaxin-7 binding, a defect in early endosomal localization and progression, as well as a failure to localize at synapses. Since V100 is trafficked on vesicles, both defects suggest an underlying

vesicle delivery problem. In contrast, selective loss of acidification does not affect early trafficking or delivery, but leads to protein accumulations in defective late-stage compartments, as reported previously (Williamson et al., 2010a).

4.3.3 V100 does not bind to the exposed SNARE domain of 'open' Syntaxin

To understand the mechanism of the V100-SNARE interaction in vesicle sorting, we mapped the interaction domain of Syntaxin1A required for V100 binding. We generated a series of Syx1A truncations as shown in Figure 4.3a and performed GST pulldown experiment with the V100 N-terminus. Surprisingly, deletion of either the Syx1A SNARE (H3N) or the Habc domain abolish binding to V100 (Figure 4.3b). Hence, V100N requires both the Habc and SNARE domains for binding and does not bind to Habc domain or the SNARE domain in isolation *in vitro*. This binding profile is suggestive of binding to a 'closed' form of Syntaxin, which requires both domains folded onto each other (Chen et al., 2008; Gerber et al., 2008b).

We designed two experiments to test this idea. First, we generated a constitutively 'open' Syntaxin by mutating conserved residues as previously done for Syx1A in *C. elegans* and mouse (Gerber et al., 2008a; Richmond et al., 2001 and schematic Figure 4.3a). GST pull-downs reveal that, compared to wild type Syx1A, 'open' Syx1A exhibits further increased binding to SNAP25, but no binding to V100 (Figure 4.3d). This finding is remarkable in that the SNARE domain that is exposed in 'open' Syx1A has been shown in numerous studies to exhibit promiscuous binding even to weak and often unspecific proteins (Jahn and Scheller, 2006a). Second, we reasoned that if V100 preferentially binds to closed Syx1A, then the combined presence of Syx1A minus the SNARE domain plus Syx1A minus the Habc domain, neither of which

individually bind V100, may reconstitute a 'closed' Syntaxin by pair-wise interaction of the two Syx1A mutants, thereby restoring the V100 interaction. Indeed, as shown in Figure 4.3e, addition of GST-Syx1A-ΔHbc and GST-Syx1A-ΔSNARE together before binding to beads, but neither alone, pulls down His-V100N. Taken together these results suggest that V100N does not bind to the Syx1A SNARE domain or Habc domain individually, but rather to the 'closed' confirmation of Syx1A, i.e. a helical bundle, *in vitro*.

4.3.4 V100 preferentially binds to a SNAP25/Syx1A t-SNARE acceptor complex

We next designed experiments to test V100 binding to full and partial ternary SNARE complexes *in vitro* and *in vivo*. First, we performed GST pull-down experiments using GST-Syx1A and different combinations of His-tagged n-Syb, Snap25 and V100N (Figure 4.4a). Consistent with previous experiments, Syx1A pulls down SNAP25 alone, V100N alone as well as SNAP25 and V100N together. Also consistent with previous findings, n-Syb pull-down by Syx1A is weak, but enhanced by addition of SNAP25. In contrast, addition of V100N does not improve the n-Syb pull-down by Syx1A. These results suggest that the interaction of V100N with Syx1A is of a different nature than the SNAP25 interaction with Syx1A. Interestingly, we find that significantly more V100N is pulled down by Syx1A when SNAP25 is added compared to addition of both SNAP25 and n-Syb, i.e. a ternary SNARE complex. Hence, addition of n-Syb effectively reduces binding of V100N to t-SNAREs. This finding suggests that V100N binding to a t-SNARE complex is stronger than to a ternary SNARE complex containing n-Syb. It further suggests that binding of n-Syb to t-SNAREs is stronger than binding of V100N to t-SNAREs.

t-SNARE complexes are thought to primarily reside on target membranes where they serve as acceptor complexes for vesicles containing cognate v-SNAREs as well as a heterogeneous group of unrelated docking and tethering factors that can stabilize the acceptor complex prior to receiving a v-SNARE (de Wit et al., 2009; Dun et al., 2010; Weninger et al., 2008). V100N binding to specific t-SNARE acceptor complexes therefore provides a potential mechanism for the observed SNARE-dependent vesicle sorting function of V100. We therefore designed an experiment to independently and rigorously test this idea by measuring V100N interaction with various SNARE combinations using fluorescein (FM) tagging. Specifically, we covalently linked an N-terminal fragment from V100 that contains coiled-coil 2 (E84 to E141) with FM, which exhibits an increase in fluorescence upon complex formation with SNAREs. On excitation at 495nm, CC2-FM has an emission maximum at 520nm (Figure 4.4a). Addition of a molar excess of Syntaxin1A increases the fluorescence emission significantly, indicative of binding to CC2-FM (Figure 4.4b). The addition of the other t-SNARE components SNAP25N and SNAP25C at similar concentrations causes a further increase in binding (Figure 4.4b, red graphs). In contrast, addition of CC2-FM to a pre-formed complex of SNARE that includes n-Syb, shows a much weaker increase in intensity compared to CC2-FM binding to t-SNAREs only. These results indicate that the CC2 fragment exhibits the strongest binding when Syx1A and SNAP25 are simultaneously present, slightly reduced binding affinity to Syx1A alone, but significantly reduced binding affinity when V100 is added to a preformed ternary SNARE complex that includes n-Syb. Hence, these data independently corroborate that V100 preferentially binds to a t-SNARE complex containing both Syntaxin1A and SNAP25.

Next, we determined the binding affinity of CC2-FM to Syx1A using the change in fluorescence, on addition of Syx1A. Fitting of the titration curve yielded an apparent dissociation constant K_d of 0.17μM (Figure 4.4c). This value indicates a low affinity binding of Syx1A to CC2-FM. Since the change in fluorescence is observed only after overnight incubation, both the k_{on} and k_{off} rates of this interaction might be slow, as has been observed previously for *in vitro* t-SNARE interactions (Pobbati et al., 2006). Low affinity binding is consistent with the finding that V100 does not bind to the exposed t-SNARE domain in the manner of a v-SNARE (Figure 4.3d) and the identification of n-Syb as a stronger competitor in the GST-Syx1A pull down (Figure 4.4a). Low affinity binding is further consistent with a transient role in docking or tethering. All taken together, our *in vitro* binding studies pinpoint a role for V100N in binding a t-SNARE acceptor complex prior to n-Syb that potentially underlies its vesicle sorting function.

Our *in vitro* findings predict that endogenous V100 in neurons should only exist in a complex with t-SNAREs under exclusion of n-Syb. To test this idea, we performed co-immunoprecipitations (co-IPs) with anti-V100 antibody from wild type fly brain protein extracts. As shown in Figure 4.4d, V100 co-immunoprecipitates both t-SNAREs Syntaxin1A and SNAP25 from fly brain extract, but not the v-SNARE n-Syb. In contrast, a Syx1A antibody co-immunoprecipitates all members of the v-/t-SNARE complex (Figure 4.4d). The co-IP result suggests that V100 exists as a V100/t-SNARE complex under exclusion of n-Syb in the fly brain. Taken together, our in vitro and in vivo findings are most consistent with a model in which V100 binding precedes v-SNARE binding.

4.3.5 V100 restricts n-Syb function in vivo

If the role for V100 in trans-SNARE assembly is to stabilize the t-SNARE acceptor complex in preparation for a transfer to synaptobrevin, we reasoned that over-expression of *n-syb* might overcome the instability of t-SNARE complexes induced by loss of *v100*. In this model, over-expression of n-syb may partially rescue the defects in neuronal function or vesicle sorting present in the *v100* null. Overexpression of *n-syb* does not rescue neurotransmission, endolysosomal trafficking or neurodegeneration in *v100* mutant photoreceptors, as predicted by the different modes of t-SNARE binding (Figure 4.5a-c and data not shown). However, quantification of photoreceptor depolarization confirms that depolarization is reduced in *v100* mutant photoreceptors expressing *n-syb*, compared to control, *n-syb* overexpression and the *v100* mutant alone (Figure 4.5c). A reduced ERG depolarization correlates with diminished photoreceptor function or health.

Immunohistochemical analysis reveals that *n-syb* overexpression in *v100* mutant photoreceptors causes an intracellular sorting defect that is absent from the *v100* mutant (Figure 4.5e) as well as *n-syb* overexpression alone (Figure 4.5f). Subcellular Chaoptin localization as an assay for cargo sorting reveals that *n-syb* overexpression in *v100* mutant photoreceptor terminals results in a prominent mislocalization of this membrane protein on the plasma membrane (Figure 4.5d-g). Interestingly, this is the opposite phenotype to the one previously reported for $v100^{R755A}$, where Chaoptin accumulations are found within Syx7 compartments (Figure 4.5h and (Williamson et al., 2010a).)

These observations indicate that n-Syb overexpression leads to increased membrane protein exocytosis only in the absence of V100. The finding thereby suggests that the presence of V100 prevents overexpressed n-Syb from increasing exocytosis and are best explained with a restrictive role of V100 for n-Syb function. Taken together with low affinity binding to Syx1A and reduced binding of V100N to t-SNARE acceptor

complexes upon addition of n-Syb lead us to hypothesize that V100N binds to t-SNARE acceptor complexes prior to n-Syb. Hence, our *in vitro* and *in vivo* findings consistently support a model in which binding to t-SNARE acceptor complexes recruits V100, and thereby the vesicle it resides on, to specific target membranes prior to v-/t-SNARE complex formation.

4.3.6 The SNARE-interacting V100 N-terminus is sufficient for sorting

Our findings suggest that the V100 N-terminus is sufficient to regulate vesicle sorting via t-SNARE interaction independent of acidification. To test the independence of the a subunit SNARE-binding N-terminus directly, we designed a chimeric protein that contains only the cytoplasmic V100 N-terminus fused to the transmembrane C-terminus of the vesicle SNARE n-Syb (Figure 4.6a). Remarkably, low level expression of the V100N::n-Syb chimera in *v100* mutant photoreceptors partially rescues neurotransmitter release to a similar extent as $v100^{R755A}$, as shown by a 50% rescue of the ERG 'on' transient (Figure 4.6b). Furthermore, we have previously reported that an ambient temperature-induced increase of $v100^{R755A}$ expression in *v100* mutant neurons leads to premature cell death during eye development (Williamson et al., 2010a). In a manner indistinguishable from $v100^{R755A}$, V100N::n-Syb expression at low levels leads to eye roughness (Figure 4.6d-i) while increasing levels in a *v100* mutant background leads to cell death (data not shown). In these experiments, expression levels of the V100 variants was controlled by temperature using the Gal4/UAS system and calibrated based on immunohistochemistry (data not shown). Correlating with worsened eye roughness, both *v100N::n-Syb* and $v100^{R755A}$ rescue the ERG 'on' transient to a lesser extent as expression levels increase (Figure 4.6c). In contrast, increased expression levels of $v100^{cc2}$ restore the 'on' transient to 25% wild type (Figure 4.6c). This finding is consistent with the

biochemical finding that SNARE interaction is not completely abolished by the mutation of seven amino acids to Alanine in coiled-coil 2 (comp. Figure 4.1d and 4.2a). Indeed, strongly overexpressed *V100*^{cc2} leads to protein levels detectable immunohistochemically at synapses (Figure S4.2).

In summary, our findings indicate that V100N::n-Syb closely mimicks the effects of V100^{R755A}, consistent with the notion that both proteins contain an intact SNARE-interacting N-terminus while losing the ability to acidify. Additionally, V100N::n-Syb exerts this effect in the absence of the other Vo subunits, suggesting that the SNARE-interacting N-terminus acts independently from the entire V-ATPase. Collectively with the *in vitro* biochemistry, our results suggest that the V100 N-terminus, independent of the v-ATPase, is sufficient to exert a sorting function by binding to t-SNARE acceptor complexes.

4.4 DISCUSSION

Mutations generated in the second coiled-coil domain of v100 abolish SNARE binding *in vitro* (Fig. 4.1d) and cause phenotypes *in vivo* that are distinct from those observed in both the v100 null and in the acidification deficient R755A mutant (Fig 4.1g, Fig. 4.2, Fig. S4.1) . These observations give credence to the claim that v100 has a second function in addition to acidification. Although much is known about the molecular mechanism for the acidification function of the V-ATPase, very little is known about the mechanism for a role in membrane fusion. In this study, we provide evidence that SNARE interactions are required for the acidification-independent function of v100, we show that the V100 N-terminus preferentially binds the closed form of Syntaxin1A (Fig. 4.3) and binds a t-SNARE complex under exclusion of Synaptobrevin (Fig 4.4). Functionally, loss of the acidification-independent role of v100 results in sorting defects *in vivo* (Fig. 4.2) and permits synaptobrevin mis-expression phenotypes that are absent in wild type (Fig. 4.5). Taken together, these results are consistent with a molecular mechanism where v100 associates with and prepares t-SNAREs for trans-SNARE complex formation.

4.4.1 Neurotransmission in Drosophila photoreceptors requires a V100/SNARE interaction

In an attempt to disrupt the documented interaction between Syx1 and the V100 N-terminus (Hiesinger et al., 2005), we induced mutations within both coiled-coil regions located in the N-terminal fragment and demonstrate *in vitro* that the mutations in CC2 result in a reduced interaction with Syx1 compared to the control v100 fragment (Fig. 4.1). Mutations in CC1 have no effect. Physiological data from transgenic flies expressing a version of v100 that has identical mutations in CC2 fails to restore

neurotransmission in photoreceptor cells, a defect present in the v100 null and restored to 50% in flies expressing v100-R755A (Fig. 4.1g). This observation in CC2 could be explained by either a defect specifically in exocytosis at the synapse or by mislocalization of V100-CC2. Immunolabeling in genetic mosaics indicates that indeed V100-CC2 does not reach the synapse when reared at room temperature (Fig. 4.2e-g'). However, flies reared at 25°C express V100-CC2 at higher levels and exhibit proper localization of V100-CC2 to the synapse (Fig. S4.2). Despite proper localization, neurotransmission is only restored to 25%, while 50% restoration is achieved by V100-R755A, a variant that possesses a wild type N-terminus. The partial rescue by CC2 is consistent with the observation that the Sxy1 interaction *in vitro* is reduced but not abolished.

4.4.2 V100 actively sorts proteinaceous cargo into a degradation pathway

The V100-CC2 mutation reduces a previously documented Syx7 interaction *in vitro* (Fig. 4.2a). Additionally, it has been shown that these two proteins are in complex *in vivo* and that V100 functions to sort cargo into Syx7-positive compartments (Williamson et al., 2010b). Ultimately, the acidification function of V100 is required to degrade this cargo, and specific disruption of acidification by expressing V100-R755A results in an exacerbated cargo accumulation phenotype relative to the *v100* null. While V100-R755A restores the V100 N-terminal-mediated sorting role, late-stage degradation compartments remain immature due to defective acidification. In this study, we confirm for V100-R755A that cargo accumulates within compartments positive for both Syx7 and V100 (Fig. S4.1o). Although Syx7 is a known early endosomal marker in *Drosophila*, the V100-R755A variant probably exhibits late-stage accumulations of Syx7 due to the fact that Syx7 is integrated into the membrane and therefore at the mercy of membrane trafficking. Consistent with this, we find for V100-R755A that the Syx7 accumulations

are negative for the Early endosome antigen-containing 2xFYVE-GFP, which labels early endosomes based on their lipidic characteristics (Fig. S4.2l).

We used the MARCM system to compare 2xFYVE levels in tissue where V100 has mutations versus contol tissue in a single genetically mosaic eye. We compared V100-R755A versus control to the v100 null versus control. Relative to identical controls, we observe a marked reduction in 2xFYVE labeling when V100-R755A is expressed compared to the v100 null (Fig. S4.1b, l), indicating an active role for the functional N-terminus of V100-R755A. By expressing V100-CC2, which contains the mutations that disrupt Syx7 interactions *in vitro*, we now observe the accumulation the early endosomal marker 2xFYVE-GFP (Fig. 4.2c''' and S4.1g). A similar MARCM experiment as described above reveals that the 2xFYVE accumulations are markedly increased versus the v100 null, opposite to the observation for V100-R755A. These results are collectively consistent with a model where V100 interacts with Syx7 to actively sort proteinaceous cargo into an endo/lysosomal pathway. Specifically blocking the early endosomal V100 sorting step results in the accumulation of early endosomal antigen 2xFYVE-GFP, whereas specifically blocking the acidification role of V100 without disrupting the fusion role results in the accumulation of undegraded cargo in late-stage, degradation-incompetent organelles.

4.4.3 The V100 N-terminal fragment preferential binding to 'closed' Syntaxin1 may provide insight into a molecular mechanism

After establishing a functionally-relevant requirement for the second coiled-coil domain in the V100 N-terminus and after determining that mutations in CC2 disrupt Syx1 interactions *in vitro*, we mapped the site on Syx1 that is required for V100

interactions. We observed a V100 N-terminal interaction with full-length Syx1, but not isolated Syx1-Habc domain or the Syx1-H3 domain (Fig. 4.3). However, experimental conditions where both the Habc domain fragment and the H3 domain fragment are present restore binding to the V100 N-terminus (Fig. 4.3e). Perhaps the V100 N-terminal fragment preferentially interacts with 'closed' Syx1. Indeed, mutations in conserved Syx1 residues previously known to render Syx1 constitutively 'open' block the Syx1, V100 N-term interaction (Fig. 4.3c). Munc18 also binds closed Syx1 and is required for synaptic vesicle exocytosis by promoting trans-SNARE complex formation through the regulated opening of Syx1, a process mediated by Munc13 (Ma et al., 2011b).

Our findings represent a first look into the molecular mechanism of the acidification-independent sorting function of the Vo-ATPase. Additional work will be necessary to determine the precise step in the process of trans-SNARE complex formation where V100 interacts with SNAREs. This may be more easily accomplished in motor or CNS neurons where synaptic function can be carefully monitored in response to evoked action potential, whereas *Drosophila* photoreceptor cells exhibit graded potentials and tonic neurotransmitter release. Additionally, it is not known whether Syx7 can assume a 'closed' conformation, or to what degree the mechanism of V100 in cargo sorting may be similar to its mechanism at the synapse.

4.4.4 The V100 N-terminus is sufficient to restore sorting in Drosophila photoreceptors

A recent study in mice proposes a role for the Vo sector c subunits in synaptic vesicle exocytosis (Di Giovanni et al., 2010). The authors show that a cytosolic fragment of the c subunit loop 3.4 directly interacts with synaptobrevin, an interaction that can interfere with neurotransmitter release when soluble fragments are present in the cytosol.

Additionally, mutations in the Vo d subunit have been shown to disrupt osteoclast fusion in mice (Lee et al., 2006). We tested the sufficiency of the *Drosophila* a1 subunit N-terminus, the V100 N-terminus, to restore the acidification-independent role of V100 in photoreceptor neurotransmission. Knowing that the Vo sector is unstable without the a subunit (Ma et al., 2011a), we reasoned that this manipulation would result in the absence of an a1 subunit-containing Vo sector while targeting the N-terminus of V100 to the synapse by fusing it to the synaptobrevin transmembrane domain. This genetic manipulation did retain the acidification defects observed for R755A (data not shown) and restored the sorting role for V100 in a similar manner as R755A (Fig 4.6). These results indicate that the other Vo sector subunits are dispensable for neurotransmission and cargo sorting in *Drosophila* photoreceptors. However, this is not inconsistent with previous findings for other subunits, since the sensory cell type in which we have conducted our study is distinct from CNS synapses or motor neuron end plates where synchronous neurotransmitter release occurs following an action potential.

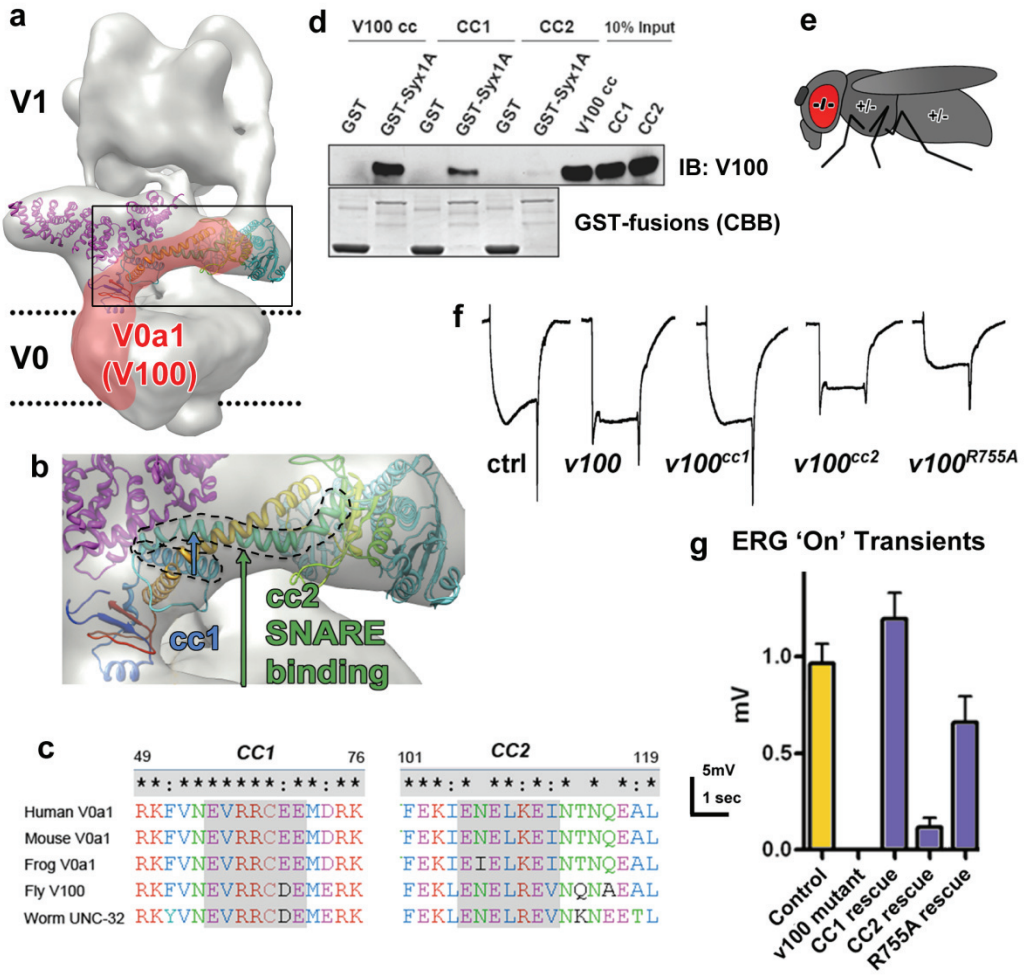

Figure 4.1: Identification of V100's SNARE binding domain and requirement for neurotransmission

(a) Overlay of a best-fit volume of the Drosophila a1 subunit V100 (red) onto the 17-A cryo-EM reconstruction of the *M. sexta* V-ATPase. Also shown are crystal structures of the yeast subunits H (magenta) and C (cyan), as well as the recently solved N-terminal domain of an a subunit homolog, subunit "I" from *Meiothermus ruber*. (b) Enlarged region inside the box in (a) with arrows directed to coiled-coil regions on the *M. ruber* I subunit which correspond to the CC1 and CC2 mutations we induced in v100. (c) Conserved residues mutated within CC1 and CC2. (d) GST-Syx1 pulldown, probing with anti-V100. (e) Schematic of the genetic mosaics used for v100 null photoreceptor analysis, a heterozygous fly supports homozygous mutant photoreceptor cells. (f) Sample traces from electroretinogram (ERG) recordings. (g) Quantified ERG results.

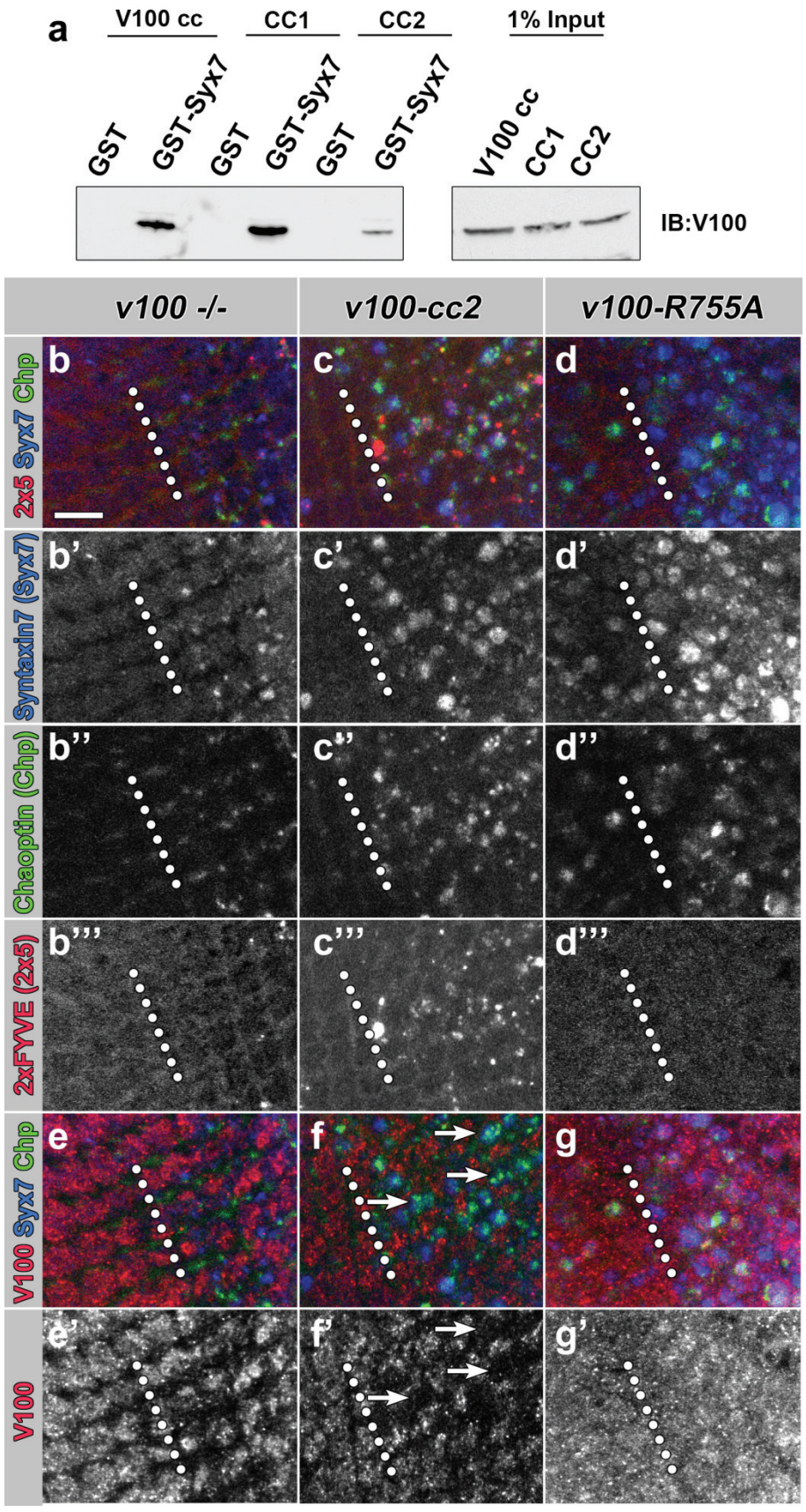
a
V100 cc
CC1
CC2
1% Input
GST
GST-Syx7
GST
GST-Syx7
GST
GST-Syx7
V100 cc
CC1
CC2
IB:V100
v100 -/-
v100-cc2
v100-R755A
2x5 Syx7 Chp
Syntaxin7 (Syx7)
Chaoptin (Chp)
2xFYVE (2x5)
V100 Syx7 Chp
V100
b
c
d
b'
c'
d'
b''
c''
d''
b'''
c'''
d'''
e
f
g
e'
f'
g'

Figure 4.2: SNARE-binding is required for sorting to synaptic and endosomal membranes.

(a) A similar GST-pulldown as in Figure 4.1, except here we use GST-Syx7, the endosomal target SNARE. (b-g') Immunolabeling of a field of axon-terminals, depicted in cross-sections through the lamina, with color-coded labels to the right on the figure. In these MARCM clones, mutant and/or transgene-expressing flies are positively labeled with 2xFYVE-GFP. Arrows highlight the presence of accumulations in $v100^{CC2}$ under the exclusion of V100 labeling.

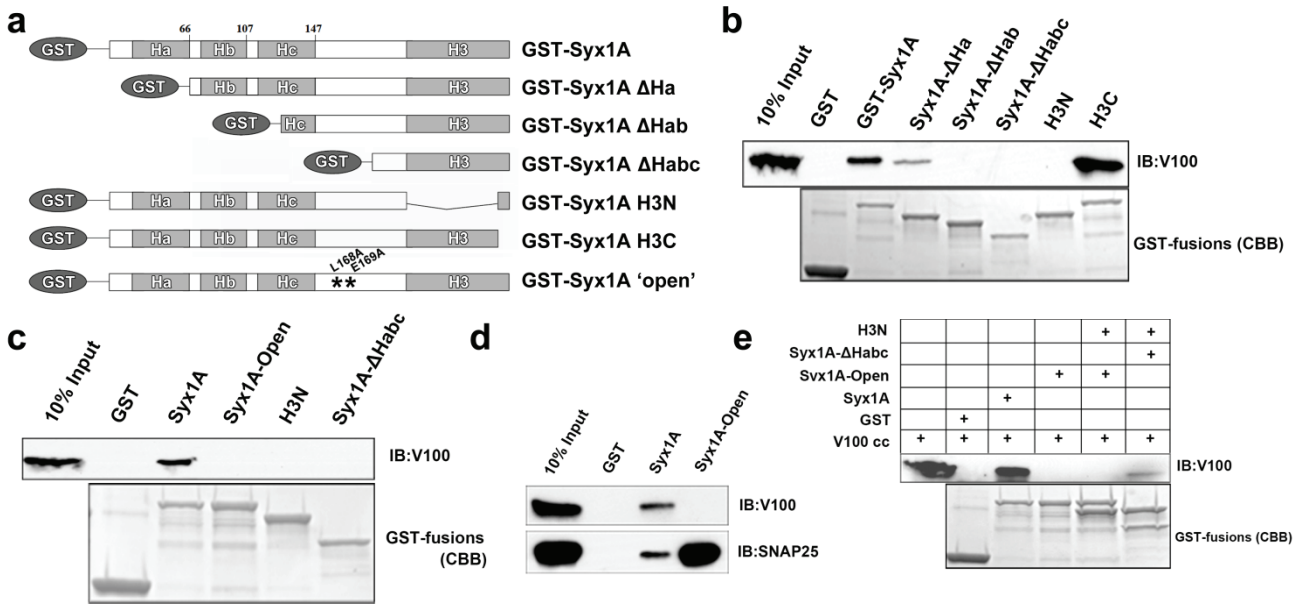

Figure 4.3: V100 does not bind to the exposed SNARE domain of 'open' Syntaxin

(a) Schematic illustrating the protein fragments used in b-e. (b) GST-pulldowns from bacterially made protein fragments as illustrated in (a). Syx1 missing Habc fails to bind V100, as does Syx1 without H3N, while full-length Syx1 binds. (c) GST-pulldowns as before, but including full-length, constitutively 'open' Syx1 that also fails to bind. (d) Positive control for 'open'-Syx1, demonstrating SNAP25 can bind. (e) Simultaneous presentation of Syx1 with either Habc or H3N deletions binds V100, while singly they do not.

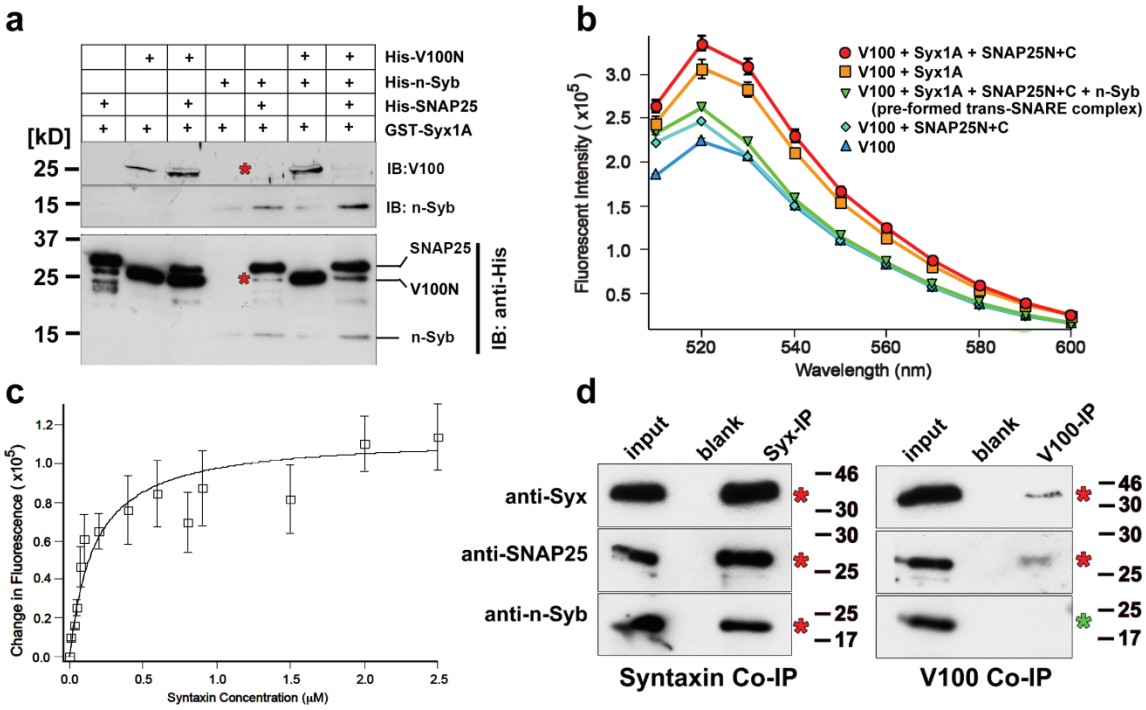

Figure 4.4: V100 preferentially binds to a SNAP25/Syx1A t-SNARE acceptor complex

(a) GST-pulldowns using bacterially made protein to determine binding preference in the context of synaptic vesicle v/t-SNARE protein as well as the V100 N-terminus. nSyb has a higher affinity for t-SNAREs than V100, although V100 strongly binds t-SNAREs when nSyb is absent. (b) Fluorescence anisometry analysis of hierarchical binding preferences among the SNARE and fluorescein-labeled V100 (CC2 domain isolated). Results are consistent as in (a). (c) Analysis of binding affinity between V100(CC2 only) and Syx1. (d) Coimmunoprecipitation from adult brain isolate, demonstrating the existence of a V100/t-SNARE complex under the exclusion of nSyb.

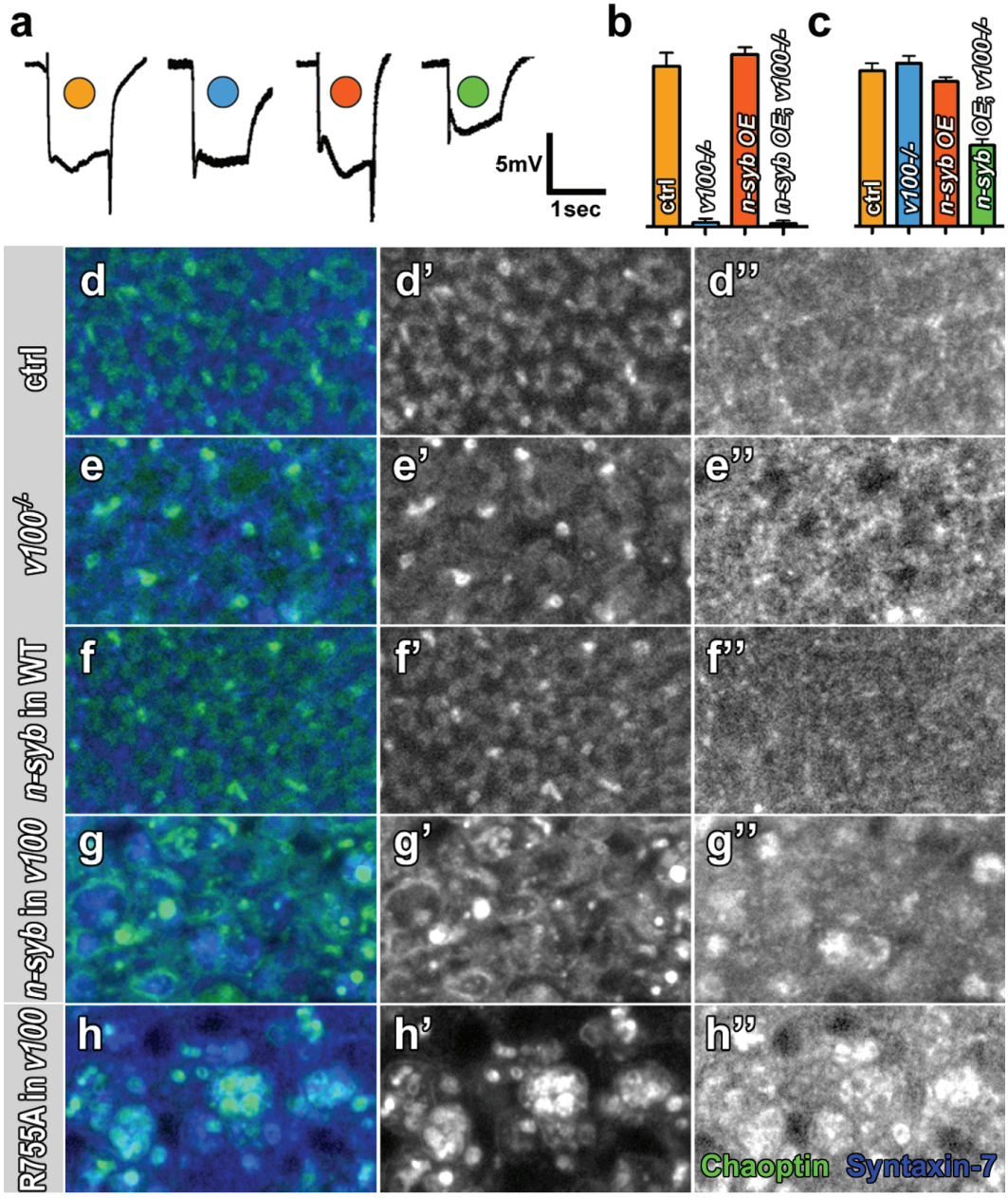

Figure 4.5: V100 restricts n-Syb function in vivo

(a) Electroretinogram (ERG) raw records from control and photoreceptor-specific v100 nulls both with and without photoreceptor-specific nSyb expression. (b-c) Quantification from (a). nSyb fails to rescue neurotransmission (b), however, v100 null photoreceptors indicate a decline in health when also expressing nSyb (c). (d-h'') Immunolabeling with anti-Chaoptin (grn) and –Syntaxin (blu) of photoreceptor terminals, shown as a cross-section through the lamina. In v100 null photoreceptors, nSyb expression drives Chaoptin to compartment or cell perimeters, while R755A develops centrally located protein aggregates.

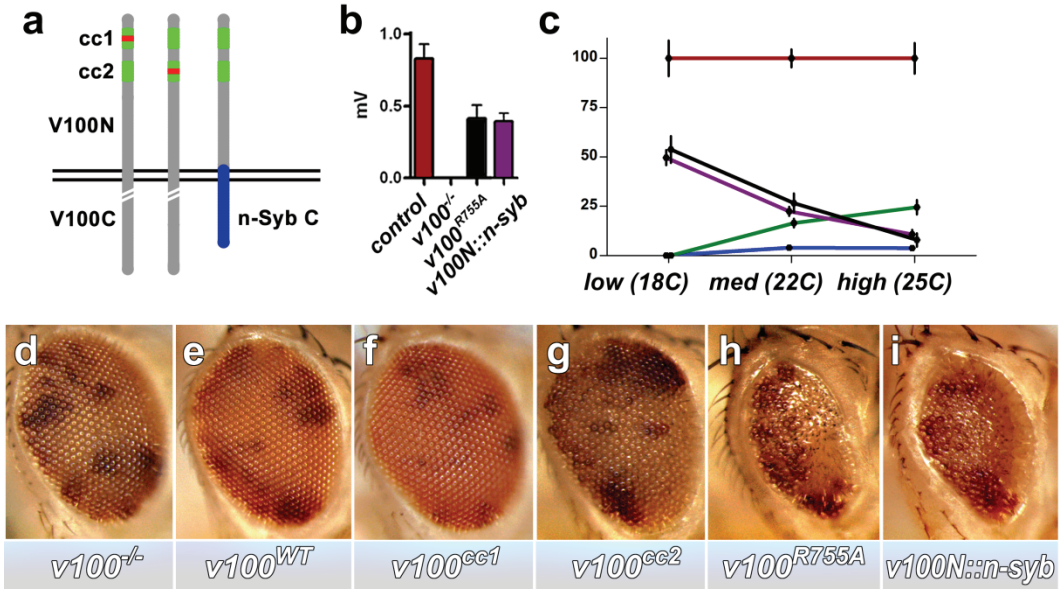

Figure 4.6: The SNARE-interacting V100 N-terminus is sufficient for sorting

(a) Graphical representation of the CC1 and CC2 mutations, as well as the V100 N-terminus/nSyb-transmembrane domain chimera (V100::n-syb). (b) The V100::n-syb construct is sufficient to restore neurotransmission in the v100 null. (c) Quantified ERG 'on' transients from animals reared at low, medium, and high temperatures, a direct correlate of the temperature-influenced gal-4/UAS system. (d-i) Eye pictures representative of the genetic background indicated. As temperatures increase, eye morphology worsens for R755A and V100::n-syb, while CC2 demonstrates moderate improvement in neurotransmission.

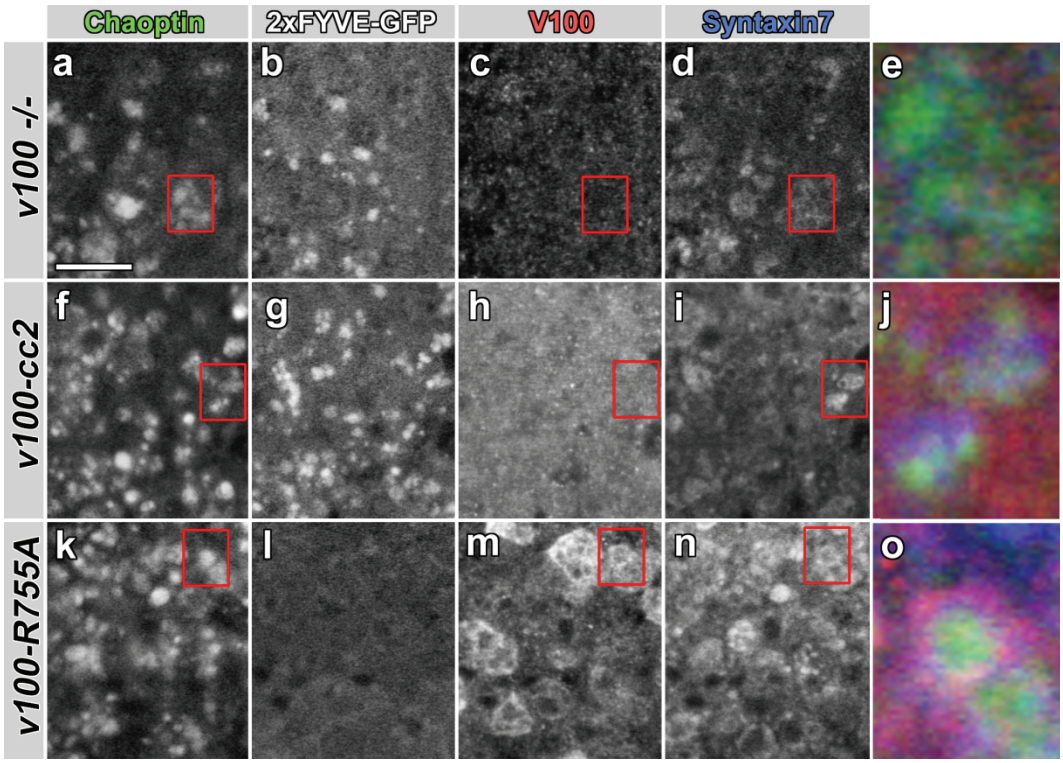

Figure S4.1: Relative to the v100 null, V100-CC2 labeling is increased in photoreceptor cell bodies

(a-o) Immunolabeling of Chaoptin (grn), V100 (red), and Syntaxin7 (blue) in photoreceptor cell bodies expressing 2xFYVE-GFP, depicted in cross-section. V100-CC2 exhibits increased 2xFYVE signal, indicating an authentic early endosomal defect. This also confirms that protein V100-CC2 is stable.

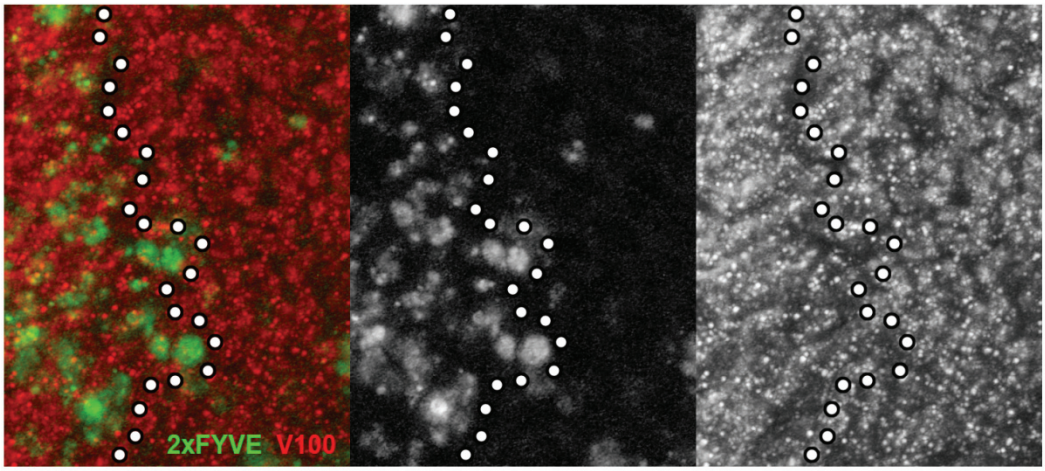

Figure S4.2: Increased expression restores V100-CC2 localization at the synapse

Immunolabeling with anti-V100 (red) at photoreceptor synapses, shown here as a cross-section through the lamina. Regions containing mutant cells that express V100-CC2 are marked with 2xFyve-GFP. No difference in V100 labeling is apparent, indicating a rescued V100-CC2 labeling at the synapse

MATERIALS AND METHODS

CONDUCTED PRIMARILY BY W. RYAN WILLIAMSON

Preparation of transgenic animals following plasmid injection

DNA injection for the generation of transgenic flies was performed by Rainbow Transgenics, Inc. At least two independent transgene insertions per chromosome were isolated. Two independent insertions for both $v100^{R755A}$ and Dendra2-*v100* on the 2nd chromosome were tested and selected for comparable expression levels to the UAS-*v100* wild type insertion when expressed in photoreceptors. The two transgenic lines chosen for each construct behaved identical in all assays.

Stock maintenance

v100 null mutant and overexpression lines have previously been described (Hiesinger et al., 2005). Allele $v100^{4}$ was the mutant allele used in all experiments. *y w; P(ry+=neo FRT)82B isogenized* flies were used as control animals. Flies were reared at room temperature, except for pupal staging experiments, where flies were reared at 25°C (100% pupal development corresponds to 103 hours).

Mosaic analysis

For photoreceptor-specific mosaics ($eyFLP^{PRonly}$) (Chotard et al., 2005; Mehta et al., 2005) the base genotype is *ey3.5FLP*;;FRT82B,*v100*/FRT82B,cl,w+. For optic lobe CNS

neuron clones (*eyFLP*^{CNS}) (Newsome et al., 2000) the base genotype is eyFLP;;FRT82B,*v100*/FRT82B,cl,w+. In order to express different reporters in either photoreceptors or all neurons, the following flies were generated:

For *eyFLP*^{PRonly}: *ey3.5FLP*;GMR-Gal4,(X*); FRT82B,*v100*/FRT82B,cl

For *eyFLP*^{CNS}: *eyFLP*,elav-Gal4;(X*); FRT82B,*v100*/FRT82B,cl

(X*) stands for one of the following UAS constructs: UAS-myr-RFP, UAS-LAMP-GFP, UAS-N-Cadherin, UAS-Fasciclin2, UAS-Roughest, UAS-*v100*^{WT} UAS-*v100*^{R755A} UAS-*v100*^{CC1} UAS-*v100*^{CC2}, or UAS-*v100N-term::nSyb*. In addition, we generated a chromosome that contains both UAS-myrRFP and UAS-lamp-GFP. *v100*^{R755A} and *v100N-term::nSyb* overexpression and control experiments were done at 18ºC, because higher levels of expression in *v100* mutant neurons cause cell death (Williamson et al., 2010b, and data not shown).

We used several variations of the MARCM technique (Lee and Luo, 1999) to generate positively marked clones with or without the expression of additional reporters or rescue constructs. In these flies, the FRT82B,cl,w+ was replaced with FRT82B,tub-Gal80. The following flies were generated:

For *eyFLP*^{CNS}: *eyFLP*,elav-Gal4;(X*);FRT82B,tub-Gal80/FRT82B,*v100*

For *eyFLP*^{PRonly}: *ey3.5FLP*; (Y*); FRT82B,tub-Gal80/FRT82B,*v100*

(X*) stands for one of the following UAS constructs: UAS-LAMP-GFP (Pulipparacharuvil et al., 2005), UAS-pHluorin (Ng et al., 2002), UAS-2xFYVE-GFP (Wucherpfennig et al., 2003);

(Y*) stands for recombined chromosomes containing GMR-Gal4 and UAS-LAMP-GFP, UAS-pHluorin, or UAS-2xFYVE-GFP.

The following genotype was used to negatively mark clones with RFP:

ey3.5FLP;GMR-Gal4,UAS-LAMP; FRT82B,UAS-RFP / FRT82B,*v100*

Immunohistochemistry

Adult brains, eyes, and eye-lamina complexes as well a pupal brains and eye-brain complexes were dissected as reported (Williamson and Hiesinger, 2010). The tissues were fixed in phosphate buffered saline (PBS) with 3.5% formaldehyde for 15 min and washed in PBS with 0.4% Triton X-100. High-resolution light microscopy was performed using the Resonance Scanning Confocal Microscope Leica SP5. Imaging data was processed and quantified using Amira 5.2 (Indeed, Berlin, Germany) and Adobe Photoshop CS4. Fluorescence data was quantified using GraphPad Prism 4. The following antibodies were used at 1:1000 dilution: anti-activated Caspase-3, Dlg, Rab7, Sun/CD63, Syx7/Avl, Rab5, Rab7, Rab11, Hrs, Syx16, Hook, Vps16, Car, Dor, Spin, and Syt. Anti-CSP, Syx, Brp (mAb nc82), Chaoptin (mAb 24B10), N-Cad (mAb DNEx8), Rst (mAb 24A5), Flamingo (mAb #74), and Fas2 (mAb 1D4) were used at 1:50. Anti-Sec15 and anti-V100 at 1:2000. All embryonic immunostaining and assessment of motor axon guidance was done using standard approaches (Hung et al., 2010) such that whole-mount embryos were fixed, washed in PBS containing 0.1% Triton, and incubated in antibodies to Fasciclin II (1:4, 1D4 supernatant, (Vactor et al., 1993)). Brightfield and DIC visualization and imaging was done using a Zeiss Axioimager upright microscope and images were captured using a Zeiss Axiocam HR camera and Zeiss Axiovision software.

Live imaging of adult and developing tissue

Brains were dissected from either pharate adults, P+20% pupae, or 3rd instar larvae in HL3 and were immobilized on a coverslip coated with sylgard using glue stitch as described (Williamson and Hiesinger, 2010). The tissue was mounted in an orientation that allows imaging of the desired region. Experiments were either performed under a Leica 63x Water-immersion lens or in a perfusion chamber (Harvard, RC-30) with slow perfusion of HL3 solution. Images were captured using resonance scanning confocal microscopy. For each scan from individual experiments the same x/y region was captured.

Synapto-pHluorin: We generated a calibration curve by first alkalizing intracellular compartments using NH_4Cl at pH7, and subsequently progressively acidifying intracellular compartments using an acidification protocol modified from (Boron and De Weer, 1976) by reducing the amount of free extracellular NH_3 using NH_4Cl washes at pH 6.5, 6.0 and 5.5. Using this method, the calibrated initial live measurements report intracompartmental pH, independent of the total amount of pHluorin. The raw data was processed in Amira 5.2 by first generating a maximum projection to eliminate the problem that differences in fluorescence vary among scans from a single experiment simply due to slight shifting of the prep in the z-direction resulting from perfusion of fluids over living tissue. Total fluorescence for each scan within a single experiment was calculated and the scans from NH_4Cl (pH controlled) scans were plotted in Prism on a Kaplan-Meier survival curve and analyzed by the four-parameter logistic equation. Next, the live fluorescence measurement was mathematically fitted onto the curve to reveal the mean live pH of the environment to which pHluorin was exposed. This was performed for several animals and the results were compiled to generate bar graphs representing the mean pH and error from the specified genotypes, tissues, and ages.

Lysotracker: Lysotracker Red was added to HL3 at 50nM. 200uL of this solution was placed onto the prepared tissue and an image was acquired within 5 minutes, as recommended by the manufacturer to prevent alkalizing effects. Live imaging was performed as described previously (Williamson and Hiesinger, 2010).

Quantification of compartment marker analyses

Comparisons of IHC label signal intensity in mutant vs. wild type photoreceptor terminals: 50% mutant photoreceptor mosaics were created with all mutant photoreceptors expressing pHluorin just to mark the mutant cells. 3D confocal stacks of three to five specimens were quantified for the ratio of total fluorescence in three cubic microns of mutant terminals divided by total fluorescence in three cubic microns of wild type terminals for each of the 20 markers individually. Wild type colocalization: Anti-V100 immunolabeling was analyzed for at least 3 specimens per colocalization experiment. Co-labelings with guinea pig antibodies (anti-Hrs, Dor, Sec15) were generated using GMR-Gal4 driven fluorescently tagged and functionally rescuing V100 in *v100* mutant neurons. For each co-labeling experiment clear and distinct V100-positive compartments were selected blindly with no other channel visible. Each V100-positive compartment was subsequently manually analyzed for colocalization with each of the 16 markers individually.

Extended-depth of field eye pictures to demonstrate degree of roughness

Flies were reared at the temperatures indicated, and adults were immobilized on glass slides with Elmer's® glue. 140µm stacks that included multiple focal planes separated by 20µm were acquired with a Leica MX16F stereoscope using In-Focus v1.60 (Meyer

Instruments & Leica Microsystems) and were processed for extended depth of field using Image-Pro Plus v6.0 by Media Cybernetics. The resulting frame was enhanced in Abobe Photoshop 4 to adjust levels, gamma, and sharpness for the purpose of highlighting the degree of eye roughness.

Electroretinograms (ERGs)

ERGs were performed as described in (Fabian-Fine et al., 2003) with the following modifications: Flies were fixed using Elmer's® non-toxic Glue-All. We used 2M NaCl in the recording and reference electrodes. Electrode voltage was amplified by a Digidata 1440A (Axon CNS/Molecular Devices), filtered through a Warner IE-210 (Warner Instruments), and recorded using Clampex 10.1 by Axon Intstruments. A post-recording filter was also provided by the Clampex software. Light stimulus was provided in 1 sec pulses by a computer-controlled white LED system (Schott MC1500). ERG data was quantified using GraphPad Prism 4.

CONDUCTED PRIMARILY BY DONG WANG AND OTHERS

Preparation of plasmids for generating transgenics

v100 was subjected to site-directed mutagenesis using full-length *v100* cDNA in a pOT2 vector (BDGP clone LD21248) and the following primers: CACCGCTTCCTATCTGGCATTGTGGGCGCTTTCCT and its reverse complement. Introduction of the mutation R755A was verified by sequencing. The resulting $v100^{R755A}$ cDNA was cloned into pUAST using EcoR1 and Xho1 restriction cutting sites as reported (Hiesinger et al., 2005). The UAS-Dendra2-*v100* construct was generated by cloning the PCR-amplified Dendra2 open reading frame into the pENTR4 vector and generating the fusion using the Gateway™ system. Site-directed mutagenesis (Stratagene) was used to introduce point mutations in the two V100 N-terminal coiled-coil domains using the following primers: TCCAGAGGAAGTTCGTCAACGCGGCGGCCGCCGCCGCTGCGATGGAGCGCAA GCTGCGTTAC (for coiled-coil domain1, hereafter 'CC1') and GAGGCCACCTTTGAGAAGCTGGCGGCCGCGGCGGCGGCGGCGAATCAGAAC GCCGAGGCCCTG (for coiled-coi domain 2, hereafter 'CC2'). For the Chimera construct, the N-terminal 415 amino acids of V100 were fused to the *Drosophila* n-Syb C-terminal coding sequence for K95-V181 by soeing PCR. All mutant constructs were introduced into a pUAST vector by conventional PCR and ligation. Sequencing confirmed the presence of the desired mutations.

Immunoprocipitations

Total proteins were extracted from adult fly heads in immunoprecipitation (IP) buffer containing 20mM Tris, 150mM NaCl, 1mM PMSF, and 1x complete protease inhibitors (Roche) at pH 7.4. The fly head extract was mixed well in 1% Triton X-100 (BioRad, Hercules, California, United States) and incubated for 1 hour at 4°C. Samples were centrifuged at 16,000g, 15 min at 4°C to remove cell debris. The resulting supernatant was incubated with 20 µl anti-V100 antibody and 8C3 anti-syx antibody (Hiesinger et al., 2005) coupled to protein A/G beads (Santa Cruz) for 1 hour at 4°C. After removing the supernatant, the beads were washed four times with the IP buffer. A/G beads without protein were used as control. The immunoprecipitates were eluted by boiling the beads in 50µl SDS sample buffer and were then analyzed by western blotting with 8C3 anti-syx, anti-SNAP25 and anti-Syb antibodies (Hiesinger et al., 2005).

Generation of bacterial expression constructs and protein purification

All sequences are from *Drosophila*. To make the His-tagged V100 N-terminus fragments, we chose the N-terminal 180 amino acids, which contains the two conserved coiled-coil domains that have been shown previously to bind Syntaxin1A *in vitro* (Hiesinger et al., 2005).The primers for this purpose are as follows: forward primer GGGGGGATCCATGGGTTCCCTATTCCGCAG, reverse primer GGGGCTCGAG CTCCTCGCCCAGCAGCTGCG. The PCR templates are V100 wild type cDNA as well as CC1 and CC2 mutated cDNA as described above. The resulting PCR products were cloned into pET28a (Novagen) to make his-tagged proteins. For Syntaxin 1A truncated GST fusion constructs, the following primers were used to perform PCR: Syx 1 (1-267 aa) forward, GGGGGGATCCATGACTAAAGACAGATTAGC;.reverse, GAGTAAAGCCCGACGAAAGCTCGAGCCCC. Syx1 ΔHa (61-267 aa) forward, GGGGGGATCCCACTCGGCCATCCTGTCCGCCCCA; reverse,

GAGTAAAGCCCGACGAAAGCT CGAGCCCC. Syx1 ΔHab (121-267 aa) forward, GGGGGGATCCACGCAGCACTCGACGTT GTCACG; reverse, GAGTAAAGCCCGACGAAAGCTCGAGCCCC. Syx1 ΔHabc (181-267 aa) forward, GGGGGGATCCACGCAGGGCATCATCATGG; reverse, GAGTAAAGCCCGACGAAA GCTCGAGCCCC. For Syntaxin7 GST fusion construct (1-258 aa), the following primers were used to perform PCR: forward, GAGTAAAGCCCGACGAAAGCTCGAGCCCC;reverse, GGGGGAATTCCACTTTGT TCCTGTAAGAGC All PCR products were cloned into the pGEXT 4T-1 vector (GE Healthcare) and sequenced. The constructs of GST-Syx1 H3N and GST-Syx1 H3C, as well as His-SNAP25 and His-Syb were described previously (Wu, et al., 1999; Hiesinger et al., 2005). The resulting plasmids were introduced into bacterial strain BL21 for expression and purification of target proteins.

Protein expression and purification were performed as standard procedure. Briefly, overnight bacterial culture was transfered into fresh LB medium at a 1:100 ratio and incubated at 37 ° C until the OD600 reached 0.6. The culture was then induced with IPTG (1mM for pET28a, 0.1mM for pGEXT) at 19 ° C overnight. The overnight culture was collected by centrifugation using a JLA 8.1000 at 5000 rpm, 4 ° C for 15 minutes. The pellet was resuspended in 10 mL standard buffer (20 mM Tris/100 mM NaCl, pH 7.4) and lysed with 1xBugbuster, 2 ul benzonase (Novagen), and protease inhibitor cocktail (Roche) for 10-20 minutes at room temperature. Centrifugation for 20 minutes at 16,000 rpm removed the cell debris. The supernatant was retained for protein purification. His-tagged or GST fusion proteins were purified as described by the manufacturer (Novagen and Pharmacia, respectively). Proteins was concentrated using Centriprep columns (Amicon) and washed twice with 4 mL of PBS.

Pull-down assays

For GST pull down assays, the indicated GST fusion proteins were bound to glutathione Sepharose™ 4B (GE Healthcare) first, then washed with standard buffer (20 mM Tris/100 mM NaCl, pH 7.4) twice. The binding assay was performed with the indicated His-tagged proteins in binding buffer (20 mM Tris/150 mM NaCl, pH 7.4/0.2% Triton X-100) and incubated at 4° C overnight. After binding, the beads were washed three times in binding buffer, and protein samples were eluted with SDS loading buffer for western blotting. For the His-protein pulll down assay, the indicated His-tagged proteins were bound to His-Bond resin (Novagen) and incubated with fly head lysate at 4° C for 2 hours. The beads were washed three times with lysis buffer (20mM Tris/150mM NaCl, 1mM PMSF, and 1x complete protease inhibitors (Roche) pH 7.4/ 1% Triton X-100). Protein samples were eluted with SDS loading buffer before western blotting.

Western blots of mutant eye-lamina complexes

For Western blots of adult eye-lamina complexes, 2-day old eyFLP; FRT82B *v100* and eyFLP; FRT82B wt eyes were dissected in HL3 as described previously (Williamson et al., 2010b). Tissues were washed twice in ice cold lysis buffer (as used for immunoprecipitation experiments) and crushed with a pestle in lysis buffer. The solution was incubated on ice for 20 minutes and then centrifuged at 4 degrees to remove solid material. 10 eye-lamina complexes per lane were run on a 12% SDS-PAGE gel.

Plastic Eye Sections

1 μm plastic sections of adult eyes were made as described (Van Vactor et al., 1991). In brief, samples were fixed using standard electron microscopy fixatives containing 2%

paraformaldehyde and 2% glutaraldehyde. Samples were subsequently dehydrated and embedded in Epon/Araldite plastic medium. Thick sections were stained with a combination of methylene blue and toluidine blue for light microscopy.

Fluorescence anisotropy by the Florante Quiocho Lab

Generation of the Drosophila subunit a1-fluorescein congugate

CC2-FM corresponds to the fluorescein labeled fragment of Fly a1 from residues E84 to E141. This fragment was sub-cloned into pTYB12 vector using SpeI and XhoI sites. A cysteine for incorporating the fluorophore was introduced right in front of E84. Protein was purified as recommended in the IMPACT manual (New England Biolabs). Briefly, cells were induced with 0.1mM IPTG at 16ºC overnight and bound to chitin beads after cell lysis in 20mM HEPES, 500mM NaCl, pH 8.0. On column cleavage was performed for 16 hours at room temperature in the same buffer with the addition of 50mM DTT. This was dialyzed with 20mM Tris-HCl, 50mM NaCl, pH 7.0. Ten times molar excess of TCEP-HCl was added to the protein to reduce the disulfide bonds. Twenty times molar excess of fluorescein maleimide (Invitrogen) dissolved in DMSO was added to the protein, drop by drop and incubated overnight at 4ºC. Labeling reaction was stopped by adding an excess of □-mercaptoethanol. The labeled protein was separated from excess dye using Zeba-desalt spin columns. Mass-spectrometric analysis was performed to confirm the molecular weight of the labeled protein. Concentration of the labeled protein was calculated by measuring the absorbance at 495nm and BioRad assay.

Generation of Drosophila Syntaxin-1A, SNAP-25 and n-Synaptobrevin

Syntaxin-1A corresponding to residues Q193 to S262 was sub-cloned into pTYB12 vector using NdeI and XhoI sites. Protein was purified as described above and the molar extinction coefficient, e = 4470 M-1cm-1, was calculated using ProtParam. Protein concentration was estimated by measuring the absorbance at 280nm. SNAP25N,

corresponding to residues K15 to K90 and SNAP25C, corresponding to residues A139 to K202 were also sub-cloned into pTYB12 vector and purified as described above. Protein concentrations were estimated using the BioRad assay. n-Synaptobrevin (syb), corresponding to residues M1 to K104 was sub-cloned into pET28 vector with a N-terminal histidine tag. This was purified using Talon beads (Clonetech) by following the manufacturer's protocol. Protein concentration was estimated using a molar extinction coefficient of e = 5500 M-1cm-1.

Fluorescence experiment

0.1 mM of CC2-FM was incubated overnight at 4ºC in various mixtures or combinations (see below) with 0.5 mM sysntaxin, SNAP25N and SNAP25C (together called plainly SNAP25) or syb in 20 mM Tris-HCl, 50 mM NaCl, pH 7.4. So, each SNARE is 5-fold greater than CC2-FM. Samples were wrapped in silver foil to avoid exposure to light. All measurements were carried on a ISS, PC-1 photon counting spectrofluorometer at room temperature using a 1mm slit (8 nm band pass) by excitation at 495nm and emission measured from 500 to 600nm.

CHAPTER SIX

Concluding remarks and future directions

What is the role for v100 in synapse development, function, and maintenance? The answer is two-fold: a SNARE-dependent sorting function participates in the regulated delivery of cargo while an acidification function is required for the maturation of degradation-competent organelles. In development, V100 sorts guidance receptors into a degradation pathway that participates in the regulatory program used in brain wiring. In synapse function, v100 interacts with Syx1 in preparation for trans-SNARE complex formation prior to neurotransmitter release. And finally, v100 defines a neuron-specific degradation pathway into which v100 sorts cargo and acidifies degradative organelles. Loss of this pathway results in progressive, adult neurodegeneration that manifests as a loss of tissue structure, accumulations of undegraded protein, and diminished electrical responses after stimulus.

This study reveals the spatial and temporal requirements for a dual-functioning neuron-specific V-ATPase, highlighting in particular the acidification-independent sorting role of v100 in neuronal cell biology. Collectively, the results convincingly demonstrate a function for v100 in membrane fusion, but the molecular mechanism remains unclear. It is clear that targeted mutations exist in the v100 N-terminus that disrupt Syx interactions and it is clear that this N-terminus preferentially binds the closed form of Syntaxin, however, it is unclear how the interaction promotes membrane fusion and how these mutations impair membrane fusion, on a molecular scale. It may be necessary to build future hypotheses in the context of a specific mode of synaptic vesicle fusion. Multiple modes of synaptic vesicle fusion have been characterized functionally,

including evoked synchronous release, evoked asynchronous release, and spontaneous release. Additionally, neurotransmitter can be released due to the collapse of a vesicle after the fusion pore is made by tension from SNARE interactions, or by a kiss-and-run event where the fusion pore is restricted and the same vesicle buds off without collapsing into the target membrane. Despite solid functional evidence for the existence of these distinct modes of membrane fusion, and despite evidence that distinct fusion modes have relevance to neuronal physiology, it remains unclear whether there are specific molecules that provide specificity, or whether these modes arise from fluctuations within the realm of possible interactions among a single set of molecules. Sorting this out is challenging because some molecules may be shared among the distinct modes and because manipulation of a particular mode may have indirect consequences for other modes. For example, loss of synaptotagmin, the calcium sensor for evoked synchronous release, results in an increase in evoked asynchronous release. This implies that the presence of synaptotagmin has a restrictive role in asynchronous release, perhaps by competing with another unknown calcium sensor for binding to SNAREs. To reach an understanding, it may be necessary to make only subtle or targeted manipulations of the system that lead to subtle, yet measurable shifts in molecular activity.

Target mutations have indeed been useful in the study of v100. Taking the lead from yeast research, we induced the R755A mutation which specifically disrupted acidification while leaving an acidification-independent sorting role intact. Also, because it was already known that coiled-coil domains are often involved in SNARE interactions, we were able to specifically disrupt SNARE interactions with the V100 N-terminus. We now know that V100 has a role in membrane fusion and that it binds closed Syntaxin1. It is also known that V100 interacts with the promiscuous calcium sensor calmodulin and that a published 'WFI' mutation disrupts this interaction. My unpublished results show

that expression of V100-WFI in photoreceptor cells restores neurotransmission as measured by an ERG recording. However, pan-neuronal expression of V100-WFI in a v100 null animal does not rescue viability or the loss of spontaneous release frequency observed in the null (also unpublished). These results suggest that the mode of release in photoreceptors are distinct from the modes in embryonic motor neurons. Also, the role of V00 in membrane fusion is calcium/calmodulin-binding-independent, while the role for v100 in membrane fusion in embryonic motor neurons is calcium/calmodulin-binding-dependent. Can V100-WFI bind Syx1? Does the V100 N-terminus release Syx1 in the presence of Calcium/calmodulin *in vitro*? Is there a genetic interaction between V100-WFI and Synaptotagmin *in vivo*? Does V100 compete with Synaptotagmin for SNARE binding? Does V100 compete with Munc18 for binding the closed form of Syntaxin? Answering these questions may add to our understanding of the molecular mechanism for V100 in membrane fusion.

In addition to the open questions related to molecular mechanism are questions related to the cell biological activities that utilize that mechanism. We have learned that v100 is required for neuronal maintenance and that loss of v100 leads to degeneration, but what is the relevance to mammalian degenerative disease? The fly has been used as a model to discover the normal cell biological functions of conserved genes associated with human neural disease, however degeneration as a process is better studied in mammalian models. Perhaps genetic manipulations or small molecules that modulate V-ATPase activity could in turn modulate the onset or severity of degeneration in mammals that possess mutations in other genes already associated with degeneration. We have presented genetic manipulations that block one of the two V-ATPase functions, but the identification of subtle manipulations would likely be more useful for this purpose. Also, specific inhibitors of V-ATPase mediated acidification are known including the

Bafilomycins and Concanamycins, however inhibitors of an acidification-independent role remain unidentified.

Why would cell biology employ the V-ATPase in membrane fusion when SNAREs are so capable? This is a problem that might be interesting to evolutionary biologists. It may be that an ancestral a subunit was solely responsible for membrane fusion and acidification. Certainly, these two tasks are frequently required in succession as vesicles are prepared for exocytosis or as organelles mature along the degradation pathways. A simpler organism would energetically benefit from having to make a single protein that can accomplish both tasks and then be reused. As organisms became more complex, membrane fusion events required additional specificity and SNARE molecules came about, along with additional methods of control, while vestigial roles in membrane fusion remain for the V-ATPase. Two recent studies are consistent with this model. In one study, an ancestral bacterial a subunit is expressed in yeast and is capable of restoring vph1 function, the yeast a subunit known to have a role in vacuolar membrane fusion, but not the other yeast a subunit, stv1, which is less conserved in the N-terminal sequence and has no known role in membrane fusion. In another study, it was shown that paramecium have over a dozen copies of the a subunit. Perhaps the paramecium evolved an alternative means of specifying membrane fusion events by modifying duplications of the ancestral a subunit. This would predict that the C-terminal fragments of the paramecium a subunits are more highly conserved than the N-termini. It would also predict that specific a subunits would sequester to specific organelles and that SNARE molecules would be fewer or absent in the genome. The molecular mechanism of the V-ATPase in membrane fusion could possibly be more easily studied in a model that uses the V-ATPase predominantly for specifity in membrane fusion events.

REFERENCES

Akbar, M.A., Ray, S., and Kramer, H. (2009). The SM protein Car/Vps33A regulates SNARE-mediated trafficking to lysosomes and lysosome-related organelles. Mol Biol Cell *20*, 1705-1714.

Araujo, S.J., and Tear, G. (2003). Axon guidance mechanisms and molecules: lessons from invertebrates. Nat Rev Neurosci *4*, 910-922.

Bartoe, J.L., McKenna, W.L., Quan, T.K., Stafford, B.K., Moore, J.A., Xia, J., Takamiya, K., Huganir, R.L., and Hinck, L. (2006). Protein interacting with C-kinase 1/protein kinase Calpha-mediated endocytosis converts netrin-1-mediated repulsion to attraction. J Neurosci *26*, 3192-3205.

Bayer, M.J., Reese, C., Buhler, S., Peters, C., and Mayer, A. (2003). Vacuole membrane fusion: V0 functions after trans-SNARE pairing and is coupled to the Ca2+-releasing channel. J Cell Biol *162*, 211-222.

Boron, W.F., and De Weer, P. (1976). Intracellular pH transients in squid giant axons caused by CO2, NH3, and metabolic inhibitors. J Gen Physiol *67*, 91-112.

Brand, A.H., and Perrimon, N. (1993). Targeted gene expression as a means of altering cell fates and generating dominant phenotypes. Development *118*, 401-415.

Broadie, K., Sink, H., Van Vactor, D., Fambrough, D., Whitington, P.M., Bate, M., and Goodman, C.S. (1993). From growth cone to synapse: the life history of the RP3 motor neuron. Dev Suppl, 227-238.

Bröcker, C., Engelbrecht-Vandré, S., and Ungermann, C. (2010). Multisubunit Tethering Complexes and Their Role in Membrane Fusion. Current biology : CB *20*, R943-R952.

Carr, C.M., and Rizo, J. (2010). At the junction of SNARE and SM protein function. Current opinion in cell biology *22*, 488-495.

Castellani, V., Falk, J., and Rougon, G. (2004). Semaphorin3A-induced receptor endocytosis during axon guidance responses is mediated by L1 CAM. Mol Cell Neurosci *26*, 89-100.

Chang, Y.Y., and Neufeld, T.P. (2009). An Atg1/Atg13 complex with multiple roles in TOR-mediated autophagy regulation. Mol Biol Cell *20*, 2004-2014.

Chen, S.Y., and Cheng, H.J. (2009). Functions of axon guidance molecules in synapse formation. Curr Opin Neurobiol *19*, 471-478.

Chen, X., Lu, J., Dulubova, I., and Rizo, J. (2008). NMR analysis of the closed conformation of syntaxin-1. J Biomol NMR *41*, 43-54.

Chen, Y.A., Scales, S.J., and Scheller, R.H. (2001). Sequential SNARE Assembly Underlies Priming and Triggering of Exocytosis. Neuron *30*, 161-170.

Chitnis, A. (2006). Why is delta endocytosis required for effective activation of notch? Dev Dyn *235*, 886-894.

Chotard, C., Leung, W., and Salecker, I. (2005). glial cells missing and gcm2 cell autonomously regulate both glial and neuronal development in the visual system of Drosophila. Neuron *48*, 237-251.

Clandinin, T.R., Lee, C.H., Herman, T., Lee, R.C., Yang, A.Y., Ovasapyan, S., and Zipursky, S.L. (2001). Drosophila LAR regulates R1-R6 and R7 target specificity in the visual system. Neuron *32*, 237-248.

Clandinin, T.R., and Zipursky, S.L. (2002). Making connections in the fly visual system. Neuron *35*, 827-841.

de Wit, H., Walter, A.M., Milosevic, I., Gulyas-Kovacs, A., Riedel, D., Sorensen, J.B., and Verhage, M. (2009). Synaptotagmin-1 docks secretory vesicles to syntaxin-1/SNAP-25 acceptor complexes. Cell *138*, 935-946.

Dermaut, B., Norga, K.K., Kania, A., Verstreken, P., Pan, H., Zhou, Y., Callaerts, P., and Bellen, H.J. (2005). Aberrant lysosomal carbohydrate storage accompanies endocytic defects and neurodegeneration in Drosophila benchwarmer. J Cell Biol *170*, 127-139.

Desai, C.J., Gindhart, J.G., Jr., Goldstein, L.S., and Zinn, K. (1996). Receptor tyrosine phosphatases are required for motor axon guidance in the Drosophila embryo. Cell *84*, 599-609.

Di Giovanni, J., Boudkkazi, S., Mochida, S., Bialowas, A., Samari, N., Lév que, C., Youssouf, F., and Brechet, A. (2010). V-ATPase membrane sector associates with synaptobrevin to modulate neurotransmitter release. Neuron *67*, 268-279.

Dickson, B.J. (2002). Molecular mechanisms of axon guidance. Science *298*, 1959-1964.

Dubois, L., Lecourtois, M., Alexandre, C., Hirst, E., and Vincent, J.P. (2001). Regulated endocytic routing modulates wingless signaling in Drosophila embryos. Cell *105*, 613-624.

Dulubova, I., Sugita, S., Hill, S., Hosaka, M., Fernandez, I., Sudhof, T.C., and Rizo, J. (1999). A conformational switch in syntaxin during exocytosis: role of munc18. EMBO J *18*, 4372-4382.

Dun, A.R., Rickman, C., and Duncan, R.R. (2010). The t-SNARE complex: a close up. Cell Mol Neurobiol *30*, 1321-1326.

El Far, O., and Seagar, M. (2011). A role for V-ATPase subunits in synaptic vesicle fusion? Journal of Neurochemistry *117*, 603-612.

Eskelinen, E.L. (2005). Maturation of autophagic vacuoles in Mammalian cells. Autophagy *1*, 1-10.

Fabian-Fine, R., Verstreken, P., Hiesinger, P.R., Horne, J.A., Kostyleva, R., Zhou, Y., Bellen, H.J., and Meinertzhagen, I.A. (2003). Endophilin promotes a late step in endocytosis at glial invaginations in Drosophila photoreceptor terminals. J Neurosci *23*, 10732-10744.

Filimonenko, M., Stuffers, S., Raiborg, C., Yamamoto, A., Malerod, L., Fisher, E.M., Isaacs, A., Brech, A., Stenmark, H., and Simonsen, A. (2007). Functional multivesicular bodies are required for autophagic clearance of protein aggregates associated with neurodegenerative disease. J Cell Biol *179*, 485-500.

Forgac, M. (2007). Vacuolar ATPases: rotary proton pumps in physiology and pathophysiology. Nature Reviews Molecular Cell Biology *8*, 917-929.

Futerman, A.H., and van Meer, G. (2004). The cell biology of lysosomal storage disorders. Nat Rev Mol Cell Biol *5*, 554-565.

Galli, T., McPherson, P.S., and De Camilli, P. (1996). The V Sector of the V-ATPase, Synaptobrevin, and Synaptophysin Are Associated on Synaptic Vesicles in a Triton X-100-resistant, Freeze-thawing Sensitive, Complex. Journal of Biological Chemistry *271*, 2193.

Garrity, P.A., Lee, C.H., Salecker, I., Robertson, H.C., Desai, C.J., Zinn, K., and Zipursky, S.L. (1999). Retinal axon target selection in Drosophila is regulated by a receptor protein tyrosine phosphatase. Neuron *22*, 707-717.

Gerber, S.H., Rah, J.-C., Min, S.-W., Liu, X., de Wit, H., Dulubova, I., Meyer, A.C., Rizo, J., Arancillo, M., Hammer, R.E.*, et al.* (2008a). Conformational Switch of Syntaxin-1 Controls Synaptic Vesicle Fusion. Science *321*, 1507-1510.

Gerber, S.H., Rah, J.C., Min, S.W., Liu, X., de Wit, H., Dulubova, I., Meyer, A.C., Rizo, J., Arancillo, M., Hammer, R.E.*, et al.* (2008b). Conformational switch of syntaxin-1 controls synaptic vesicle fusion. Science *321*, 1507-1510.

Ghosh, P., Dahms, N.M., and Kornfeld, S. (2003). Mannose 6-phosphate receptors: new twists in the tale. Nature Reviews Molecular Cell Biology *4*, 202-213.

Grenningloh, G., Rehm, E.J., and Goodman, C.S. (1991). Genetic analysis of growth cone guidance in Drosophila: fasciclin II functions as a neuronal recognition molecule. Cell *67*, 45-57.

Hara, T., Nakamura, K., Matsui, M., Yamamoto, A., Nakahara, Y., Suzuki-Migishima, R., Yokoyama, M., Mishima, K., Saito, I., Okano, H.*, et al.* (2006). Suppression of basal autophagy in neural cells causes neurodegenerative disease in mice. Nature *441*, 885-889.

He, H., Yang, T., Terman, J.R., and Zhang, X. (2009). Crystal structure of the plexin A3 intracellular region reveals an autoinhibited conformation through active site sequestration. Proc Natl Acad Sci U S A *106*, 15610-15615.

Hiesinger, P.R., Fayyazuddin, A., Mehta, S.Q., Rosenmund, T., Schulze, K.L., Zhai, R.G., Verstreken, P., Cao, Y., Zhou, Y., Kunz, J.*, et al.* (2005). The v-ATPase V0 subunit a1 is required for a late step in synaptic vesicle exocytosis in Drosophila. Cell *121*, 607-620.

Hiesinger, P.R., Reiter, C., Schau, H., and Fischbach, K.F. (1999). Neuropil pattern formation and regulation of cell adhesion molecules in Drosophila optic lobe development depend on synaptobrevin. J Neurosci *19*, 7548-7556.

Hiesinger, P.R., Scholz, M., Meinertzhagen, I.A., Fischbach, K.F., and Obermayer, K. (2001). Visualization of synaptic markers in the optic neuropils of Drosophila using a new constrained deconvolution method. J Comp Neurol *429*, 277-288.

Hiesinger, P.R., Zhai, R.G., Zhou, Y., Koh, T.W., Mehta, S.Q., Schulze, K.L., Cao, Y., Verstreken, P., Clandinin, T.R., Fischbach, K.F.*, et al.* (2006). Activity-independent prespecification of synaptic partners in the visual map of Drosophila. Curr Biol *16*, 1835-1843.

Hung, R.J., Yazdani, U., Yoon, J., Wu, H., Yang, T., Gupta, N., Huang, Z., van Berkel, W.J., and Terman, J.R. (2010). Mical links semaphorins to F-actin disassembly. Nature *463*, 823-827.

Jahn, R., and Scheller, R.H. (2006a). SNAREs--engines for membrane fusion. Nat Rev Mol Cell Biol *7*, 631-643.

Jahn, R., and Scheller, R.H. (2006b). SNAREs—engines for membrane fusion. Nature Reviews Molecular Cell Biology *7*, 631-643.

Jefferies, K.C., Cipriano, D.J., and Forgac, M. (2008). Function, structure and regulation of the vacuolar (H+)-ATPases. Archives of biochemistry and biophysics *476*, 33-42.

Kane, P.M. (2006). The where, when, and how of organelle acidification by the yeast vacuolar H+-ATPase. Microbiology and molecular biology reviews *70*, 177.

Kane, P.M. (2007). The long physiological reach of the yeast vacuolar H+-ATPase. J Bioenerg Biomembr *39*, 415-421.

Kaphingst, K., and Kunes, S. (1994). Pattern formation in the visual centers of the Drosophila brain: wingless acts via decapentaplegic to specify the dorsoventral axis. Cell *78*, 437-448.

Karet, F.E., Finberg, K.E., Nelson, R.D., Nayir, A., Mocan, H., Sanjad, S.A., Rodriguez-Soriano, J., Santos, F., Cremers, C.W.R.J., and Di Pietro, A. (1999). Mutations in the gene encoding B1 subunit of H+-ATPase cause renal tubular acidosis with sensorineural deafness. Nature genetics *21*, 84-90.

Kawasaki-Nishi, S., Nishi, T., and Forgac, M. (2001). Arg-735 of the 100-kDa subunit a of the yeast V-ATPase is essential for proton translocation. Proc Natl Acad Sci U S A *98*, 12397-12402.

Keleman, K., Rajagopalan, S., Cleppien, D., Teis, D., Paiha, K., Huber, L.A., Technau, G.M., and Dickson, B.J. (2002). Comm sorts robo to control axon guidance at the Drosophila midline. Cell *110*, 415-427.

Keleman, K., Ribeiro, C., and Dickson, B.J. (2005). Comm function in commissural axon guidance: cell-autonomous sorting of Robo in vivo. Nat Neurosci *8*, 156-163.

Kolotuev, I., Apaydin, A., and Labouesse, M. (2009). Secretion of Hedgehog-related peptides and WNT during Caenorhabditis elegans development. Traffic *10*, 803-810.

Komatsu, M., Waguri, S., Chiba, T., Murata, S., Iwata, J., Tanida, I., Ueno, T., Koike, M., Uchiyama, Y., Kominami, E*., et al.* (2006). Loss of autophagy in the central nervous system causes neurodegeneration in mice. Nature *441*, 880-884.

Kornak, U., Reynders, E., Dimopoulou, A., van Reeuwijk, J., Fischer, B., Rajab, A., Budde, B., Nurnberg, P., Foulquier, F., Lefeber, D*., et al.* (2008). Impaired glycosylation and cutis laxa caused by mutations in the vesicular H+-ATPase subunit ATP6V0A2. Nat Genet *40*, 32-34.

Kornak, U., Schulz, A., Friedrich, W., Uhlhaas, S., Kremens, B., Voit, T., Hasan, C., Bode, U., Jentsch, T.J., and Kubisch, C. (2000). Mutations in the a3 subunit of the vacuolar H(+)-ATPase cause infantile malignant osteopetrosis. Hum Mol Genet *9*, 2059-2063.

Krishnakumar, S.S., Radoff, D.T., Kümmel, D., Giraudo, C.G., Li, F., Khandan, L., Baguley, S.W., Coleman, J., Reinisch, K.M., Pincet, F*., et al.* (2011). A conformational switch in complexin is required for synaptotagmin to trigger synaptic fusion. Nat Struct Mol Biol *18*, 934-940.

Lee, C.H., Herman, T., Clandinin, T.R., Lee, R., and Zipursky, S.L. (2001). N-cadherin regulates target specificity in the Drosophila visual system. Neuron *30*, 437-450.

Lee, R.C., Clandinin, T.R., Lee, C.H., Chen, P.L., Meinertzhagen, I.A., and Zipursky, S.L. (2003). The protocadherin Flamingo is required for axon target selection in the Drosophila visual system. Nat Neurosci *6*, 557-563.

Lee, S.H., Rho, J., Jeong, D., Sul, J.Y., Kim, T., Kim, N., Kang, J.S., Miyamoto, T., Suda, T., Lee, S.K.*, et al.* (2006). v-ATPase V0 subunit d2-deficient mice exhibit impaired osteoclast fusion and increased bone formation. Nat Med *12*, 1403-1409.

Lee, T., and Luo, L. (1999). Mosaic analysis with a repressible cell marker for studies of gene function in neuronal morphogenesis. Neuron *22*, 451-461.

Liegeois, S., Benedetto, A., Garnier, J.M., Schwab, Y., and Labouesse, M. (2006). The V0-ATPase mediates apical secretion of exosomes containing Hedgehog-related proteins in Caenorhabditis elegans. J Cell Biol *173*, 949-961.

Lin, D.M., Fetter, R.D., Kopczynski, C., Grenningloh, G., and Goodman, C.S. (1994). Genetic analysis of Fasciclin II in Drosophila: defasciculation, refasciculation, and altered fasciculation. Neuron *13*, 1055-1069.

Lin, D.M., and Goodman, C.S. (1994). Ectopic and increased expression of Fasciclin II alters motoneuron growth cone guidance. Neuron *13*, 507-523.

Lloyd, T.E., Atkinson, R., Wu, M.N., Zhou, Y., Pennetta, G., and Bellen, H.J. (2002). Hrs regulates endosome membrane invagination and tyrosine kinase receptor signaling in Drosophila. Cell *108*, 261-269.

Lu, H., and Bilder, D. (2005). Endocytic control of epithelial polarity and proliferation in Drosophila. Nat Cell Biol *7*, 1232-1239.

Ma, B., Xiang, Y., and An, L. (2011a). Structural bases of physiological functions and roles of the vacuolar H+-ATPase. Cellular Signalling *23*, 1244-1256.

Ma, C., Li, W., Xu, Y., and Rizo, J. (2011b). Munc13 mediates the transition from the closed syntaxin–Munc18 complex to the SNARE complex. Nat Struct Mol Biol *18*, 542-549.

Machen, T.E., Leigh, M.J., Taylor, C., Kimura, T., Asano, S., and Moore, H.P. (2003). pH of TGN and recycling endosomes of H+/K+-ATPase-transfected HEK-293 cells: implications for pH regulation in the secretory pathway. Am J Physiol Cell Physiol *285*, C205-214.

Manolson, M.F., Wu, B., Proteau, D., Taillon, B.E., Roberts, B.T., Hoyt, M.A., and Jones, E.W. (1994). STV1 gene encodes functional homologue of 95-kDa yeast vacuolar H(+)-ATPase subunit Vph1p. J Biol Chem *269*, 14064-14074.

Margittai, M., Fasshauer, D., Pabst, S., Jahn, R., and Langen, R. (2001). Homo-and heterooligomeric SNARE complexes studied by site-directed spin labeling. Journal of Biological Chemistry *276*, 13169.

Marshansky, V., and Futai, M. (2008). The V-type H+-ATPase in vesicular trafficking: targeting, regulation and function. Current opinion in cell biology *20*, 415-426.

Mast, J.D., Prakash, S., Chen, P.L., and Clandinin, T.R. (2006). The mechanisms and molecules that connect photoreceptor axons to their targets in Drosophila. Semin Cell Dev Biol *17*, 42-49.

Maurel-Zaffran, C., Suzuki, T., Gahmon, G., Treisman, J.E., and Dickson, B.J. (2001). Cell-autonomous and -nonautonomous functions of LAR in R7 photoreceptor axon targeting. Neuron *32*, 225-235.

Maxfield, F.R., and McGraw, T.E. (2004). Endocytic recycling. Nature reviews Molecular cell biology *5*, 121.

Maximov, A., Tang, J., Yang, X., Pang, Z.P., and Südhof, T.C. (2009). Complexin Controls the Force Transfer from SNARE Complexes to Membranes in Fusion. Science *323*, 516-521.

Mehta, S.Q., Hiesinger, P.R., Beronja, S., Zhai, R.G., Schulze, K.L., Verstreken, P., Cao, Y., Zhou, Y., Tepass, U., Crair, M.C.*, et al.* (2005). Mutations in Drosophila sec15 reveal a function in neuronal targeting for a subset of exocyst components. Neuron *46*, 219-232.

Misura, K., Gonzalez, L.C., May, A.P., Scheller, R.H., and Weis, W.I. (2001). Crystal structure and biophysical properties of a complex between the N-terminal SNARE region of SNAP25 and syntaxin 1a. Journal of Biological Chemistry *276*, 41301.

Mizushima, N., Levine, B., Cuervo, A.M., and Klionsky, D.J. (2008). Autophagy fights disease through cellular self-digestion. Nature *451*, 1069-1075.

Morel, N., Dedieu, J.C., and Philippe, J.M. (2003). Specific sorting of the a1 isoform of the V-H+ATPase a subunit to nerve terminals where it associates with both synaptic vesicles and the presynaptic plasma membrane. J Cell Sci *116*, 4751-4762.

Moriyama, Y., Maeda, M., and Futai, M. (1992). The role of V-ATPase in neuronal and endocrine systems. Journal of experimental biology *172*, 171.

Newsome, T.P., Asling, B., and Dickson, B.J. (2000). Analysis of Drosophila photoreceptor axon guidance in eye-specific mosaics. Development *127*, 851-860.

Ng, M., Roorda, R.D., Lima, S.Q., Zemelman, B.V., Morcillo, P., and Miesenbock, G. (2002). Transmission of olfactory information between three populations of neurons in the antennal lobe of the fly. Neuron *36*, 463-474.

Nichols, B.J., Ungermann, C., Pelham, H.R.B., Wickner, W.T., and Haas, A. (1997). Homotypic vacuolar fusion mediated by t- and v-SNAREs. Nature *387*, 199-202.

Nishi, T., and Forgac, M. (2002). The vacuolar (H+)-ATPases--nature's most versatile proton pumps. Nat Rev Mol Cell Biol *3*, 94-103.

Nixon, R.A., Yang, D.S., and Lee, J.H. (2008). Neurodegenerative lysosomal disorders: a continuum from development to late age. Autophagy *4*, 590-599.

O'Donnell, M., Chance, R.K., and Bashaw, G.J. (2009). Axon growth and guidance: receptor regulation and signal transduction. Annu Rev Neurosci *32*, 383-412.

Pang, Z.P., and Südhof, T.C. (2010). Cell biology of Ca2+-triggered exocytosis. Current opinion in cell biology *22*, 496-505.

Pelissier, A., Chauvin, J.P., and Lecuit, T. (2003). Trafficking through Rab11 endosomes is required for cellularization during Drosophila embryogenesis. Curr Biol *13*, 1848-1857.

Peri, F., and Nusslein-Volhard, C. (2008). Live imaging of neuronal degradation by microglia reveals a role for v0-ATPase a1 in phagosomal fusion in vivo. Cell *133*, 916-927.

Perin, M.S., Fried, V.A., Stone, D.K., Xie, X.S., and Sudhof, T.C. (1991). Structure of the 116-kDa polypeptide of the clathrin-coated vesicle/synaptic vesicle proton pump. J Biol Chem *266*, 3877-3881.

Peters, C., Bayer, M.J., Buhler, S., Andersen, J.S., Mann, M., and Mayer, A. (2001). Trans-complex formation by proteolipid channels in the terminal phase of membrane fusion. Nature *409*, 581-588.

Pietrement, C., Sun-Wada, G., Da Silva, N., McKee, M., Marshansky, V., Brown, D., Futai, M., and Breton, S. (2006). Distinct expression patterns of different subunit isoforms of the V-ATPase in the rat epididymis. Biology of reproduction *74*, 185.

Pobbati, A.V., Stein, A., and Fasshauer, D. (2006). N- to C-Terminal SNARE Complex Assembly Promotes Rapid Membrane Fusion. Science *313*, 673-676.

Pulipparacharuvil, S., Akbar, M.A., Ray, S., Sevrioukov, E.A., Haberman, A.S., Rohrer, J., and Kramer, H. (2005). Drosophila Vps16A is required for trafficking to lysosomes and biogenesis of pigment granules. J Cell Sci *118*, 3663-3673.

Ramos, R.G., Igloi, G.L., Lichte, B., Baumann, U., Maier, D., Schneider, T., Brandstatter, J.H., Frohlich, A., and Fischbach, K.F. (1993). The irregular chiasm C-roughest locus of Drosophila, which affects axonal projections and programmed cell death, encodes a novel immunoglobulin-like protein. Genes Dev *7*, 2533-2547.

Razi, M., Chan, E.Y., and Tooze, S.A. (2009). Early endosomes and endosomal coatomer are required for autophagy. J Cell Biol *185*, 305-321.

Reiter, C., Schimansky, T., Nie, Z., and Fischbach, K.F. (1996). Reorganization of membrane contacts prior to apoptosis in the Drosophila retina: the role of the IrreC-rst protein. Development *122*, 1931-1940.

Richmond, J.E., Weimer, R.M., and Jorgensen, E.M. (2001). An open form of syntaxin bypasses the requirement for UNC-13 in vesicle priming. Nature *412*, 338-341.

Rink, J., Ghigo, E., Kalaidzidis, Y., and Zerial, M. (2005). Rab conversion as a mechanism of progression from early to late endosomes. Cell *122*, 735-749.

Sann, S., Wang, Z., Brown, H., and Jin, Y. (2009). Roles of endosomal trafficking in neurite outgrowth and guidance. Trends Cell Biol *19*, 317-324.

Schneider, T., Reiter, C., Eule, E., Bader, B., Lichte, B., Nie, Z., Schimansky, T., Ramos, R.G., and Fischbach, K.F. (1995). Restricted expression of the irreC-rst protein is required for normal axonal projections of columnar visual neurons. Neuron *15*, 259-271.

Senti, K.A., Usui, T., Boucke, K., Greber, U., Uemura, T., and Dickson, B.J. (2003). Flamingo regulates R8 axon-axon and axon-target interactions in the Drosophila visual system. Curr Biol *13*, 828-832.

Seol, J.H., Shevchenko, A., and Deshaies, R.J. (2001). Skp1 forms multiple protein complexes, including RAVE, a regulator of V-ATPase assembly. Nature cell biology *3*, 384-391.

Seto, E.S., Bellen, H.J., and Lloyd, T.E. (2002). When cell biology meets development: endocytic regulation of signaling pathways. Genes Dev *16*, 1314-1336.

Sollner, T., Whiteheart, S.W., Brunner, M., Erdjument-Bromage, H., Geromanos, S., Tempst, P., and Rothman, J.E. (1993). SNAP receptors implicated in vesicle targeting and fusion. Nature *362*, 318-324.

Spitzweck, B., Brankatschk, M., and Dickson, B.J. (2010). Distinct protein domains and expression patterns confer divergent axon guidance functions for Drosophila Robo receptors. Cell *140*, 409-420.

Stowers, R.S., Megeath, L.J., Gorska-Andrzejak, J., Meinertzhagen, I.A., and Schwarz, T.L. (2002). Axonal transport of mitochondria to synapses depends on milton, a novel Drosophila protein. Neuron *36*, 1063-1077.

Stowers, R.S., and Schwarz, T.L. (1999). A genetic method for generating Drosophila eyes composed exclusively of mitotic clones of a single genotype. Genetics *152*, 1631-1639.

Sudhof, T.C. (2004). The synaptic vesicle cycle. Annual review of neuroscience *27*, 509-547.

Sudhof, T.C., and Rothman, J.E. (2009). Membrane fusion: grappling with SNARE and SM proteins. Science *323*, 474-477.

Sun-Wada, G.H., Toyomura, T., Murata, Y., Yamamoto, A., Futai, M., and Wada, Y. (2006). The a3 isoform of V-ATPase regulates insulin secretion from pancreatic beta-cells. J Cell Sci *119*, 4531-4540.

Sweeney, S.T., and Davis, G.W. (2002). Unrestricted synaptic growth in spinster-a late endosomal protein implicated in TGF-beta-mediated synaptic growth regulation. Neuron *36*, 403-416.

Terman, J.R., Mao, T., Pasterkamp, R.J., Yu, H.H., and Kolodkin, A.L. (2002). MICALs, a family of conserved flavoprotein oxidoreductases, function in plexin-mediated axonal repulsion. Cell *109*, 887-900.

Ting, C.Y., and Lee, C.H. (2007). Visual circuit development in Drosophila. Curr Opin Neurobiol *17*, 65-72.

Toei, M., Saum, R., and Forgac, M. (2010). Regulation and isoform function of the V-ATPases. Biochemistry *49*, 4715-4723.

Toonen, R.F.G., and Verhage, M. (2007). Munc18-1 in secretion: lonely Munc joins SNARE team and takes control. Trends in neurosciences *30*, 564-572.

Tooze, S.A., and Schiavo, G. (2008). Liaisons dangereuses: autophagy, neuronal survival and neurodegeneration. Curr Opin Neurobiol *18*, 504-515.

Toyomura, T., Murata, Y., Yamamoto, A., Oka, T., Sun-Wada, G.H., Wada, Y., and Futai, M. (2003). From lysosomes to the plasma membrane. Journal of Biological Chemistry *278*, 22023.

Truman, J.W., Taylor, B.J., and Awad, T.A. (1993). Formation of the Adult Nervous System. In The Development of Drosophila melanogaster, M. Bate, and A. Martinez-Arias, eds. (Cold Spring Harbor, Cold Spring Harbor Laboratory Press), pp. 1245-1275.

Vaccari, T., Duchi, S., Cortese, K., Tacchetti, C., and Bilder, D. (2010). The vacuolar ATPase is required for physiological as well as pathological activation of the Notch receptor. Development *137*, 1825-1832.

Vactor, D.V., Sink, H., Fambrough, D., Tsoo, R., and Goodman, C.S. (1993). Genes that control neuromuscular specificity in Drosophila. Cell *73*, 1137-1153.

Van Vactor, D. (1998). Adhesion and signaling in axonal fasciculation. Curr Opin Neurobiol *8*, 80-86.

Van Vactor, D.L., Jr., Cagan, R.L., Kramer, H., and Zipursky, S.L. (1991). Induction in the developing compound eye of Drosophila: multiple mechanisms restrict R7 induction to a single retinal precursor cell. Cell *67*, 1145-1155.

Verstreken, P., Koh, T.W., Schulze, K.L., Zhai, R.G., Hiesinger, P.R., Zhou, Y., Mehta, S.Q., Cao, Y., Roos, J., and Bellen, H.J. (2003). Synaptojanin is recruited by endophilin to promote synaptic vesicle uncoating. Neuron *40*, 733-748.

Wada, Y., Sun-Wada, G.H., Tabata, H., and Kawamura, N. (2008). Vacuolar-type proton ATPase as regulator of membrane dynamics in multicellular organisms. J Bioenerg Biomembr *40*, 53-57.

Wagner, C.A., Finberg, K.E., Breton, S., Marshansky, V., Brown, D., and Geibel, J.P. (2004). Renal vacuolar H+-ATPase. Physiological reviews *84*, 1263.

Wang, T., Lao, U., and Edgar, B.A. (2009). TOR-mediated autophagy regulates cell death in Drosophila neurodegenerative disease. J Cell Biol *186*, 703-711.

Weninger, K., Bowen, M.E., Choi, U.B., Chu, S., and Brunger, A.T. (2008). Accessory proteins stabilize the acceptor complex for synaptobrevin, the 1:1 syntaxin/SNAP-25 complex. Structure *16*, 308-320.

Williamson, W.R., and Hiesinger, P.R. (2010). Preparation of developing and adult Drosophila brains and retinae for live imaging. J Vis Exp.

Williamson, W.R., Wang, D., Haberman, A.S., and Hiesinger, P.R. (2010a). A dual function of V0-ATPase a1 provides an endolysosomal degradation mechanism in Drosophila melanogaster photoreceptors. J Cell Biol *189*, 885-899.

Williamson, W.R., Wang, D., Haberman, A.S., and Hiesinger, P.R. (2010b). A dual function of V0-ATPase a1 provides an endolysosomal degradation mechanism in Drosophila photoreceptors. J Cell Biol.

Wucherpfennig, T., Wilsch-Brauninger, M., and Gonzalez-Gaitan, M. (2003). Role of Drosophila Rab5 during endosomal trafficking at the synapse and evoked neurotransmitter release. J Cell Biol *161*, 609-624.

Xu, H., Lee, S.J., Suzuki, E., Dugan, K.D., Stoddard, A., Li, H.S., Chodosh, L.A., and Montell, C. (2004). A lysosomal tetraspanin associated with retinal degeneration identified via a genome-wide screen. EMBO J *23*, 811-822.

Xu, T., and Forgac, M. (2001). Microtubules are involved in glucose-dependent dissociation of the yeast vacuolar [H+]-ATPase in vivo. Journal of Biological Chemistry *276*, 24855.

Yan, Y., Denef, N., and Schupbach, T. (2009). The vacuolar proton pump, V-ATPase, is required for notch signaling and endosomal trafficking in Drosophila. Dev Cell *17*, 387-402.

Yu, S.Y., Yoo, S.J., Yang, L., Zapata, C., Srinivasan, A., Hay, B.A., and Baker, N.E. (2002). A pathway of signals regulating effector and initiator caspases in the developing Drosophila eye. Development *129*, 3269-3278.

Zhang, J., Schulze, K.L., Hiesinger, P.R., Suyama, K., Wang, S., Fish, M., Acar, M., Hoskins, R.A., Bellen, H.J., and Scott, M.P. (2007). Thirty-one flavors of Drosophila rab proteins. Genetics *176*, 1307-1322.